

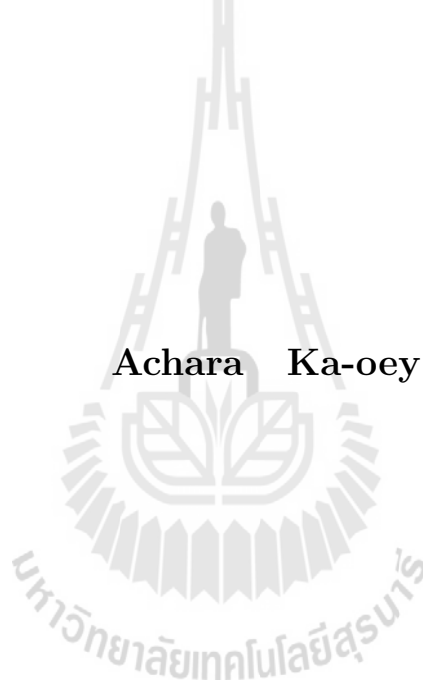
สเปกตรัมสภาพนำไฟฟ้าที่ขึ้นกับสปีนของระบบที่มีคู่ควบสปีนกับวงโคจร  
แบบรีซบาและเดรสเซลฮอส



วิทยานิพนธ์นี้เป็นส่วนหนึ่งของการศึกษาตามหลักสูตรปริญญาวิทยาศาสตรดุษฎีบัณฑิต  
สาขาวิชาฟิสิกส์  
มหาวิทยาลัยเทคโนโลยีสุรนารี  
ปีการศึกษา 2556

**SPIN-DEPENDENT CONDUCTANCE  
SPECTRUM IN SYSTEMS WITH RASHBA  
AND DRESSELHAUS SPIN-ORBIT  
COUPLING**

**Achara Ka-oey**



**A Thesis Submitted in Partial Fulfillment of the Requirements for the**

**Degree of Doctor of Philosophy in Physics**

**Suranaree University of Technology**

**Academic Year 2013**

# PARTICLE AND SPIN TRANSPORT IN SYSTEMS WITH RASHBA AND DRESSELHAUS SPIN-ORBIT COUPLING

Suranaree University of Technology has approved this thesis submitted in partial fulfillment of the requirements for the Degree of Doctor of Philosophy.

Thesis Examining Committee

---

(Prof. Dr. Santi Maensiri)

Chairperson

---

(Assoc. Prof. Dr. Puangratana Pairor)

Member (Thesis Advisor)

---

(Assoc. Prof. Dr. Yongyut Laosiritaworn)

Member

---

(Asst. Prof. Dr. Michael F. Smith)

Member

---

(Asst. Prof. Dr. Worawat Meevasana)

Member

---

(Prof. Dr. Sukit Limpijumnong)

Vice Rector for Academic Affairs  
and Innovation

---

(Assoc. Prof. Dr. Prapun Manyum)

Dean of Institute of Science

อัจฉรา กาเอ๊ย : สเปกตรัมสภาพนำไฟฟ้าที่ขึ้นกับสปินของระบบที่มีคู่ควบสปินกับวงโคจรแบบ  
รีชาและเดรสเซลฮอส (SPIN-DEPENDENT CONDUCTANCE SPECTRUM IN SYSTEMS  
WITH RASHBA AND DRESSSELHAUS SPIN-ORBIT COUPLING) อาจารย์ที่ปรึกษา :  
รองศาสตราจารย์ ดร.พวงรัตน์ ไพเราะ, 99 หน้า.

วิทยานิพนธ์นี้เป็นการศึกษาเชิงทฤษฎีเกี่ยวกับการส่งผ่านอนุภาคและสปินในระบบรอยต่อ  
ระหว่างโลหะกับระบบแก๊สอิเล็กตรอนสองมิติที่มีคู่ควบสปินกับวงโคจรแบบเดรสเซลฮอสและรีชา  
โดยจำลองลักษณะการเคลื่อนที่ของอนุภาคและสปินด้วยแบบจำลองอิสระเพื่อศึกษาผลของการหมุนแกน  
ผลึกของระบบแก๊สอิเล็กตรอนสองมิติ ความแรงของคู่ควบสปินกับวงโคจรและความแรงของกำแพงศักย์  
ตรงรอยต่อที่มีต่อสภาพการนำไฟฟ้าและสปินโพลาไรเซชัน

การคำนวณสภาพการนำไฟฟ้าและสปินโพลาไรเซชันในระบบรอยต่อระหว่างโลหะกับระบบ  
แก๊สอิเล็กตรอนสองมิติที่มีคู่ควบสปินกับวงโคจรแบบเดรสเซลฮอสเพียงชนิดเดียว พบว่าการหมุนแกน  
ผลึกของระบบแก๊สอิเล็กตรอนสองมิติไม่ส่งผลต่อผลรวมของสภาพการนำไฟฟ้าในระบบ แต่ส่งผลต่อ  
การเปลี่ยนแปลงของสปินโพลาไรเซชันคือ ค่าสปินโพลาไรเซชันจะมีค่าสูงสุดเมื่อหมุนแกนผลึกเป็นมุม  
 $\pm(2n+1)\pi/4$  และมีค่าต่ำสุดเมื่อหมุนแกนผลึกเป็นมุม  $\pm n\pi/2$  เมื่อ  $n = 0, 1, 2, 3, \dots$  สำหรับผลของ  
ความแรงของคู่ควบสปินกับวงโคจรแบบเดรสเซลฮอสพบว่าเมื่อเพิ่มค่าความแรงของคู่ควบสปินกับวง  
โคจรจะทำให้สภาพการนำไฟฟ้ามีค่าลดลงแต่กลับทำให้สปินโพลาไรเซชันมีค่ามากขึ้น ในทางตรงกัน  
ข้ามการเพิ่มค่าความแรงของกำแพงศักย์ตรงรอยต่อจะทำให้ค่าสภาพการนำไฟฟ้าและสปินโพลาไรเซชัน  
มีค่าลดลง นอกจากนี้แถบสเปกตรัมของสภาพการนำไฟฟ้ายังสามารถใช้วัดค่าพลังงานของระบบเดรส-  
เซลฮอสได้อีกด้วย

สำหรับระบบรอยต่อระหว่างโลหะกับระบบแก๊สอิเล็กตรอนสองมิติที่มีคู่ควบสปินและวงโคจร  
แบบรีชามีผลกับเดรสเซลฮอสพบว่า จากแถบสเปกตรัมของสภาพการนำไฟฟ้านอกจากจะสามารถวัดค่า  
พลังงานของระบบผสมรีชากับเดรสเซลฮอสได้แล้ว ยังสามารถวัดค่าผลต่างของพลังงานที่มี  
ความสัมพันธ์โดยตรงกับผลต่างระหว่างความแรงของคู่ควบสปินกับวงโคจรทั้งสองชนิดได้อีกด้วย และ  
จากการศึกษาของการหมุนแกนผลึกของระบบแก๊สอิเล็กตรอนสองมิติพบว่า ค่าสภาพการนำไฟฟ้าและ  
สปินโพลาไรเซชันของระบบมีค่าสูงสุดเมื่อหมุนแกนผลึกเป็นมุม  $(2n+1)\pi/4$  และให้ค่าต่ำสุดเมื่อ  
หมุนแกนผลึกเป็นมุม  $-(2n+1)\pi/4$  ซึ่งผลที่ได้ตรงกันข้ามกันกับผลของสปินโพลาไรเซชัน ผลการ  
เปลี่ยนแปลงความแรงของคู่ควบสปินกับวงโคจรแบบรีชามีผลกับเดรสเซลฮอสเมื่อกำหนดให้ค่าความแรงของคู่ควบสปินกับ  
วงโคจรแบบเดรสเซลฮอสคงที่พบว่า ที่ระดับแรงดันไฟฟ้าต่างๆ ค่าผลรวมของสภาพการนำไฟฟ้าจะมี  
ค่าแปรผันตามค่าความแรงของคู่ควบสปินกับวงโคจรแบบรีชาจนถึงค่าวิกฤตค่าหนึ่ง หลังจากนั้นค่า  
สภาพการนำไฟฟ้าจะมีค่าลดลงเมื่อเพิ่มค่าความแรงของคู่ควบสปินกับวงโคจร ในส่วนของสปินโพลาไร-  
เซชันกลับพบว่าจะมีค่าเพิ่มขึ้นตามค่าความแรงของคู่ควบสปินกับวงโคจร และเมื่อพิจารณาผลของความ

แรงของกำแพงศักย์พบว่า การเพิ่มค่าความแรงของกำแพงศักย์จะส่งผลให้ผลรวมของค่าสภาพการนำไฟฟ้าลดลงแต่กลับส่งผลให้ค่าสปีนโพลาริเซชันมีค่าเพิ่มขึ้น นอกจากนี้ยังพบว่าการส่งผ่านของอนุภาคในระบบรอยต่อดังกล่าวนอกจากจะทำให้เกิดค่าสภาพการนำไฟฟ้าและสปีนโพลาริเซชันในแนวตั้งฉากกับรอยต่อแล้ว ยังสามารถทำให้เกิดค่าสภาพการนำไฟฟ้าและสปีนโพลาริเซชันในแนวขนานกับรอยต่อได้อีกด้วย



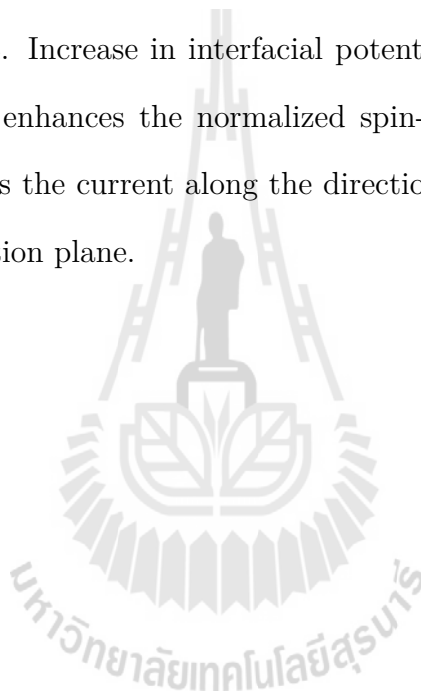
ACHARA KA-OEY : SPIN-DEPENDENT CONDUCTANCE  
SPECTRUM IN SYSTEMS WITH RASHBA AND DRESSELHAUS  
SPIN-ORBIT COUPLING. THESIS ADVISOR : ASSOC. PROF.  
PUANGRATANA PAIROR, Ph.D. 99 PP.

DRESSELHAUS SPIN-ORBIT COUPLING/RASHBA SPIN-ORBIT  
COUPLING/CONDUCTANCE SPECTRA/SPIN-POLARIZATION OF  
CONDUCTANCE/CRYSTALLOGRAPHIC ORIENTATION

This thesis is a theoretical study of the particle and spin transport across the interface between a metal and a two-dimensional electron gas with Rashba and Dresselhaus spin-orbit coupling. The conductance spectra and the normalized spin polarization of conductance are calculated using a scattering formalism. The effect of the crystallographic orientation of the 2DEG, the spin-orbit coupling strength, and the potential barrier strength on conductance spectra and its normalized spin polarization are considered.

In the absence of Rashba spin-orbit coupling, the conductance spectrum is found to be invariant with the crystallographic orientation. On the contrary, the normalized spin polarization is not invariant with the crystallographic orientation. The magnitude of the normalized spin polarization has a maximum value, when the (100) crystal axis is rotated at  $\theta = \pm(2n + 1)\pi/4$  away from the junction normal and minimum value at  $\theta = \pm n\pi/2$  where  $n = 0, 1, 2, 3, \dots$ . Both of the total conductance spectrum and the normalized spin polarization of conductance can be enhanced by increasing the Dresselhaus spin-orbit coupling strength, but can be suppressed by increasing the barrier strength. The Dresselhaus coupled energy can be determined from the conductance spectrum.

When both Rashba and Dresselhaus spin-orbit coupling exist, the conductance spectrum shows two distinctive features. From the positions of these features, the Rashba and Dresselhaus couples energy can be determined the Rashba-Dresselhaus energy and  $E_{\Delta}$ . Both the conductance spectrum and the normalized spin polarization of conductance are not invariant with the crystallographic orientation. The conductance spectrum has a maximum value, when rotate the (100) crystal axis makes  $\theta = (2n + 1)\pi/4$  with the junction normal and minimum value at  $\theta = -(2n + 1)\pi/4$ . Increase in interfacial potential barrier suppresses the total conductance but enhances the normalized spin-polarization of conductance. Moreover, there exists the current along the direction perpendicular to the interface normal the junction plane.



School of Physics

Academic Year 2013

Student's Signature \_\_\_\_\_

Advisor's Signature \_\_\_\_\_

## ACKNOWLEDGEMENTS

I would like to express my sincere thanks to my thesis advisor, Assoc. Prof. Dr. Puangratana Pairor for her invaluable help and constant encouragement throughout the course of this research.

In addition, I am grateful for the lecturers in the School of Physics for their suggestion and all their help.

I would like to thank Prof. Dr. Santi Maensiri, Assoc. Prof. Dr. Yongyut Laosiritaworn, Assist. Prof. Dr. Michael F. Smith, and Assist. Prof. Dr. Worawat Meevasana for accepting to serve in my committee, and for helpful comments and suggestions.

This work has been financial support from the Thailand Research Fund through the Royal Golden Jubilee Ph.D. Program (Grant No. PHD/0218/2548.)

I would like to thanks all physics staffs and graduate student at SUT for their friendly and sincerely.

Finally, I would like to thanks my parents, my sister, Ton and his family for their love and encouragement.

Achara Ka-oey



# CONTENTS

	Page
ABSTRACT IN THAI . . . . .	I
ABSTRACT IN ENGLISH . . . . .	III
ACKNOWLEDGEMENTS . . . . .	V
CONTENTS . . . . .	VI
LIST OF FIGURES . . . . .	VIII
LIST OF SYMBOLS . . . . .	XVI
<b>CHAPTER</b>	
<b>I INTRODUCTION . . . . .</b>	<b>1</b>
1.1 Motivation . . . . .	1
1.2 Research Procedure . . . . .	14
1.3 Outline of Thesis . . . . .	14
<b>II TUNNELING BETWEEN A NORMAL METAL AND A 2DEG WITH ONLY DRESSSELHAUS SPIN-ORBIT COU- PLING . . . . .</b>	<b>16</b>
2.1 Density of States . . . . .	16
2.2 Model and Formalism . . . . .	18
2.2.1 Basic Model . . . . .	18
2.2.2 The Wave Functions and Matching Conditions . . . . .	22
2.2.3 Conductance and Normalized Spin Polarization of Conduc- tance . . . . .	23
2.3 Results and Discussions . . . . .	26

## CONTENTS (Continued)

	Page
2.4 Conclusions . . . . .	31
<b>III TUNNELING BETWEEN A NORMAL METAL AND A 2DEG WITH BOTH RASHBA AND DRESSELHAUS SPIN- ORBIT COUPLING . . . . .</b>	<b>35</b>
3.1 Density of States . . . . .	36
3.2 Model and Formalism . . . . .	37
3.2.1 Basic model . . . . .	37
3.2.2 The Wave Functions and Matching Conditions . . . . .	40
3.2.3 Conductance and Normalized Spin Polarization of Conduc- tance . . . . .	41
3.3 Results and Discussions . . . . .	43
3.4 Conclusions . . . . .	46
<b>IV CONCLUSIONS . . . . .</b>	<b>60</b>
REFERENCES . . . . .	64
APPENDICES	
APPENDIX A TUNNELING BETWEEN A NORMAL METAL AND A 2DEG WITH ONLY RASHBA SPIN-ORBIT COUPLING DOUBLE JUNCTIONS . . . . .	73
APPENDIX B PUBLICATION I . . . . .	82
APPENDIX C PUBLICATION II . . . . .	86
CURRICULUM VITAE . . . . .	99

# LIST OF FIGURES

Figure		Page
1.1	A unit cell of a zinc blende structure, such as GaAs, where the shaded dots represent Ga atoms and the bold dots represent As atoms . . . . .	2
1.2	(a) The energy spectrum of an electrons in a two-dimensional Dresselhaus system. (b) The sketches of the energy spectrum of the electron in Dresselhaus system as a function of $k_x$ , for zero (top) and nonzero (bottom) $k_y$ . The dashed lines represent the energy spectrum of the electron with energy $E^+$ and the solid lines represent energy spectrum of the electron with energy $E^-$ . . . . .	4
1.3	The energy contours of an electron in the two-dimensional Dresselhaus system for (a) $E > 0$ and (b) $E < 0$ . Dashed lines represent the energy contour of the electron with energy $E^+$ and solid lines represent energy contour of the electron with energy $E^-$ . The arrows depict the spin direction of the electrons at the $\vec{k}$ state on the contours. . . . .	5
1.4	Schematic diagram of the semiconductors heterostucture grown in $z$ (001) direction, like GaAs and AlGaAs. A 2DEG with RSOC occurs at the interface. . . . .	6

## LIST OF FIGURES (Continued)

Figure		Page
1.5	(a) The band structure of an electron in the two-dimensional Rashba system. (b) The sketches of the energy spectrum as a function of $k_x$ for zero (top) and nonzero (bottom) $k_y$ . Dashed lines represent the energy spectrum of the electron with energy $E^+$ and solid lines represent energy spectrum of the electron with energy $E^-$ .	7
1.6	The energy contours of an electron in the two-dimensional Rashba system for (a) $E > 0$ and (b) $E < 0$ . The dashed lines represent the energy contour of an electron with energy $E^+$ and the solid lines represent energy contour of the electron with energy $E^-$ . The arrows depict the spin direction of the electrons at the $\vec{k}$ state on the contours. . . . .	8
1.7	Schematic diagram of the semiconductors heterostructure grown in $z$ (001) direction, like GaAs and AlGaAs. 2DEG with RDSOC occurs at the interface between GaAs and AlGaAs. . . . .	9
1.8	(a) The band structure of an electron in a two-dimensional Rashba-Dresselhaus system. (b) The sketches of the energy spectrum as a function of $k_x$ for zero (top) and nonzero (bottom) $k_y$ . The dashed lines represent the energy spectrum of the electron with energy $E^+$ and the solid lines represent energy spectrum of the electron with energy $E^-$ . . . . .	10

## LIST OF FIGURES (Continued)

Figure	Page
1.9	The energy contours of an electron in a two-dimensional Rashba-Dresselhaus system (a) for $E > 0$ and (b) $E < 0$ . The dashed lines represent the energy contour of the electron with energy $E^+$ and the solid lines represent energy contour of the electron with energy $E^-$ . The arrows depict the spin direction of the electrons at the $\vec{k}$ state on the contours. . . . .
11	
1.10	Schematic diagram of the junction of the system considered in this thesis. A metal is in the $x < 0$ region and the $x > 0$ region is occupied by a 2DEG with spin-orbit coupling. . . . .
13	
2.1	(a) The energy spectrum of the electrons in a two-dimensional Dresselhaus system. (b) The sketches of the energy spectrum of the electron in Dresselhaus system as a function of $k_x$ . Dashed lines represent the energy spectrum of the electron with energy $E^+$ and solid lines represent energy spectrum of the electron with energy $E^-$ .
17	
2.2	The DOS of a 2DEG with Dresselhaus spin-orbit coupling. The dotted line represents the DOS of the electron in the $E^-$ branch, the dashed line represents the electron in the $E^+$ branch and solid line represents the total DOS. . . . .
19	
2.3	A Metal/Dresselhaus system junction. . . . .
20	

## LIST OF FIGURES (Continued)

Figure	Page
2.4	The energy spectrum of the electrons in a metal (left) and the Dresselhaus system (right). The arrows pointing left or right, represent electron states that are considered in the scattering process. We assumed the incoming state is equal to 1, $r_{\uparrow}$ and $r_{\downarrow}$ are reflected states with spin-up and spin-down, $t_{+}$ and $t_{-}$ are outgoing states of the electron with $E^{+}$ and $E^{-}$ , respectively. . . . . 21
2.5	The total conductance of the M/DS junction as a function of applied voltage ( $eV$ ) at various values of $Z$ , where $\beta_0 = 0.05 q_F$ , $m_D = 0.05 m_e$ , $Z = 0$ , and $\theta = 0$ . . . . . 26
2.6	The normalized spin polarization of conductance of the M/DS junction as a function of applied voltage( $eV$ ) at various values of $Z$ , where $\beta_0 = 0.05q_F$ , $m_D = 0.05m_e$ , and $\theta = 0$ . . . . . 28
2.7	Plots of the total conductance and the normalized spin polarization of conductance as a function of $Z$ , where $m_D = 0.05 m_e$ , $\beta_0 = 0.05q_F$ , and $\theta = 0$ . . . . . 29
2.8	The total conductance of the M/DS junction as a function of applied voltage( $eV$ ) at various $\theta$ , where $\beta_0 = 0.05 q_F$ , $m_D = 0.05m_e$ , and $\theta = 0$ . . . . . 30
2.9	The normalized spin polarization of conductance of the M/DS junction as a function of applied voltage( $eV$ ) at various $\theta$ , where $\beta_0 = 0.05 q_F$ , $m_D = 0.05m_e$ , and $Z = 0$ . . . . . 31

## LIST OF FIGURES (Continued)

Figure		Page
2.10	The total conductance of the M/DS junction as a function of $\beta_0$ at various applied voltages, where $eV = E_D$ , $m_D = 0.05 m_e$ , and $Z = 0$ .	32
2.11	The normalized spin polarization of conductance of the M/DS junction as a function of $\beta_0$ at various applied voltages, where $eV = E_D$ , $m_D = 0.05 m_e$ , and $Z = 0$ .	33
2.12	The normalized spin polarization of conductance in the Metal/Dresselhaus system junction as a function of $\theta$ at various applied voltages. where $\beta_0 = 0.05 q_F$ , $m_D = 0.05 m_e$ , and $Z = 0$ . The solid line shows $G_P$ is in $eV < 0$ region, and dashed line is in $eV > 0$ region.	34
3.1	(a) The energy spectrum of the electron in a two-dimensional Rashba-Dresselhaus system. (b) The sketches of the energy spectrum of the electron in Rashba-Dresselhaus system as a function of $k_x$ . Dashed lines represent the energy spectrum of the electron with energy $E^+$ and solid lines represent energy spectrum of the electron with energy $E^-$ .	36
3.2	The DOS of a 2DEG with Rashba and Dresselhaus spin-orbit coupling. The dotted line represents the DOS of the electron in the $E^-$ branch, the dashed line represents the electron in the $E^+$ branch and the solid line represents the total DOS, where $E_D = \frac{\hbar^2 \beta_0^2}{2m_{RD}}$ , $m_{RD} = 0.05m_e$ , $\beta_0 = 0.025q_F$ , and $k_0 = 0.05q_F$ .	48

## LIST OF FIGURES (Continued)

Figure		Page
3.3	A Metal/Rashba-Dresselhaus system junction. . . . .	49
3.4	The energy spectra of the electrons in a metal (left) and the Rashba-Dresselhaus system (right). The arrows pointing left or right, represent the electron states that are considered in the scattering process. We assumed the incoming state equal 1, $r_{\uparrow}$ and $r_{\downarrow}$ are reflected states with spin-up and spin-down, and $t_{+}$ and $t_{-}$ are outgoing states of the electron with $E^{+}$ and $E^{-}$ , respectively. . . . .	49
3.5	The total conductance spectrum as a function of applied voltage at various values of $Z$ , where $k_0 = 0.05q_F$ , $\beta_0 = 0.025q_F$ , $m_{RD} = 0.05 m_e$ , and $\theta = -\pi/4$ rad. . . . .	50
3.6	Plots of the normalized spin polarization of conductance as a function of applied voltage at various values of $Z$ , where $m_{RD} = 0.05 m_e$ , $k_0 = 0.05q_F$ , $\beta_0 = 0.025q_F$ , and $\theta = -\pi/4$ rad. . . . .	51
3.7	Plots of the total conductance and the normalized spin polarization of conductance as a function of $Z$ , where $m_{RD} = 0.05 m_e$ , $k_0 = 0.05q_F$ , $\beta_0 = 0.025q_F$ , and $\theta = 0$ . . . . .	52
3.8	The total conductance spectrum as a function of applied voltage at various $\theta$ , where $m_{RD} = 0.05 m_e$ , $k_0 = 0.05q_F$ , $\beta_0 = 0.025q_F$ , $Z = 0.0$ . . . . .	53
3.9	Plots of the normalized spin polarization of conductance as a function of applied voltage at various $\theta$ , where $m_{RD} = 0.05 m_e$ , $k_0 = 0.05q_F$ , $\beta_0 = 0.025q_F$ , and $Z = 0.0$ . . . . .	54



## LIST OF FIGURES (Continued)

Figure		Page
3.10	The total conductance spectrum as a function of Rashba spin-orbit coupling strength at various values of $\theta$ , where $m_{RD} = 0.05 m_e$ , $\beta_0 = 0.025q_F$ , $Z = 0.0$ , and $\theta = -\frac{\pi}{4}$ rad. . . . .	55
3.11	Plot of the normalized spin polarization of conductance as a function of Rashba spin-orbit coupling strength at various values of $\theta$ , where $m_{RD} = 0.05 m_e$ , $\beta_0 = 0.025q_F$ , and $\theta = -\frac{\pi}{4}$ rad. . . . .	56
3.12	Plot of the total conductance as a function of $\theta$ at various values of applied voltage, where $m_{RD} = 0.05 m_e$ , $k_0 = 0.05q_F$ , $\beta_0 = 0.025q_F$ , and $Z = 0.0$ . . . . .	57
3.13	Plot of the normalized spin polarization of conductance as a function of $\theta$ at various values of applied voltage, where $m_{RD} = 0.05 m_e$ , $k_0 = 0.05q_F$ , $\beta_0 = 0.025q_F$ , and $Z = 0.0$ . . . . .	58
3.14	The plot of the conductance perpendicular to the junction( $G_{Total,XY}$ ) as a function of applied voltage at various values of $\theta$ , where $k_0 = 0.05q_F$ , $\beta_0 = 0.025q_F$ , $Z = 0.0$ , and $\theta = 0$ rad. . . . .	59
A.1	A Metal/Rashba system/Metal double junction. . . . .	74
A.2	The total conductance of the M/RS/M double junctions as a function of applied voltage ( $eV$ ) when we set $Z_1 = Z_2 = Z$ , where $k_0 = 0.05 q_F$ , $m_R = 0.05 m_e$ , and $L = 280//q_F$ . . . . .	77

## LIST OF FIGURES (Continued)

Figure	Page
A.3	<p>The normalized of spin polarization of conductance of the M/RS/M double junctions as a function of applied voltage (<math>eV</math>) when we set <math>Z_1 = Z_2 = Z</math>, where <math>k_0 = 0.05 q_F</math>, <math>m_R = 0.05 m_e</math>, and <math>L = 280//q_F</math>. 78</p>
A.4	<p>The total conductance and the normalized spin polarization of conductance of the M/RS/M double junctions as a function of the interfacial scattering potential between a normal metal and a 2DEG with RSOC (<math>Z_1</math>) when fixed <math>Z_2 = 0</math>, where <math>k_0 = 0.05 q_F</math>, <math>m_R = 0.05 m_e</math>, and <math>L = 280//q_F</math>. The left column shows the total conductance and the right column shows the normalized spin polarization of conductance, when the top figure for <math>eV = -0.5 E_R</math> and the bottom figure for <math>eV = E_R</math>. . . . . 80</p>
A.5	<p>The total conductance and the normalized spin polarization of conductance of the M/RS/M double junctions as a function of the interfacial scattering potential between a 2DEG with RSOC and a normal metal (<math>Z_2</math>) when fixed <math>Z_1 = 0</math>, where <math>k_0 = 0.05 q_F</math>, <math>m_R = 0.05 m_e</math>, and <math>L = 280//q_F</math>. The left column shows the total conductance and the right column shows the normalized spin polarization of conductance, when the top figure for <math>eV = -0.5 E_R</math> and the bottom figure for <math>eV = E_R</math>. . . . . 81</p>

## LIST OF SYMBOLS

$k, q$	Wave vector
$\beta$	Dresselhaus Spin-orbit coupling constant
$\beta_0$	Dresselhaus Spin-orbit coupling strenght
$\lambda$	Rashba Spin-orbit coupling constant
$k_0$	Rashba Spin-orbit coupling strenght
$\hbar$	Plank constant
$j$	Current density
$G$	Conductance
$D$	Density of state
$n$	Electron carrier density
$eV$	Bias voltage
$P$	Spin polarization of conductance
$Z$	Potential barrier strength
$\gamma$	Material constant
$m_e$	Electron effective mass in metal
$m_D$	Electron effective mass in Dresselhaus system
$m_{RD}$	Electron effective mass in Rashba-Dresselhaus system
$E_F$	Fermi energy of metal
$E_{FD}$	Fermi energy of Dresselhaus system
$E_{FRD}$	Fermi energy of Rashba-Dresselhaus system
$\sigma$	Pauli spin matrices
$\theta$	Angle of the orientation

# CHAPTER I

## INTRODUCTION

### 1.1 Motivation

Spintronics is an emerging field that studies how to exploit the intrinsic spin of the electron in addition to its fundamental electronic charge in solid-state devices (Wolf et al., 2001; Zutic et al., 2004; Barnas et al., 1990). This ability has led to dramatic improvement in electronic systems and devices, such as memory elements, logic elements, spin transistors and spin valves. Current efforts in designing and manufacturing spintronic devices have involved two different approaches. The first has been perfecting the existing giant magnetoresistance-based technology by either developing new materials with larger normalized spin polarization of electrons, or making improvements on the existing devices for better spin filtering. The second, more radical, effort has focused on finding novel ways of both generation and utilization of spin-polarized currents. The latter includes the investigation of spin transport in semiconductors and looking for the ways, in which semiconductors can function as spin polarizers and spin valves. The materials that possessed the potential to be manipulated in such ways are, for example, the semiconductors with spin-orbit coupling (Hu and Matsuyama, 2001; Datta and Das, 1989; Zutic et al., 2004). The spin-orbit coupling in these materials gives rise to spin splitting of energy band lifting the degeneracy of up-spin and down-spin states. There are two well-known kinds of such spin-orbit coupling; Dresselhaus spin-orbit coupling(DSOC), and the Rashba-Bychkov spin-orbit coupling(RSOC).

In the system lacking of the bulk inversion symmetry, like a zinc blende

structure (in Figure 1.1), there exists the Dresselhaus spin-orbit coupling (Dresselhaus, 1955). The widely known semiconductors that have such spin-orbit coupling are the III-IV semiconductor compounds, like InAs, GaAs, GaSb, InP and InSb (Dresselhaus, 1955; Wepfer et al., 1971; Perel et al., 2003; Desrat et al., 2006; Studer et al., 2010). This interaction takes the form (Dresselhaus, 1955; Silva, 1992)

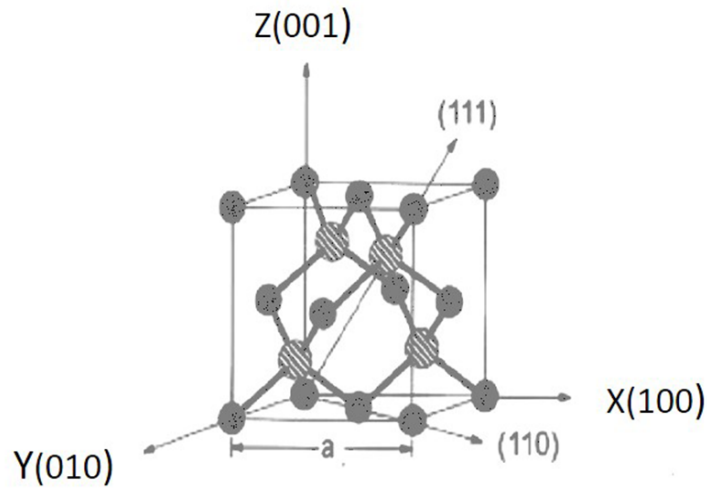


**Figure 1.1** A unit cell of a zinc blende structure, such as GaAs, where the shaded dots represent Ga atoms and the bold dots represent As atoms

$$H_{DSOC} = \gamma [\sigma_x k_x (k_y^2 - k_z^2) + \sigma_y k_y (k_z^2 - k_x^2) + \sigma_z k_z (k_x^2 - k_y^2)], \quad (1.1)$$

where  $\vec{k} = (k_x, k_y, k_z)$  is the wave vector of electron. Each component of the wave vector are parallel to the main crystal axes (100), (010) and (001) respectively.  $\gamma$  is the material constant.  $\sigma_x, \sigma_y$  and  $\sigma_z$  are the Pauli spin matrices. If the electrons are confined to move in the  $xy$  plane, the interaction can be simplified to

$$H_{DSOC} = \beta(\sigma_x k_x - \sigma_y k_y) + \gamma(\sigma_x k_x k_y^2 - \sigma_y k_y k_x^2), \quad (1.2)$$

where  $\beta = -\gamma \langle k_z^2 \rangle$  is the Dresselhaus spin-orbit coupling constant, and  $\langle k_z^2 \rangle$  is the expected value of  $k_z^2$ . For the III-IV semiconductor compounds, the typical magnitude of the cubic terms in the wave vector compared to that of the linear term is given by the ratio of the Fermi energy  $E_F$  of the in-plane motion to the kinetic energy of the quantized degree of freedom in the growth direction. The magnitude for  $\vec{k} = (k_x, k_y)$  on the Fermi surface, i.e., for  $k_x^2 + k_y^2 = k_F^2$ : the ratios  $k_x^2 / \langle k_z^2 \rangle$  and  $k_y^2 / \langle k_z^2 \rangle$  have an upper limit of  $k_F^2 / \langle k_z^2 \rangle$  and are zero for the certain orientation of  $\vec{k}$ . Therefore, the linear term is dominant in the case of strong confinement, i.e., for  $\langle k_z^2 \rangle \gg k_F^2$ . The DSOC spin-orbit interaction for a two-dimensional system (2DEG) can be then written as (Perel et al., 2003)

$$H_{DSOC} = \frac{\hbar^2 \beta_0}{m_D} (\sigma_x k_x - \sigma_y k_y), \quad (1.3)$$

where  $\beta_0 = \frac{m_D \beta}{\hbar^2}$  is the strength parameter of DSOC.

In the effective mass model, the Hamiltonian of the two-dimensional system with DSOC takes the form

$$H_{DS} = \frac{p^2}{2m_D} + \frac{\hbar^2 \beta_0}{m_D} (\sigma_x k_x - \sigma_y k_y), \quad (1.4)$$

where  $\vec{p}$  is the momentum of an electron, and  $m_D$  is the effective mass of an electron. The energy spectrum is found to be

$$E^\pm(\vec{k}) = \frac{\hbar^2}{2m_D} k^2 \pm \frac{\hbar^2 \beta_0}{m_D} |k|, \quad (1.5)$$

where  $k = \sqrt{k_x^2 + k_y^2}$ . The spin part of the eigenfunction with  $E^+$  and  $E^-$  states is

$$|+\rangle = \frac{1}{\sqrt{2}} \begin{bmatrix} \frac{k_x + ik_y}{\sqrt{k_x^2 + k_y^2}} \\ 1 \end{bmatrix}, \quad (1.6)$$

and

$$|-\rangle = \frac{1}{\sqrt{2}} \begin{bmatrix} -\frac{k_x + ik_y}{\sqrt{k_x^2 + k_y^2}} \\ 1 \end{bmatrix}, \quad (1.7)$$

respectively.

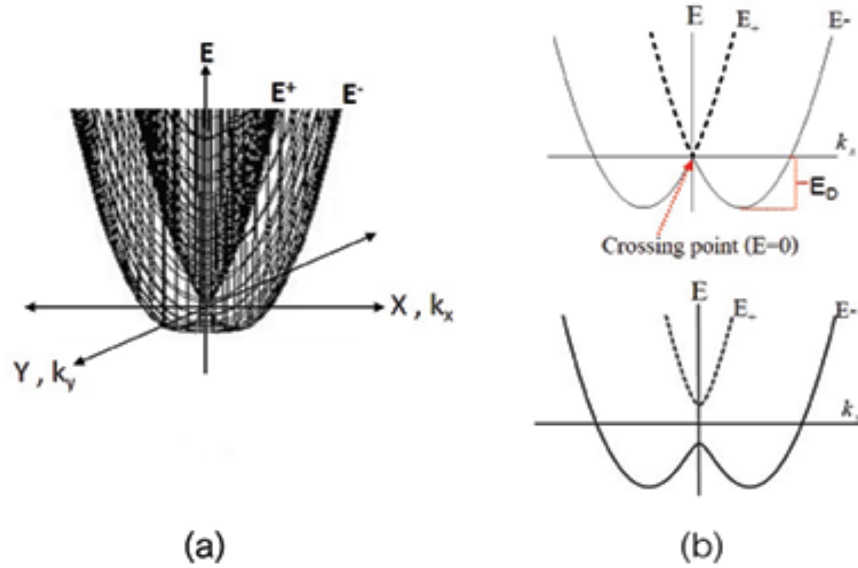


**Figure 1.2** (a) The energy spectrum of an electrons in a two-dimensional Dresselhaus system. (b) The sketches of the energy spectrum of the electron in Dresselhaus system as a function of  $k_x$ , for zero (top) and nonzero (bottom)  $k_y$ . The dashed lines represent the energy spectrum of the electron with energy  $E^+$  and the solid lines represent energy spectrum of the electron with energy  $E^-$ .

The energy spectrum of an electron in the two-dimensional Dresselhaus system are shown in Figure 1.2. Notice that for only  $k_y = 0$  the  $E^+$  and  $E^-$  bands meet at  $k_x = 0$ . It should also be pointed out that  $E^\pm = E^\pm(|k|)$ , independent of the  $\vec{k}$  direction. The energy contours of  $|+\rangle$  and  $|-\rangle$  states are shown in Figure 1.3. The contours are invariant through the rotation around the  $z$  axis. The spin states of the electrons at some  $\vec{k}$  states are graphically shown by the arrows on the contours. Unlike the energy contours, the spin states are not invariant with

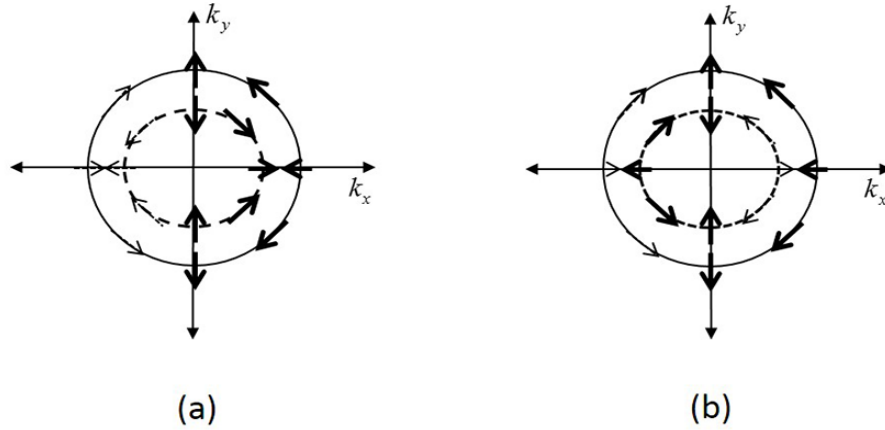


**Figure 1.3** The energy contours of an electron in the two-dimensional Dresselhaus system for (a)  $E > 0$  and (b)  $E < 0$ . Dashed lines represent the energy contour of the electron with energy  $E^+$  and solid lines represent energy contour of the electron with energy  $E^-$ . The arrows depict the spin direction of the electrons at the  $\vec{k}$  state on the contours.

respect to the rotation around the  $z$  axis.

Many researchers measured the strength of DSOC by various techniques like Raman scattering (Jusserand et al., 1992), magnetotransport (Dresselhaus et al., 1992; Miller et al., 2003; Krich and Halperin, 2007), Hall and Shubnikov-de Hass oscillations (Studer et al., 2010). The typical value of the Dresselhaus spin-orbit coupling constant is between  $0.5 \times 10^{-13} - 2.5 \times 10^{-13}$  eV.m.

The Rashba spin-orbit coupling (RSOC) exist in the system lacking of the structural inversion symmetry, like surface alloys Bi/Ag(111) and Pb/Ag(111) (Bychkov and Rashba, 1984; Pacile et al., 2006; Ast et al., 2007a; Premper et al., 2007; Ast et al., 2007b; Vajna et al., 2012) and semiconductor heterostructures, such as AlGaAs/GaAs and InSb/InAlSb (Tolozá Sandoval et al., 2010; Usaj and Balseiro, 2004). For the heterostructure, like GaAs/AlGaAs in the (001) direction, the electrons are trapped at the interface and can move only in the interface plane



(see Figure 1.4). The Rashba spin-orbit interaction takes the form (Rashba, 1960; Bychkov and Rashba, 1984; Wepfer et al., 1971; Desrat et al., 2006)

$$H_{RSOC} = \lambda \hat{z} \cdot (\vec{k} \times \vec{\sigma}), \quad (1.8)$$

where  $\lambda$  is the Rashba spin-orbit coupling constant,  $\vec{\sigma}$  are Pauli spin matrices,  $\hat{z}$  is a unit vector perpendicular to the plane of motion, and  $\vec{k}$  is the wave vector. For a system defined in Figure 1.5, the Hamiltonian is simplified to

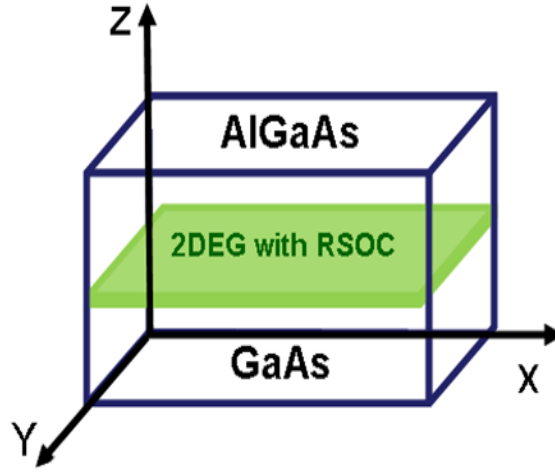


**Figure 1.4** Schematic diagram of the semiconductors heterostructure grown in  $z$  (001) direction, like GaAs and AlGaAs. A 2DEG with RSOC occurs at the interface.

$$H_{RSOC} = \frac{\hbar^2 k_0}{m_R} (\sigma_x k_y - \sigma_y k_x), \quad (1.9)$$

where  $k_0 = \frac{m_R \lambda}{\hbar^2}$  is the strength parameter of RSOC, and  $m_R$  is the effective mass of the electron in the Rashba system. In the effective mass model, the Hamiltonian

of the system with RSOC takes the form

$$H_{RS} = \frac{p^2}{2m_R} + \frac{\hbar^2 k_0}{m_R} (\sigma_x k_y - \sigma_y k_x) \quad (1.10)$$

The energy dispersion relation of the electrons in these system are

$$E^\pm(\vec{k}) = \frac{\hbar^2}{2m_R} k^2 \pm \frac{\hbar^2 k_0}{m_{RS}} |k|, \quad (1.11)$$

where  $k = \sqrt{k_x^2 + k_y^2}$ . The spin part of the eigenfunction for the  $E^+$  and  $E^-$  state is

$$|+\rangle = \frac{1}{\sqrt{2}} \begin{bmatrix} \frac{ik_x + k_y}{\sqrt{k_x^2 + k_y^2}} \\ 1 \end{bmatrix}, \quad (1.12)$$

$$|-\rangle = \frac{1}{\sqrt{2}} \begin{bmatrix} -\frac{ik_x + ik_y}{\sqrt{k_x^2 + k_y^2}} \\ 1 \end{bmatrix}, \quad (1.13)$$

respectively.

The energy spectrum of the electron in the two-dimensional Rashba system are shown in Figure 1.5. Similar to the Dresselhaus case, for  $k_y = 0$  both  $E^+$  and  $E^-$  bands meet at  $k_x = 0$ , and the energy contours are invariant under the rotation around the  $z$  axis. The spin states of the electrons at some values of  $\vec{k}$  state are depict by the arrows on the contours.

Many researchers measured the strength of the RSOC by using many techniques such as the weak antilocalization analysis (Koga et al., 2002), photocurrent measurement (Ganichev et al., 2004), the scanning-tunneling spectroscopy (Ast et al., 2007b), the Shubnikovde Haas oscillations (Engels et al., 1997; Hu et al., 1999) and angle-resolved photoelectron spectroscopy (Ast et al., 2007a; LaShell et al., 1996; Henk et al., 2004; Popovic et al., 2005; Cercellier et al., 2004). The typical value of the Rashba spin-orbit coupling strength is about  $1 \times 10^{-11} - 4 \times 10^{-11}$  eV.m. It was also found that the strength of RSOC can be tunned by applying

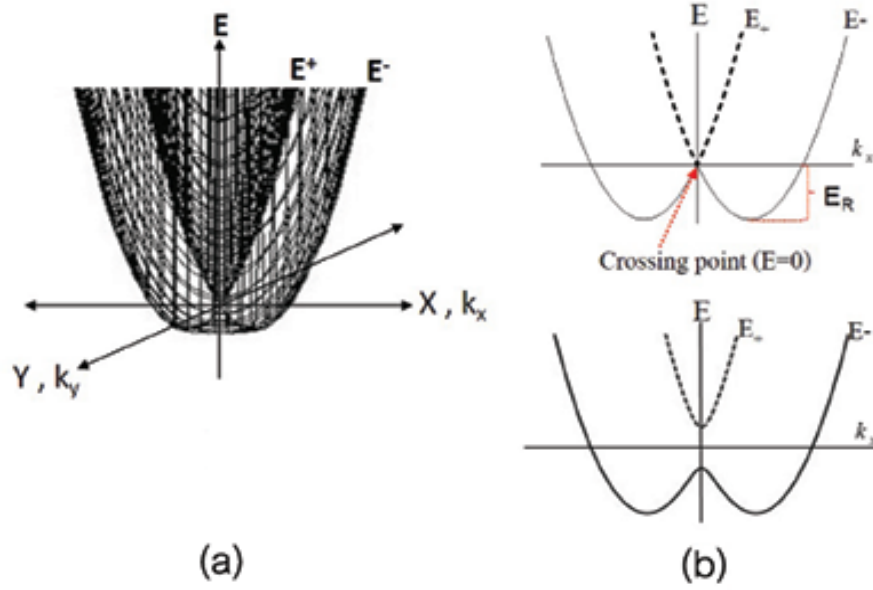


**Figure 1.5** (a) The band structure of an electron in the two-dimensional Rashba system. (b) The sketches of the energy spectrum as a function of  $k_x$  for zero (top) and nonzero (bottom)  $k_y$ . Dashed lines represent the energy spectrum of the electron with energy  $E^+$  and solid lines represent energy spectrum of the electron with energy  $E^-$ .

gate voltage perpendicular to the 2DEG plane and adsorption of adatoms (Bychkov and Rashba, 1984; Rashba, 1960; Grundler, 2000; Nitta et al., 1997).

Both types of the spin-orbit couplings can also co-exist in the systems like InAs/GaSb, InAs/AlSb, GaAs/AlGaAs and InGaAs/InAlAs. Figure 1.7 depicts the 2DEG in which both types of spin-orbit coupling can coexist (Nitta et al., 1997; Das et al., 1989; Toloza Sandoval et al., 2012; Studer et al., 2009a). The Hamiltonian of the electron in these systems can be written as

$$H_{RDSOC} = \frac{\hbar^2 k_0}{m_{RD}} (\sigma_x k_y - \sigma_y k_x) + \frac{\hbar^2 \beta_0}{m_{RD}} (\sigma_x k_x - \sigma_y k_y), \quad (1.14)$$

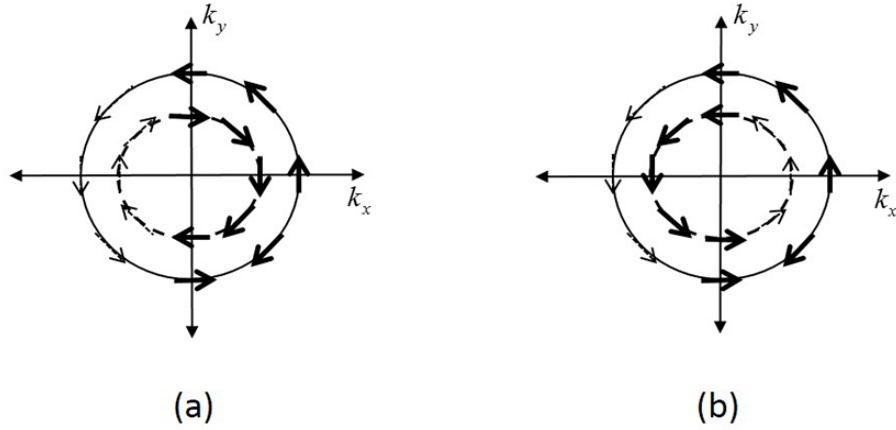


**Figure 1.6** The energy contours of an electron in the two-dimensional Rashba system for (a)  $E > 0$  and (b)  $E < 0$ . The dashed lines represent the energy contour of an electron with energy  $E^+$  and the solid lines represent energy contour of the electron with energy  $E^-$ . The arrows depict the spin direction of the electrons at the  $\vec{k}$  state on the contours.

In the effective mass model, the Hamiltonian takes the form

$$H_{RDS} = \frac{p^2}{2m_{RD}} + \frac{\hbar^2 k_0}{m_{RD}} (\sigma_x k_y - \sigma_y k_x) + \frac{\hbar^2 \beta_0}{m_{RD}} (\sigma_x k_x - \sigma_y k_y), \quad (1.15)$$

where  $m_{RD}$  is the electron effective mass of electron in the Rashba-Dresselhaus system. The energy dispersion relation is

$$E^\pm(k_x, k_y) = \frac{\hbar^2 k^2}{2m_{RD}} \pm \frac{\hbar^2}{m_{RD}} \sqrt{(\beta_0^2 + k_0^2) |k|^2 + 4\beta_0 k_0 k_x k_y}, \quad (1.16)$$

where  $k = \sqrt{k_x^2 + k_y^2}$ . The spin part of the eigen function for the  $E^+$  and  $E^-$  state is

$$|+\rangle = \frac{1}{\sqrt{2}} \begin{bmatrix} \frac{(\beta_0 k_x + k_0 k_y) + i(\beta_0 k_y + k_0 k_x)}{\sqrt{(\beta_0^2 + k_0^2)(k_x^2 + k_y^2) + 4\beta_0 k_0 k_x k_y}} \\ 1 \end{bmatrix}, \quad (1.17)$$

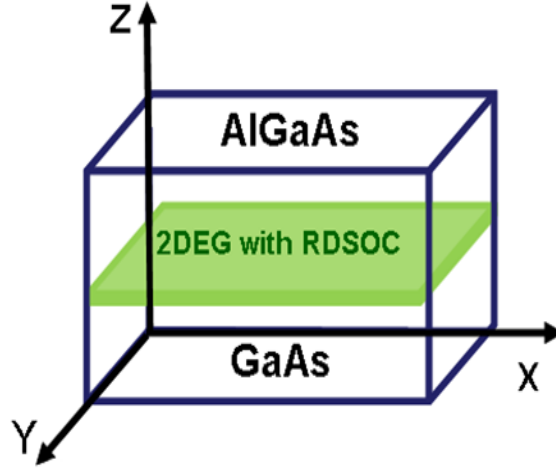


**Figure 1.7** Schematic diagram of the semiconductors heterostructure grown in  $z$  (001) direction, like GaAs and AlGaAs. 2DEG with RDSOC occurs at the interface between GaAs and AlGaAs.

$$|-\rangle = \frac{1}{\sqrt{2}} \begin{bmatrix} -\frac{(\beta_0 k_x + k_0 k_y) + i(\beta_0 k_y + k_0 k_x)}{\sqrt{(\beta_0^2 + k_0^2)(k_x^2 + k_y^2) + 4\beta_0 k_0 k_x k_y}} \\ 1 \end{bmatrix}, \quad (1.18)$$

respectively.

The energy spectrum of the electron in the two-dimensional Rashba and Dresselhaus system is shown in Figure 1.8(a). Unlike the system with only either Rashba or Dresselhaus spin-orbit coupling, the energy contours of Rashba and Dresselhaus system are not invariant under the rotation around the  $z$  axis. Also  $E^\pm(-k_x, k_y) \neq E^\pm(k_x, k_y)$  (see Figure 1.8(b)). In Figure 1.9, the energy contours and the spin directions at a few corresponding  $\vec{k}$  states are shown.

The strength of RSOC is usually stronger than that of DSOC, and when they both exist, they can be determined by many techniques such as the Shubnikov-de Hass oscillations (Park et al., 2013), persistent charge and spin cur-

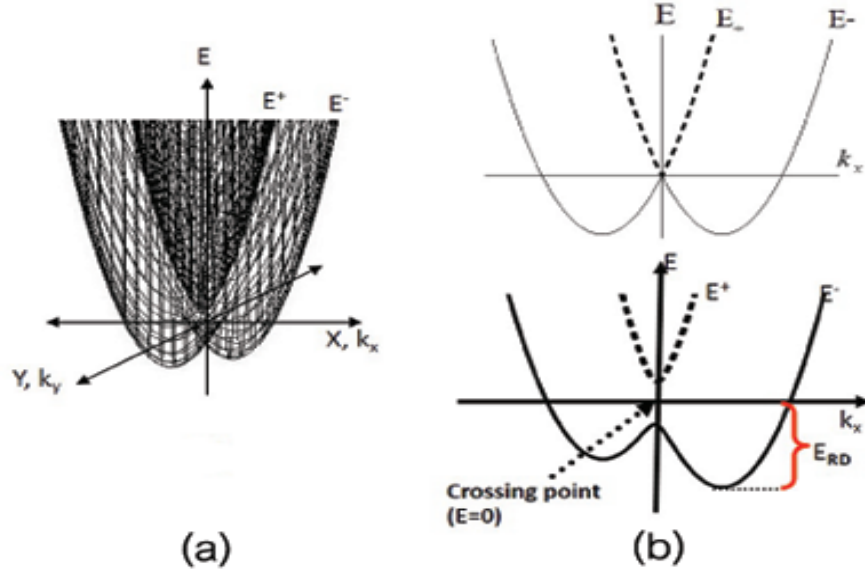


**Figure 1.8** (a) The band structure of an electron in a two-dimensional Rashba-Dresselhaus system. (b) The sketches of the energy spectrum as a function of  $k_x$  for zero (top) and nonzero (bottom)  $k_y$ . The dashed lines represent the energy spectrum of the electron with energy  $E^+$  and the solid lines represent energy spectrum of the electron with energy  $E^-$ .

rents in a mesoscopic ring (Maiti, 2011),  $k \cdot p$  calculation (Pfeffer and Zawadzki, 1999), and the spin-dependent photo current, electron spin resonance, weak antilocalization and time-resolved Kerr rotation (Nitta et al., 1997; Ganichev et al., 2004; Studer et al., 2009a; Studer et al., 2009b; Meier et al., 2007; Giglberger et al., 2007; Frolov et al., 2009; Knap et al., 1996). The typical ratio between Rashba and Dresselhaus spin-orbit constant ( $\alpha/\beta$ ) is about 1.5 – 7.6.

Many types of junctions involving the systems with either type of interaction also have been studied in order to find ways to control spin transport. For instance, in study of Rashba system/ferromagnetic metal junction, it was found that the spin injection across junction can be reduced or enhanced by RSOC (Jiang

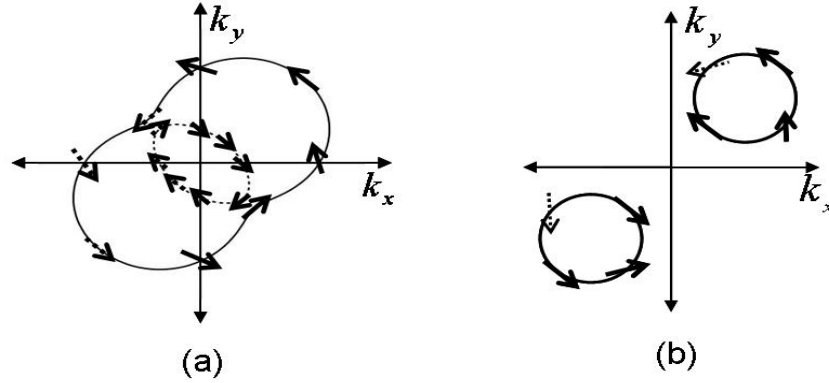


**Figure 1.9** The energy contours of an electron in a two-dimensional Rashba-Dresselhaus system (a) for  $E > 0$  and (b)  $E < 0$ . The dashed lines represent the energy contour of the electron with energy  $E^+$  and the solid lines represent energy contour of the electron with energy  $E^-$ . The arrows depict the spin direction of the electrons at the  $\vec{k}$  state on the contours.

and Jalil, 2003; Yokoyama et al., 2006). Also, in Rashba system/Superconductor junction, it was found that in the limit of low insulating barrier, the tunneling conductance was suppressed by the RSOC, where in the tunneling limit the RSOC can enhance the conductance (Sawa et al., 2007). Similar results can also be found in Dresselhaus system/Superconductor junction (Lee and Choi, 2005). Perel and co-worker (Perel et al., 2003) studied the electron tunneling through a symmetric semiconductor barrier, and found the polarization efficiency is increased with the strength of DSOC and the barrier width. Similarly, the overall conductance and the normalized spin polarization of conductance of Metal/Dresselhaus system junction can be enhanced by the spin-flip scattering from applying voltages below spin splitting energy (Srisongmuang and Kaoey, 2012). Jantayod (Jantayod, 2013) also found that the normalized spin polarization of current can be enhanced by increasing the carrier density and it weakly depends on the interfacial scattering.

There are also many other works that studied the tunneling properties in a junction, in which one or more materials containing both types of spin orbit coupling. For instance, it was found that the transmission probability, the transport normalized spin polarization and the conductance can be modulated by the Rashba and Dresselhaus strength as well as the strength of the interface barrier (Xiao and Deng, 2010; Xu and Guo, 2005; Lu and Li, 2010). More specifically, when the barrier strength is increased, there appear two resonant peaks in the electron transmission probability. However, the transmission probability is decreased to zero as the barrier is stronger. Linder and co-worker (Linder et al., 1997) proposed a method for generating pure spin current in Metal/2DEG with both types of the spin-orbit couplings, by rotating the spin polarizing of the incident current. They also found that the pure transverse spin current could be generated in the normal metal, when the incident current was completely unpolarized. Furthermore, the transverse charge current can be tuned by rotating the magnetization of the polarizing ferromagnet. Liang and co-worker (Liang et al., 2009) showed that one could control the normalized spin polarization direction of the spin current by tuning the ratio of the RSOC and DSOC strength.

The fact that both the energy contours and the spin states of the system with both types of spin-orbit couplings are not invariant with respect to the rotation about the  $z$  axis can also lead to many other interesting effects. For instance, Park and co-worker, found that the strength of spin orbit coupling parameters from the beat pattern in the Shubnikov-de Hass oscillations depends on the crystal direction (Park et al., 2013). In this thesis we will explore more on how this dependence on the crystallographic orientation will affect the particle and spin transport across the interface between a metal and the system with both types of the spin-orbit couplings. In particular, we will study the conductance, and



the normalized spin polarization of conductance, and the current flow along the interface plane.

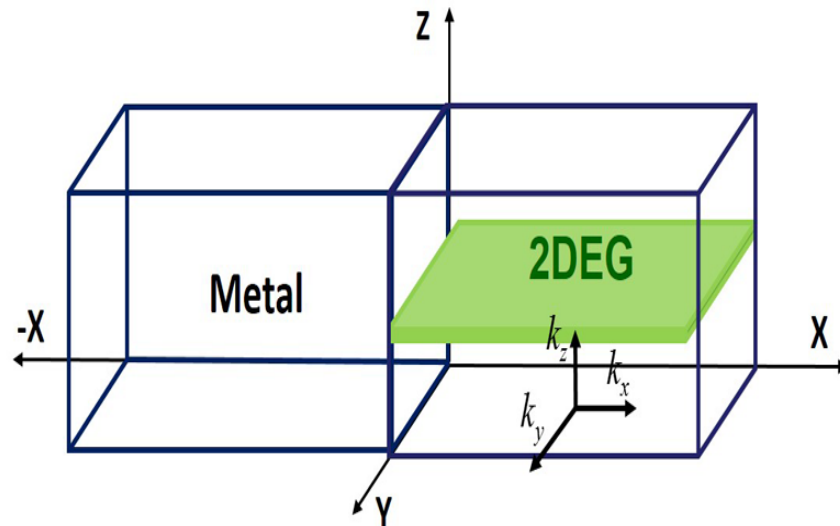


**Figure 1.10** Schematic diagram of the junction of the system considered in this thesis. A metal is in the  $x < 0$  region and the  $x > 0$  region is occupied by a 2DEG with spin-orbit coupling.

## 1.2 Research Procedure

We modeled our junction as a two-dimensional infinite system, in which a metal is in the  $x < 0$  region where in the  $x > 0$  region the media is occupied by a 2DEG with spin-orbit couplings, as shown in Figure 1.10. The effective mass model is used to describe the electronic properties of the system. A scattering method is used to study the particle and spin transport. Two types of junction are considered. The first one is the junction where the right side of which is the Dresselhaus system and the second one is the junction where the right side of which has both Rashba and Dresselhaus spin-orbit coupling. It is assumed that

the interface is smooth. The barrier at the interface is represented by a Dirac delta-function potential. From the Hamiltonian, the eigenstates and energy dispersion relation can be obtained. With appropriate eigenstates, the wave function for electrons in each region can be formed. It is a summation of incoming and outgoing states of the same energy and the momentum with the same component along the interface. The reflection and transmission amplitudes can be obtained by applying the matching conditions for the wave function at the interface. The matching conditions are the continuity of the wave function and the discontinuity of the slopes of the wave functions due to the Dirac delta-function potential and the spin-orbit interactions. The transmission and reflection probabilities can then be calculated and used to obtain conductance and the normalized spin polarization of conductance.

### 1.3 Outline of Thesis

The organization of this thesis is as follows.

The next chapter includes the study of a metal/Dresselhaus system junction. The electronic and spin properties of an electron in the Dresselhaus system will be described, and the calculation of the conductance spectrum and the normalized spin polarization of conductance will be shown. The effect of the crystal orientation of the Dresselhaus side, the DSOC strength, and the barrier strength will be considered.

In Chapter III, the conductance spectrum and the normalized spin polarization of conductance of the junction between metal and Rashba-Dresselhaus system will be presented. The effect of the crystal orientation of the Rashba-Dresselhaus system, the RDSOC strength, and the barrier strength will be considered. Finally, the conclusion of this work is given in Chapter IV.

# CHAPTER II

## TUNNELING BETWEEN A NORMAL METAL AND A 2DEG WITH ONLY DRESSELHAUS SPIN-ORBIT COUPLING

In this chapter, the particle and spin transport across the interface between a normal metal and a 2DEG with only DSOC (M/DS junction) are considered. The scattering method is used to obtain the conductance and the normalized spin polarization of conductance as a function of applied voltage. The effect of the crystallographic orientation of the 2DEG, the barrier strength, and the spin-orbit strength are considered. In the next section, the density of states (DOS) of a 2DEG with Dresselhaus spin-orbit coupling will be examined. In Section 2.2, the method to obtain the conductance and the spin-polarization of conductance will be presented. The numerical results and discussions will be in Section 2.3.

### 2.1 Density of States

The DOS of the electrons in a two-dimensional Dresselhaus system is

$$D(E) = \frac{2}{A} \sum_{\vec{k}} \delta(E - E_{\vec{k}}), \quad (2.1)$$

where  $A$  is the area of the system,  $\vec{k}$  is the wave vector of the electron, and the sum is overall possible values of  $\vec{k}$ . In our case  $E_{\vec{k}} = \frac{\hbar^2}{2m_D} (k^2 \pm 2\beta_0|k|)$  (see Figure 2.1) when  $\beta_0$  is the strength of Dresselhaus spin-orbit coupling . By changing the

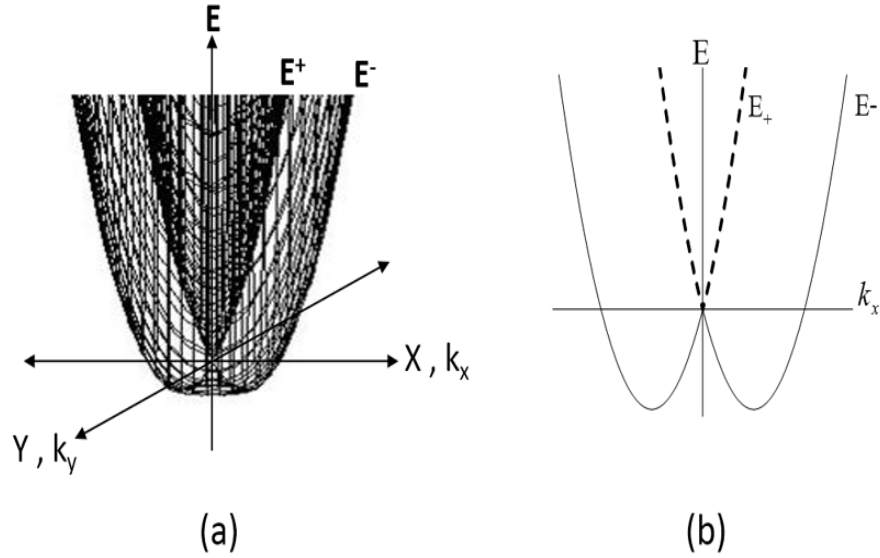


**Figure 2.1** (a) The energy spectrum of the electrons in a two-dimensional Dresselhaus system. (b) The sketches of the energy spectrum of the electron in Dresselhaus system as a function of  $k_x$ . Dashed lines represent the energy spectrum of the electron with energy  $E^+$  and solid lines represent energy spectrum of the electron with energy  $E^-$ .

summation to the integral, we obtain

$$D(E) = \frac{1}{\pi} \int_{-\infty}^{\infty} \delta(E - E_{\vec{k}}) k dk, \quad (2.2)$$

Changing the integration variable to  $E_{\vec{k}}$ , we have

$$D^{\pm}(E) = \frac{m_D}{\pi \hbar^2} \int_{-\frac{\hbar^2 \beta_0^2}{2m_D}}^{\infty} \delta(E - E_{\vec{k}}) \left( 1 \mp \frac{\beta_0}{\sqrt{\frac{2m_D E_{\vec{k}}}{\hbar^2} + \beta_0^2}} \right) dE_{\vec{k}}, \quad (2.3)$$

where upper and lower signs represent the DOS of electrons in the  $E^+$  and  $E^-$

branches. The DOS in  $E > 0$  region of each branches is then

$$D^\pm(E > 0) = \frac{m_D}{\pi\hbar^2} \left( 1 \mp \frac{\beta_0}{\sqrt{\frac{2m_D E_{\vec{k}}}{\hbar^2} + \beta_0^2}} \right), \quad (2.4)$$

and when the  $E < 0$  region, the DOS is

$$D^\pm(E < 0) = \frac{m_D}{\pi\hbar^2} \left( \mp 1 + \frac{\beta_0}{\sqrt{\frac{2m_D E_{\vec{k}}}{\hbar^2} + \beta_0^2}} \right) \quad (2.5)$$

The total DOS can be obtained from

$$D_{total}(E) = D^+(E) + D^-(E) \quad (2.6)$$

$$D_{total}(E) = \begin{cases} \frac{m_D}{\pi\hbar^2} \frac{\beta_0}{\sqrt{\frac{2m_D E}{\hbar^2} + \beta_0^2}}, & E < 0; \\ \frac{2m_D}{\pi\hbar^2}, & E > 0. \end{cases} \quad (2.7)$$

The DOS are plotted in Figure 2.2, where  $E_D = \frac{\hbar^2 \beta_0^2}{2m_D}$ . The dotted line represents the DOS of electron in the  $E^-$  branch, the dashed line for electron in the  $E^+$  branch and the solid line for the total DOS. In  $E < 0$  region, there is only  $E^-$  branch, the DOS has a singularity at  $E = -E_D$ . In  $E > 0$  region, both branches exist. The total DOS in  $E > 0$  region is constant due to the two-dimensionality of the system.

## 2.2 Model and Formalism

### 2.2.1 Basic Model

We modeled our junction (M/DS junction) as a two-dimensional infinite system, in which a normal metal is in  $x < 0$  and a 2DEG with DSOC is in  $x > 0$  as shown in Figure 2.3. It is assumed that the interface is smooth and the barrier at the interface is represented by a Dirac delta-function potential,  $H\delta(x)$  where

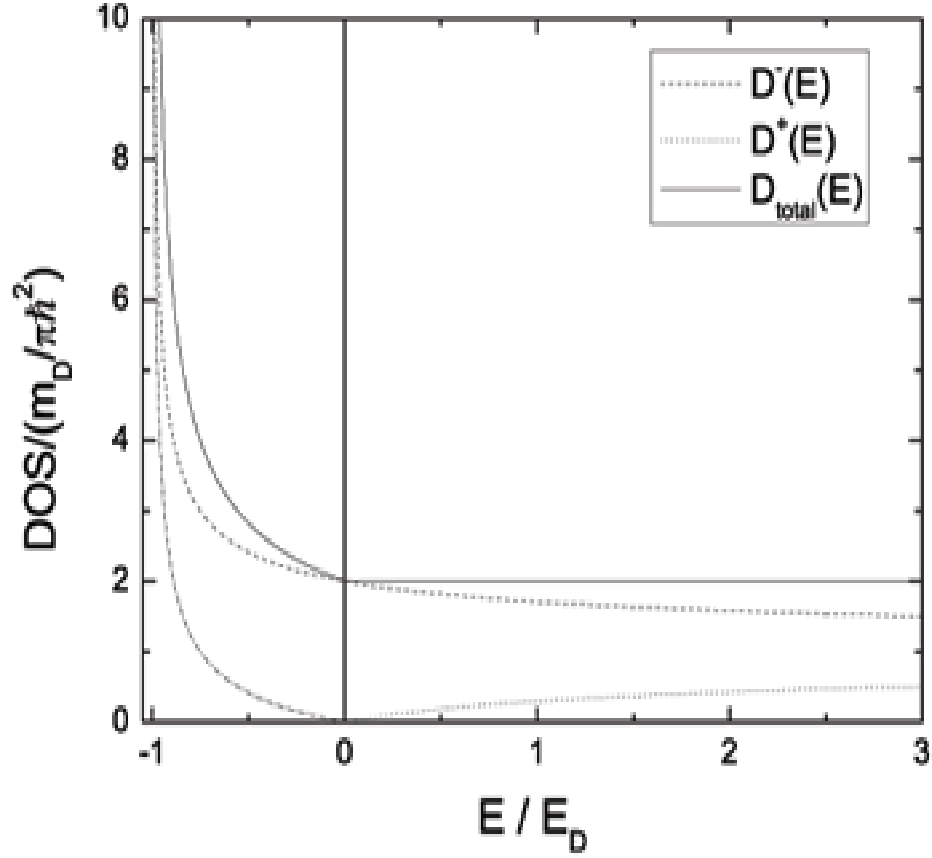


**Figure 2.2** The DOS of a 2DEG with Dresselhaus spin-orbit coupling. The dotted line represents the DOS of the electron in the  $E^-$  branch, the dashed line represents the electron in the  $E^+$  branch and solid line represents the total DOS.

$H$  is the scattering potential strength at the interface. The Hamiltonian of the electron in M/DS junction is written as

$$H(x) = \frac{\hat{p}^2}{2m(x)} - E_{FD}\Theta(x) - E_F\Theta(-x) + H\delta(x) + \frac{\hbar^2\beta_0\Theta(x)}{m_D}(\sigma_x(k_x \cos 2\theta + k_y \sin 2\theta) - \sigma_y(k_y \cos 2\theta - k_x \sin 2\theta)), \quad (2.8)$$

where  $\hat{p} = -i\hbar(\hat{x}\frac{\partial}{\partial x} + \hat{y}\frac{\partial}{\partial y})$  is the momentum operator, the effective mass  $m(x) = m_e\Theta(-x) + m_D\Theta(x)$  which is position dependent,  $m_e$  and  $m_D$  are the effective

electron mass in the metal and in Dresselhaus system, respectively,  $\Theta(x)$  is the Heaviside step function,  $\theta$  is the angle between the (100) crystal axis and the surface normal,  $E_F$  is the Fermi energy of the metal, and  $E_{FD}$  is the Fermi energy of the Dresselhaus system.

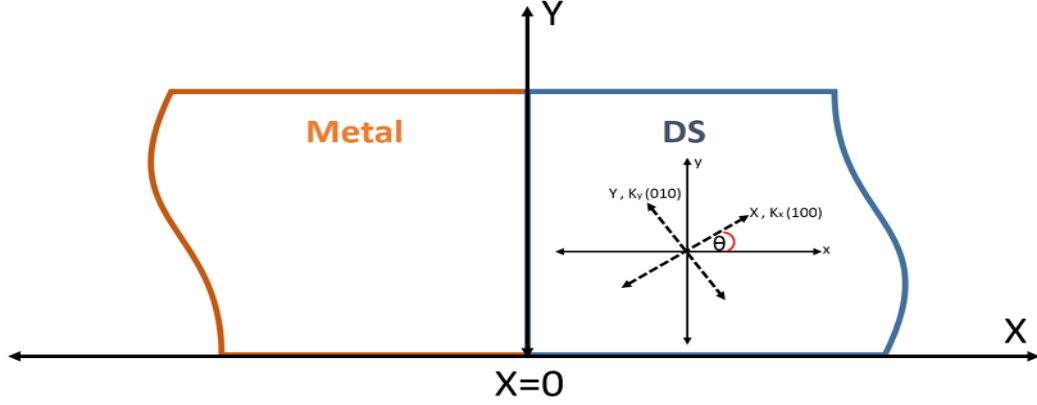


**Figure 2.3** A Metal/Dresselhaus system junction.

In the metal,  $x < 0$ , the energy dispersion relation for both spin-up and spin-down are equal to (see Figure 2.4)

$$E(q) = \frac{\hbar^2 q^2}{2m_e}, \quad (2.9)$$

where  $\vec{q}$  is the wave vector of electron in the metal,  $q = \sqrt{q_x^2 + q_y^2}$ . The eigenstates of electron with spin-up and spin-down are

$$|\uparrow\rangle = \frac{1}{\sqrt{2}} \begin{bmatrix} -i \\ 1 \end{bmatrix}, \quad (2.10)$$

and

$$|\downarrow\rangle = \frac{1}{\sqrt{2}} \begin{bmatrix} i \\ 1 \end{bmatrix}, \quad (2.11)$$

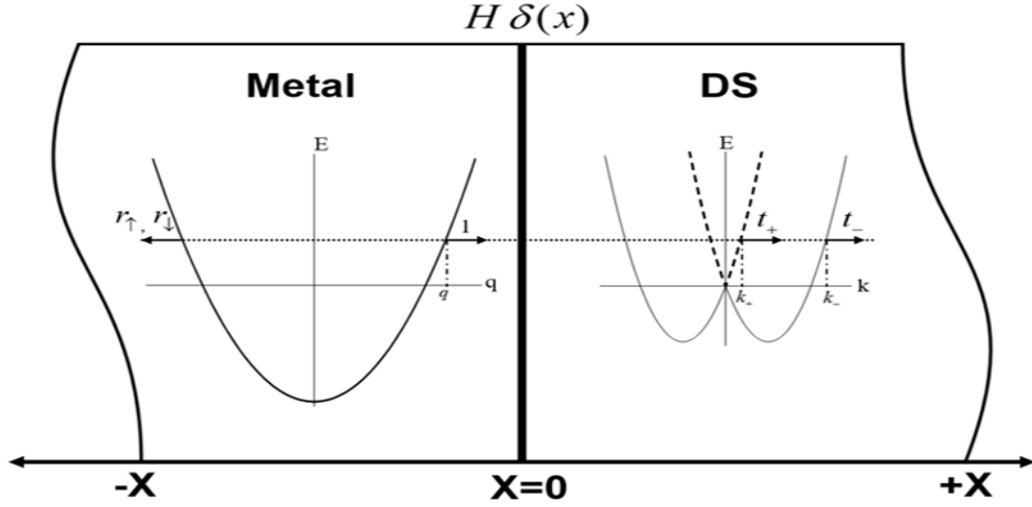


**Figure 2.4** The energy spectrum of the electrons in a metal (left) and the Dresselhaus system (right). The arrows pointing left or right, represent electron states that are considered in the scattering process. We assumed the incoming state is equal to 1,  $r_\uparrow$  and  $r_\downarrow$  are reflected states with spin-up and spin-down,  $t_+$  and  $t_-$  are outgoing states of the electron with  $E^+$  and  $E^-$ , respectively.

respectively, where the magnitude of the wave vector  $q_x$  as a function of energy is written as

$$q_x(E, q_y) = \sqrt{\frac{2m_e E}{\hbar^2} - q_y^2}, \quad (2.12)$$

In the Dresselhaus system,  $x > 0$ , the energy dispersion relation of Dresselhaus system is equal to (see Figure 2.4)

$$E^\pm(k_x, k_y) = \frac{\hbar^2}{2m_D} \left( (k_x^2 + k_y^2) \pm 2\beta_0 \sqrt{k_x^2 + k_y^2} \right), \quad (2.13)$$

where  $\vec{k} = (k_x, k_y)$  is the wave vector of electron in the Dresselhaus system. The



eigenstats of electron with  $E^+$  and  $E^-$  states are

$$|+\rangle = \frac{1}{\sqrt{2}} \begin{bmatrix} \frac{k_x^+ \cos 2\theta + k_y \sin 2\theta + i(k_y \cos 2\theta - k_x^+ \sin 2\theta)}{\sqrt{k_x^{+2} + k_y^2}} \\ 1 \end{bmatrix}, \quad (2.14)$$

and

$$|-\rangle = \frac{1}{\sqrt{2}} \begin{bmatrix} -\frac{k_x^- \cos 2\theta + k_y \sin 2\theta + i(k_y \cos 2\theta - k_x^- \sin 2\theta)}{\sqrt{k_x^{-2} + k_y^2}} \\ 1 \end{bmatrix}, \quad (2.15)$$

respectively, where the magnitude of the wave vector  $k_x$  as a function of energy ( $E$ ), and  $k_y$  is written as

$$k_x^\pm(E, k_y) = \pm \sqrt{\left( \sqrt{\frac{2m_D E}{\hbar^2} + \beta_0^2 \mp \beta_0} \right)^2 - k_y^2}. \quad (2.16)$$

## 2.2.2 The Wave Functions and Matching Conditions

We consider ballistic transport across the interface. Thus the wave function of the electron in metal side takes form

$$\begin{aligned} \Psi_M(q_x, q_y, x) = & \frac{1}{\sqrt{2}} \left( \begin{bmatrix} \pm i \\ 1 \end{bmatrix} e^{iq_x x} + r_\uparrow \begin{bmatrix} -i \\ 1 \end{bmatrix} e^{-iq_x x} \right. \\ & \left. + r_\downarrow \begin{bmatrix} i \\ 1 \end{bmatrix} e^{-iq_x x} \right) e^{iq_y y} \end{aligned} \quad (2.17)$$

where the  $\pm$  in the first term refer to the electron with spin-up (the spin state point to  $+y$  direction) and spin-down (the spin state point to  $-y$  direction) respectively. The first term represents the incoming state, the second and third terms are the reflecting state, where  $R_\uparrow$  and  $R_\downarrow$  are the reflection probability amplitude of electron with spin-up and spin-down respectively, and  $\vec{q} = (q_x, q_y)$  is the wave vectors of electron in the normal metal.

The wave function of electron with energy  $E$  in the two-dimensional Dresselhaus system can be written as

$$\begin{aligned} \Psi_D(k_x, k_y, \theta, x) = & \frac{1}{\sqrt{2}} \left( t_+ \begin{bmatrix} \varphi(k_x^+, k_y, \theta) \\ 1 \end{bmatrix} e^{ik_x^+ x} \right. \\ & \left. + t_- \begin{bmatrix} -\varphi(k_x^-, k_y, \theta) \\ 1 \end{bmatrix} e^{ik_x^- x} \right) e^{ik_y y} \end{aligned} \quad (2.18)$$

This wave function is the linear combination of two outgoing states of electron in the Dresselhaus system, where  $t_+$  and  $t_-$  are the transmission probability amplitudes of the electron with energy  $E_+$  and  $E_-$  respectively.

The appropriate matching conditions at the interface ( $x = 0$ ) of M/DS junction are the continuity of wave function and the discontinuity of slope of wave function at the interface:

$$\Psi_D|_{x=0^+} = \Psi_M|_{x=0^-}, \quad (2.19)$$

and

$$\frac{m_e}{m_D} \frac{\partial \Psi_D}{\partial x} \Big|_{x=0^+} - \frac{\partial \Psi_M}{\partial x} \Big|_{x=0^-} = (2q_F Z - i \frac{m_e}{m_D} \beta_0 (\sigma_x \cos 2\theta + \sigma_y \sin 2\theta)) \Psi_D|_{x=0^+}, \quad (2.20)$$

where  $Z = \frac{m_e H}{\hbar^2 q_F}$  is a dimensionless parameter of the strength of the barrier at the interface.

### 2.2.3 Conductance and Normalized Spin Polarization of Conductance

From the matching conditions to the suitable wave functions, we can calculate the reflection and transmission amplitudes and thus their associated prob-

abilities as

$$R_\sigma = |r_\sigma|^2, \quad (2.21)$$

$$T_+(E) = |t_+|^2 v_x^+, \quad (2.22)$$

$$T_-(E) = |t_-|^2 v_x^-, \quad (2.23)$$

where  $R_\sigma$  are the reflection probabilities of spin state  $\sigma$ , and  $T_+$ ,  $T_-$  are the corresponding transmission probability for the plus and minus branches, respectively.

The transmission probabilities for spin-up and spin-down are defined as

$$T_\uparrow(E) = |\langle \uparrow | t_+ \rangle|^2 v_x^+ + |\langle \uparrow | t_- \rangle|^2 v_x^-, \quad (2.24)$$

$$T_\downarrow(E) = |\langle \downarrow | t_+ \rangle|^2 v_x^+ + |\langle \downarrow | t_- \rangle|^2 v_x^-, \quad (2.25)$$

the group velocities of the electron are

$$v_x^\pm = \frac{m_e k_x^\pm}{m_D q_x} \left( 1 \pm \frac{\beta_0}{\sqrt{k_x^{\pm 2} + k_y^2}} \right). \quad (2.26)$$

The current density flows to the right is given by

$$J_x^e = \sum_k n_k v_{qx} e, \quad (2.27)$$

where  $n_k = \sum_{i=1}^2 (1 - R_{i\uparrow}(E_k) + R_{i\downarrow}(E_k)) f(E_k)$ ,  $i = 1, 2$  correspond to the spin orientation of the incident electron,  $f(E_k)$  is the Fermi Dirac distribution function,  $v_{qx}$  is the group velocity, and  $e$  is the electron charge. The electric current density flows across the junction when applied voltage  $V$  is written as

$$J_x^e(eV) = \sum_{k_x > 0, k_y} e v_x \sum_{i=1}^2 (1 - (R_{i\uparrow}(E_k) + R_{i\downarrow}(E_k))) (f(E_k - eV) - f(E_k)), \quad (2.28)$$

The tunneling conductance is

$$G(V) = \frac{dJ_x^e(eV)}{dV}, \quad (2.29)$$

and at zero temperature

$$G(V) = \frac{e^2}{h} \frac{Aq_F}{2\pi} \int_{k_{y,min}}^{k_{y,max}} (1 - R_{i\uparrow}(eV) + R_{i\downarrow}(eV)) dk_y. \quad (2.30)$$

The conductance spectrum of the electron with spin-up state can be obtained from

$$G_{\uparrow}(V) = \frac{e^2}{h} \frac{Aq_F}{2\pi} \int_{k_{y,min}}^{k_{y,max}} (1 - R_{i\uparrow}(eV) + R_{i\downarrow}(eV) - T_{i\downarrow}(eV)) dk_y, \quad (2.31)$$

and the conductance spectrum of the electron with spin-down state takes form

$$G_{\downarrow}(V) = \frac{e^2}{h} \frac{Aq_F}{2\pi} \int_{k_{y,min}}^{k_{y,max}} (1 - R_{i\uparrow}(eV) + R_{i\downarrow}(eV) - T_{i\uparrow}(eV)) dk_y. \quad (2.32)$$

We also define the total conductance  $G_{Total}$  as the summation of the conductance of electron with spin-up and spin-down, i.e.

$$G_{Total} = G_{\uparrow} + G_{\downarrow}. \quad (2.33)$$

The difference conductance  $\Delta G$  is the differentiation between the conductance of electron with spin-up and electron with spin-down, i.e.

$$\Delta G = G_{\uparrow} - G_{\downarrow}, \quad (2.34)$$

and the normalized spin polarization of conductance  $G_P$  is defined

$$G_P = \frac{\Delta G}{G_{Total}}. \quad (2.35)$$

### 2.3 Results and Discussions

We set the effective mass of the electron in Dresselhaus system;  $m_D = 0.05m_e$  through this section, and the dresselhaus spin-orbit coupling strength;  $\beta_0 = 0.025q_F$ . We calculate all of the conductance in the unit of  $\frac{e^2}{h} \frac{Aq_F}{2\pi}$ .

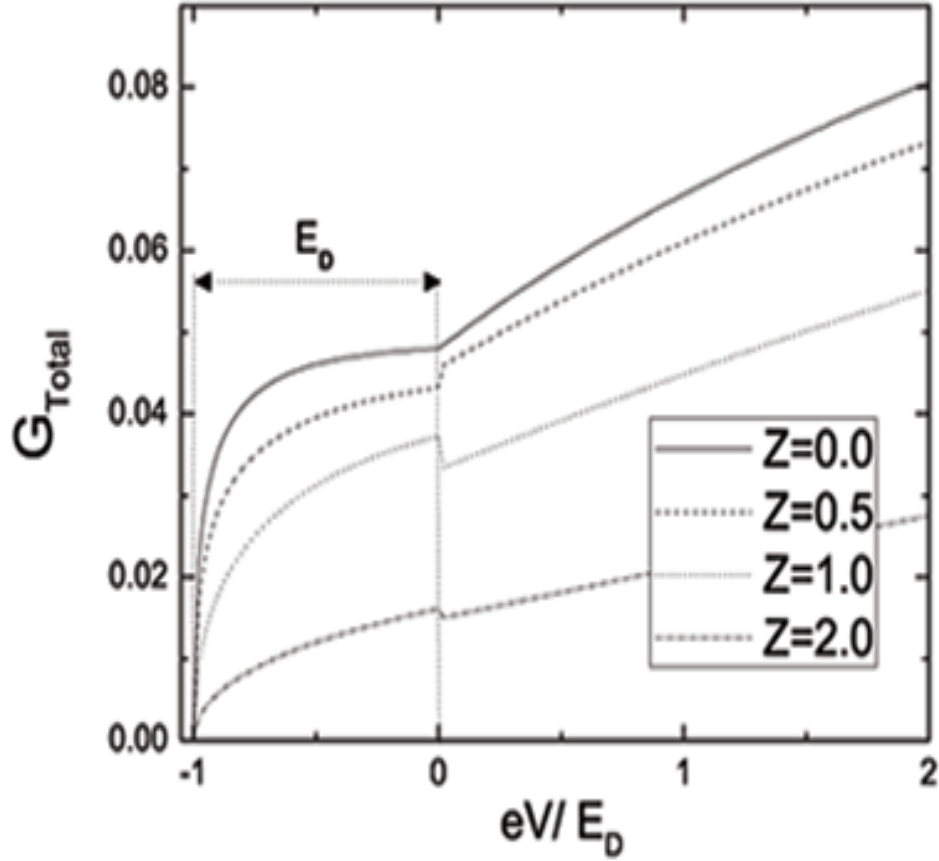


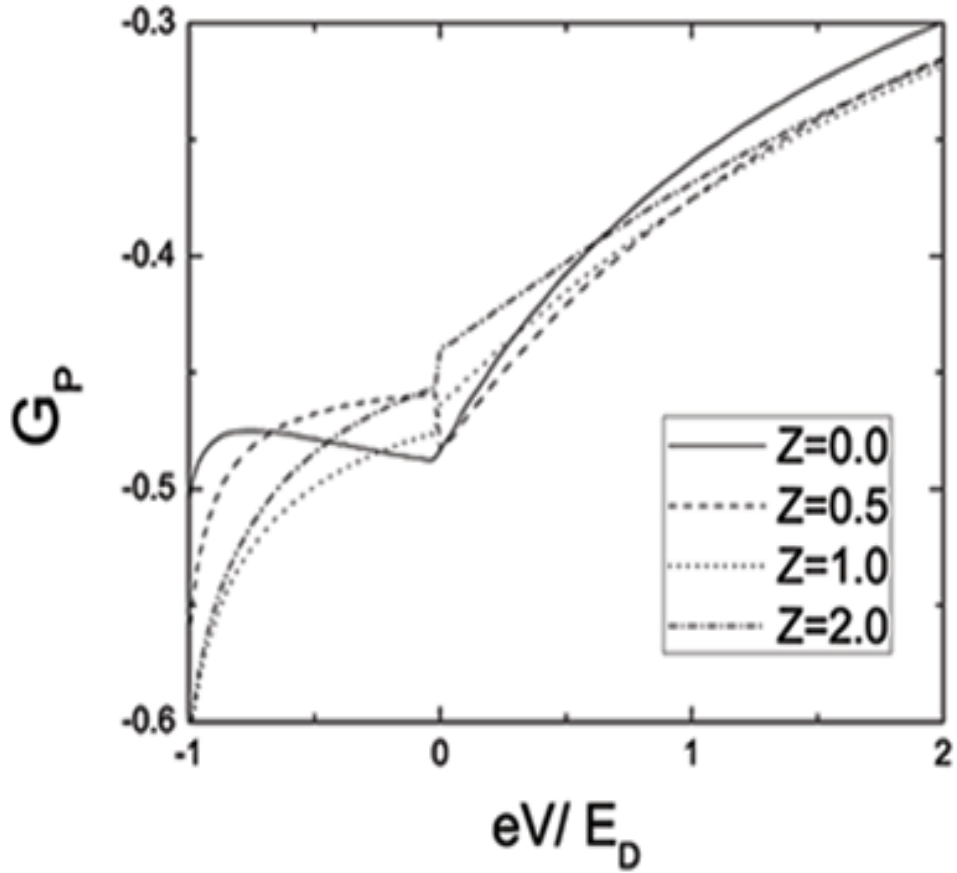
**Figure 2.5** The total conductance of the M/DS junction as a function of applied voltage ( $eV$ ) at various values of  $Z$ , where  $\beta_0 = 0.05 q_F$ ,  $m_D = 0.05 m_e$ ,  $Z = 0$ , and  $\theta = 0$ .

In Figure 2.5, the conductance spectra for  $\theta = 0$  for various values of  $Z$  are shown. There are two prominent features. The first one is at the bottom of the Dresselhaus band where the conductance spectrum value starts to be non-zero. The second one is at the voltage value is higher than the bottom of the Dres-

selhaus band by  $E_D = \frac{\hbar^2 \beta_0^2}{2m_D}$ . This two features are robust against the change in  $Z$ . This discontinuity in the slope of the conductance can be used to determine the Dresselhaus energy ( $E_D$ ), which measures from the energy scale between the beginning of the spectrum to the discontinuity point. However, as  $Z$  increases, the conductance decreases as expected (Srisongmuang and Kaoey, 2012). We also see that the total conductance gives the highest value when  $Z = 0$  and it decreases when  $Z$  increase. The total conductance shows step value at  $eV = 0$  with different patterns for nonzero of  $Z$ . For small  $Z = 0.5$ , the total conductance in  $eV < 0$  region is smaller than  $eV > 0$  region. The total conductance increases when applied more voltage. However, for a bigger  $Z$  ( $Z = 1, 2$ ) the total conductance in  $eV < 0$  region is higher than  $eV > 0$  region. We also found that at  $Z = 0.65$  is the first point that gives the total conductance in  $eV < 0$  region is higher than  $eV > 0$  region.

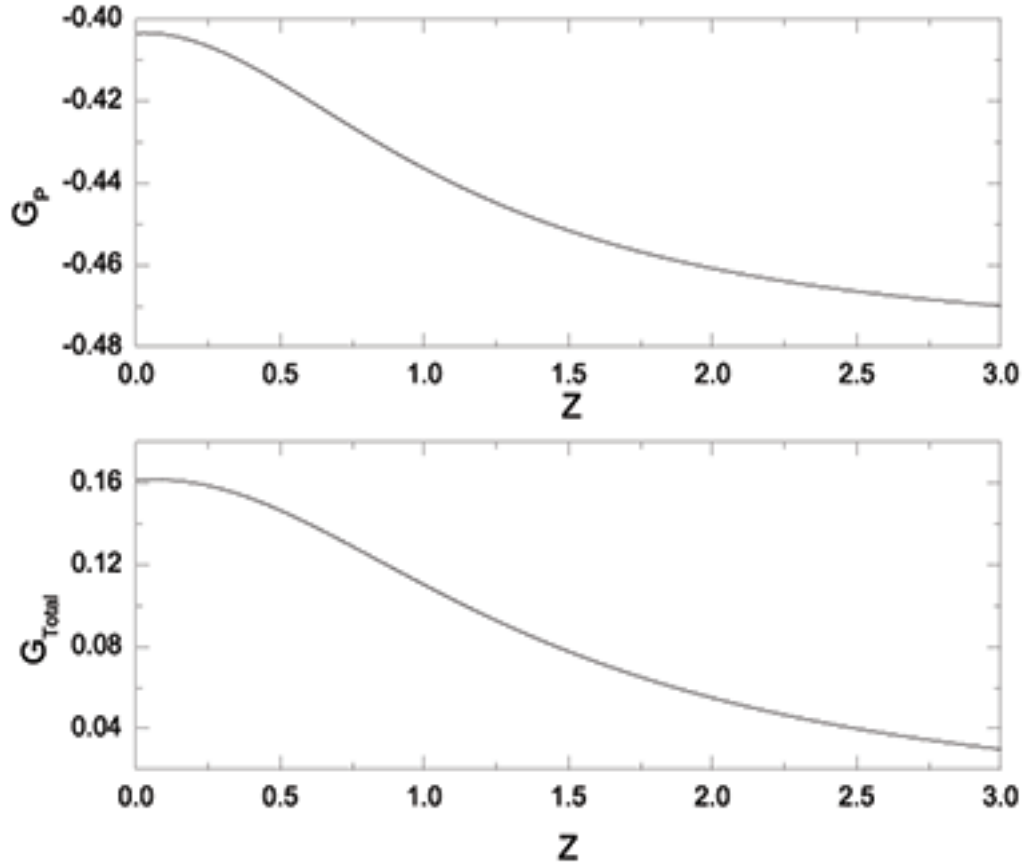
The magnitude of normalized spin polarization of conductance, decreases when the applied voltage increases. The normalized spin polarization of conductance is increased with the barrier strength as shown in Figure 2.6. There is a step at  $eV = 0$  similar to the total conductance spectra. For small  $Z$  ( $Z = 0, 0.5$ ), the normalized spin polarization of conductance in  $eV < 0$  region is smaller than  $eV > 0$  region, but for a bigger  $Z$  ( $Z = 1, 2$ ), the normalized spin polarization of conductance in  $eV < 0$  region is higher than  $eV > 0$  region.

Figure 2.7 shows the total conductance and the normalized spin polarization of conductance as a function of  $Z$ . The total conductance decrease when  $Z$  increases, but the normalized spin polarization conductance increase when  $Z$  increases. The optimum point which give maximum values of both total conductance and normalized spin polarization of conductance is between  $Z = 0.6$  and  $Z = 0.7$ .



**Figure 2.6** The normalized spin polarization of conductance of the M/DS junction as a function of applied voltage ( $eV$ ) at various values of  $Z$ , where  $\beta_0 = 0.05q_F$ ,  $m_D = 0.05m_e$ , and  $\theta = 0$ .

The plots of total conductance and normalized spin polarization of conductance of junction between a normal metal and a two-dimensional electron with only Dresselhaus spin-orbit coupling as a function of applied voltage ( $eV$ ) at various values of  $\theta$  shown in Figure 2.8 and Figure 2.9. The total conductance spectrum is invariant with the crystallographic orientation. However, the normalized spin polarization of conductance are strongly depend on the  $\theta$ . Especially, in the  $eV > 0$ , the magnitudes of normalized spin polarization of conductance are risen when  $\theta$  are considered, and decreased when  $eV$  is increases. The maximum values of the



**Figure 2.7** Plots of the total conductance and the normalized spin polarization of conductance as a function of  $Z$ , where  $m_D = 0.05 m_e$ ,  $\beta_0 = 0.05 q_F$ , and  $\theta = 0$ .

magnitudes of normalized spin polarization of conductance are occur at  $eV = 0$ . For  $eV < 0$ , the magnitudes of normalized spin polarization of conductance are risen when  $\theta$  are considered, and also increased when  $eV$  is increases. While  $\theta = 0$ , the magnitudes of normalized spin polarization of conductance is slightly increase with the applied voltage.

The plots of total conductance and normalized spin polarization of conductance of junction between a normal metal and a two-dimensional electron with only Dresselhaus spin-orbit coupling as a function of  $\beta_0$  at various values of  $\theta$  are shown in Figure 2.10 and Figure 2.11. The total conductance is increased with



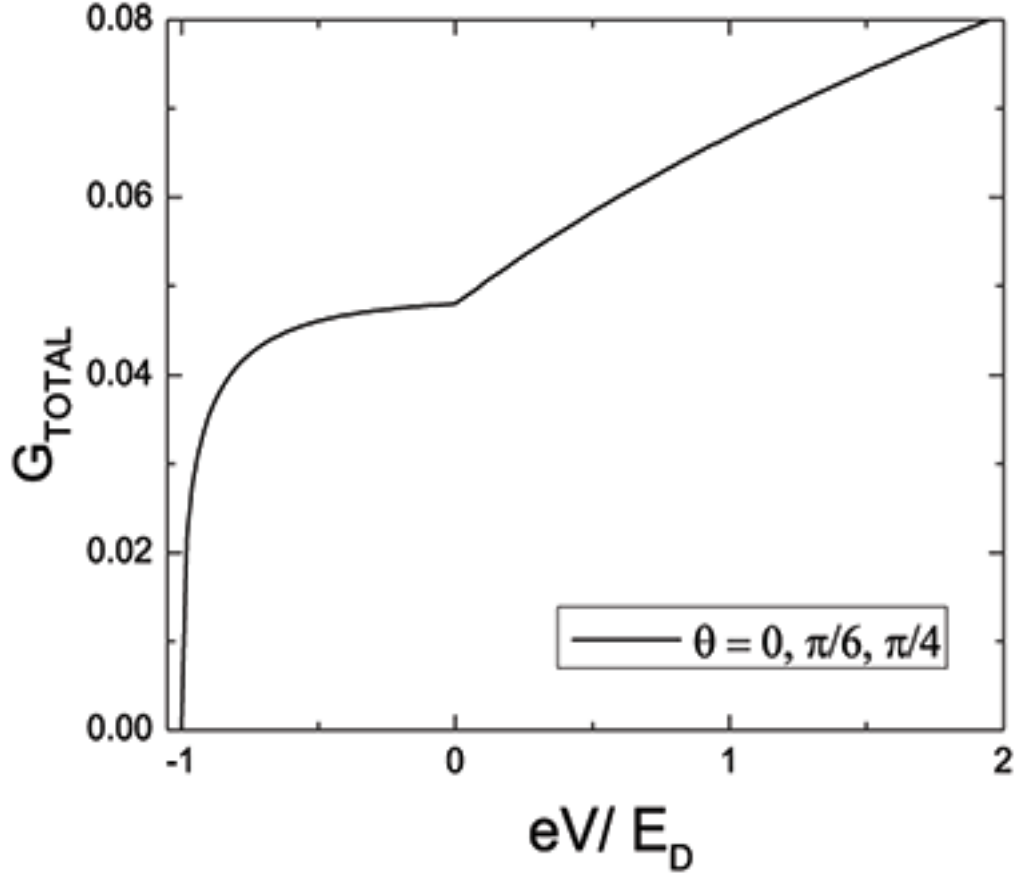


**Figure 2.8** The total conductance of the M/DS junction as a function of applied voltage ( $eV$ ) at various  $\theta$ , where  $\beta_0 = 0.05 q_F$ ,  $m_D = 0.05 m_e$ , and  $\theta = 0$ .

the Dresselhaus spin-orbit coupling strength.

The plot of the spin-polarization of conductance as a function of  $\beta$  for changes with  $\theta$ . When  $\theta = 0$ , it is zero. For nonzero  $\theta$ , the magnitudes of the normalized spin polarization of conductance are increased. The normalized spin-polarization of conductance is negative indicate that the numbers of electron with spin-up is fewer than that of electron with spin-down.

The normalized spin polarization of conductance changes with  $\theta$  and shows an oscillation with period of  $\pi$  rad. For  $eV > 0$ , the magnitude of the normalized spin polarization of conductance is a maximum, when the (100) crystal axis makes

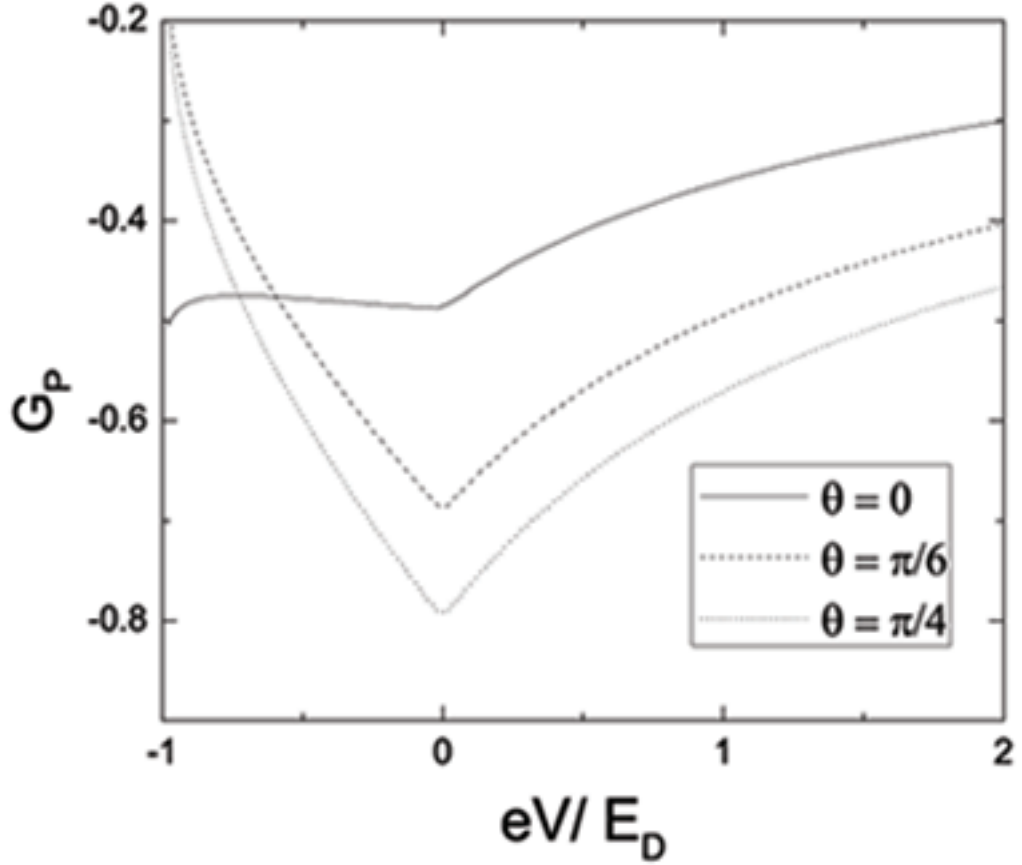


**Figure 2.9** The normalized spin polarization of conductance of the M/DS junction as a function of applied voltage ( $eV$ ) at various  $\theta$ , where  $\beta_0 = 0.05 q_F$ ,  $m_D = 0.05m_e$ , and  $Z = 0$ .

$\theta = \pm(2n + 1)\pi/4$  and is zero at  $\pm n\pi/2$  where  $n = 0, 1, 2, 3, \dots$ . For  $eV < 0$ , both of the maximum and zero values were not exactly at  $\theta = \pm(2n + 1)\pi/4$  and  $\pm n\pi/2$  (see Figure 2.12).

## 2.4 Conclusions

We calculated the total conductance and the normalized spin polarization of conductance across the junction between a normal metal and a 2DEG with only DSOC. We found that the total conductance and the normalized spin polarization

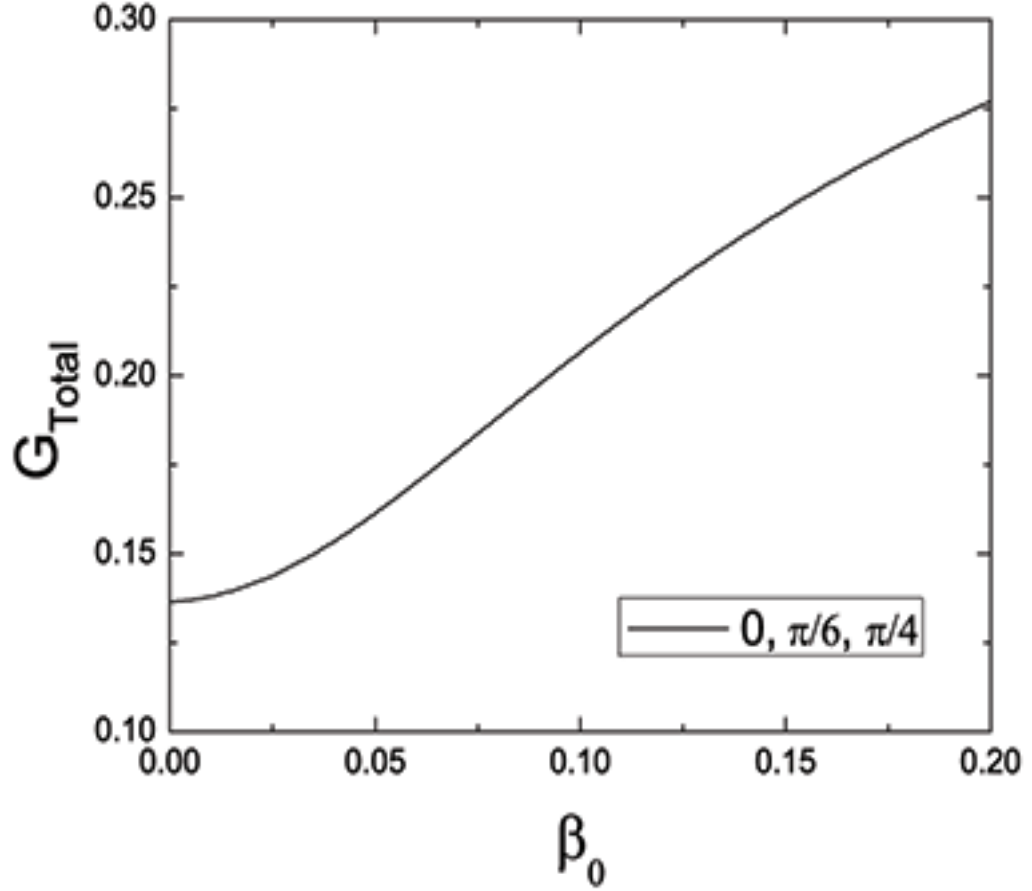


**Figure 2.10** The total conductance of the M/DS junction as a function of  $\beta_0$  at various applied voltages, where  $eV = E_D$ ,  $m_D = 0.05 m_e$ , and  $Z = 0$ .

of conductance can be enhanced by increasing the Dresselhaus strength, and can be suppressed by increasing the potential barrier strength. The Dresselhaus coupling energy can be determined from the beginning of the conductance spectra to the discontinuity point in the conductance spectra similar to (Srisongmuang and Kaoey, 2012).

The crystallographic orientation of the 2DEG, only offset the normalized spin polarization. Its magnitude oscillates with  $\theta$  in a period of  $\pi$ . The maximum magnitude occurs when the (100) crystal axis makes  $\theta = \pm(2n + 1)\pi/4$  with the interface normal, while the zero magnitude occurs when  $\theta = \pm n\pi/2$ , where  $n$  is a

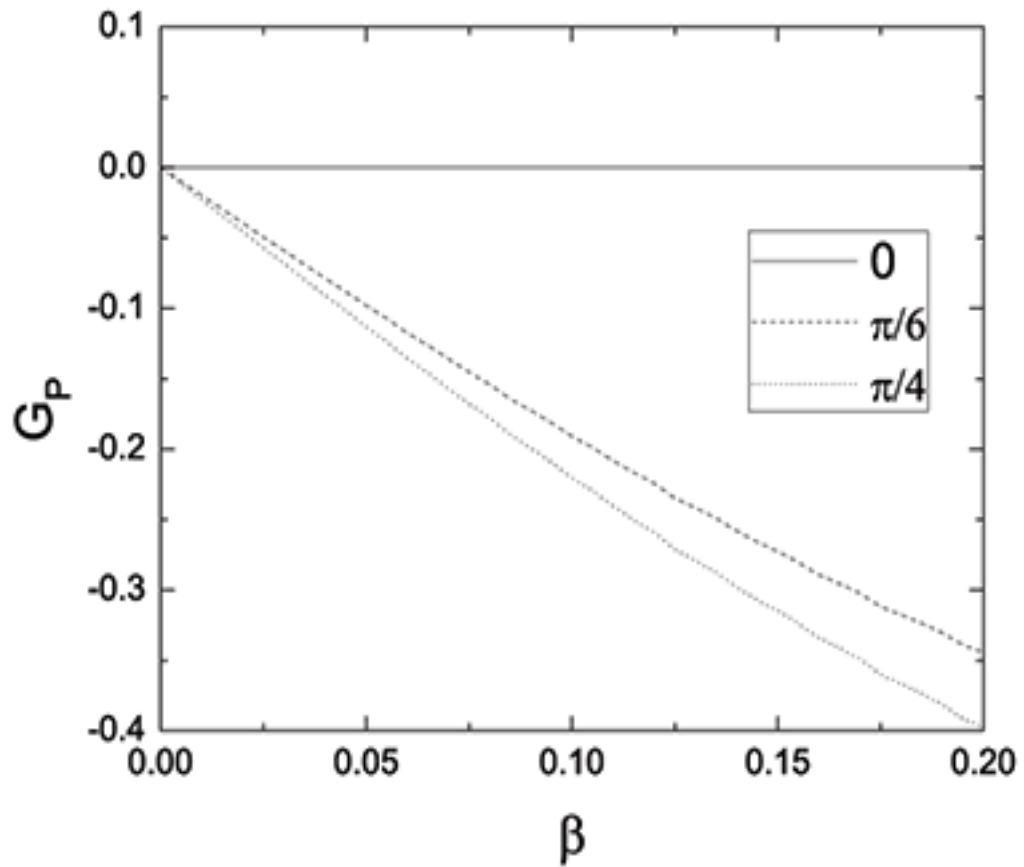


**Figure 2.11** The normalized spin polarization of conductance of the M/DS junction as a function of  $\beta_0$  at various applied voltages, where  $eV = E_D$ ,  $m_D = 0.05 m_e$ , and  $Z = 0$ .

non-negative integer.

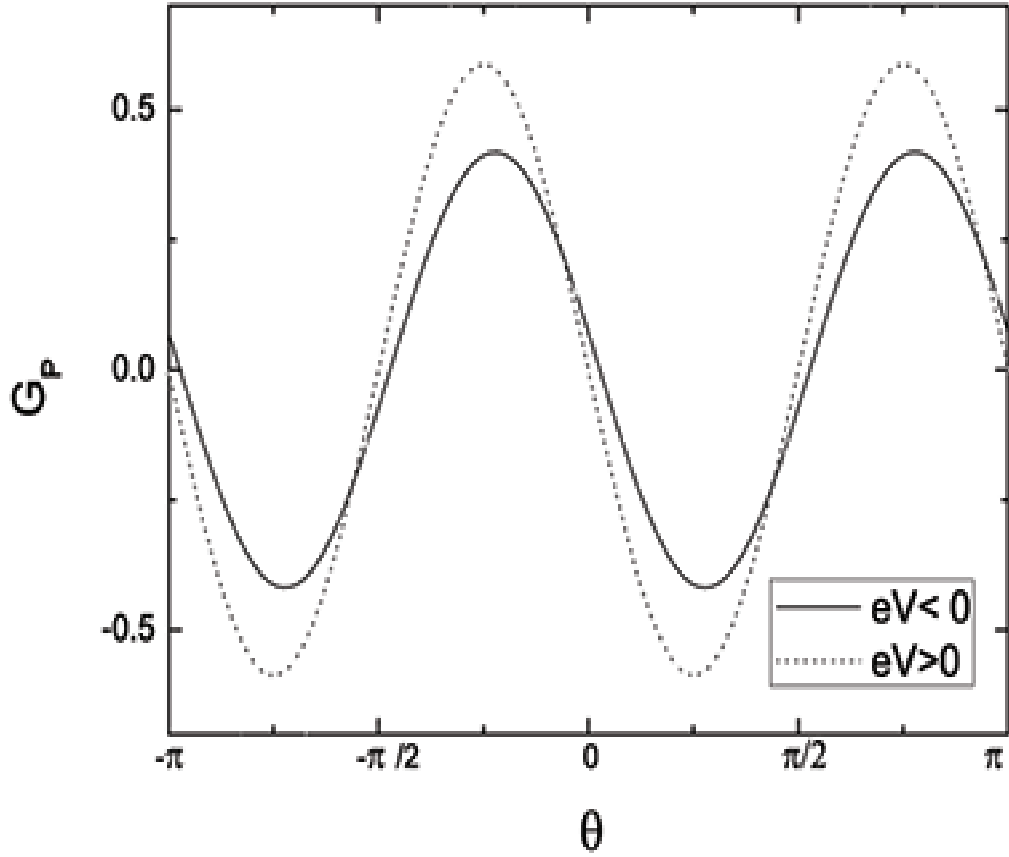


**Figure 2.12** The normalized spin polarization of conductance in the Metal/Dresselhaus system junction as a function of  $\theta$  at various applied voltages. where  $\beta_0 = 0.05 q_F$ ,  $m_D = 0.05 m_e$ , and  $Z = 0$ . The solid line shows  $G_P$  is in  $eV < 0$  region, and dashed line is in  $eV > 0$  region.

# CHAPTER III

## TUNNELING BETWEEN A NORMAL METAL AND A 2DEG WITH BOTH RASHBA AND DRESSELHAUS SPIN-ORBIT COUPLING

In this chapter, the particle and spin transport across the interface between a normal metal and a 2DEG with both types of spin-orbit couplings (M/RDS junction) are considered. Similar to the approach used in previous chapter, the scattering method is used to obtain the conductance and the normalized spin polarization of conductance as a function of applied voltage. In this chapter we will see the effect of the crystallographic orientation of the 2DEG on both conductance and normalized spin polarization of conductance. The effect of barrier strength and the spin-orbit strength are also considered. In the next section, the DOS of the electron in the 2DEG with both Rashba and Dresselhaus spin-orbit coupling (RDSOC) will be examined in Section 3.1. In Section 3.2, the approach used to obtain the conductance and the spin-polarization of conductance will be described in details. The numerical results and discussions will be in Section 3.3.

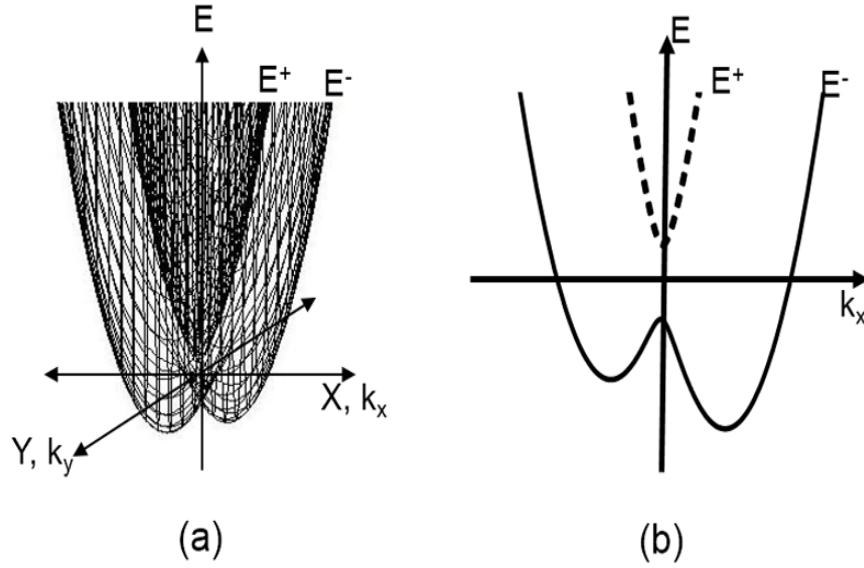


**Figure 3.1** (a) The energy spectrum of the electron in a two-dimensional Rashba-Dresselhaus system. (b) The sketches of the energy spectrum of the electron in Rashba-Dresselhaus system as a function of  $k_x$ . Dashed lines represent the energy spectrum of the electron with energy  $E^+$  and solid lines represent energy spectrum of the electron with energy  $E^-$ .

### 3.1 Density of States

The DOS of the electron in the Rashba-Dresselhaus system can be calculate from

$$D(E) = \frac{2}{A} \sum_{\vec{k}} \delta(E - E_{\vec{k}}), \quad (3.1)$$

where  $A$  is the area of the system,  $\vec{k}$  is the wave vector of the electron, the sum is over all possible values of  $\vec{k}$ , and  $E_{\vec{k}} = \frac{\hbar^2 k^2}{2m_{RD}} \pm \frac{\hbar^2}{m_{RD}} \sqrt{(\beta_0^2 + k_0^2)|k|^2 + 4\beta_0 k_0 k_x k_y}$  when  $\beta_0$  is the strength of Dresselhaus spin-orbit coupling, and  $k_0$  is the strength of Rashba spin-orbit coupling (see 3.1). By changing the summation to the integral

$$D(E) = \frac{1}{\pi} \int_{-\infty}^{\infty} \int_0^{\infty} \delta(E - E_{\vec{k}}) dk_x dk_y, \quad (3.2)$$

By changing the integration variable to  $E_{\vec{k}}$ , we obtain

$$D^{\pm}(E) = \frac{m_{RD}}{2\pi^2\hbar^2} \int_{-k_y}^{k_y} \int_{\epsilon}^{\infty} \frac{C^{\pm}(E)}{C(E^{\pm})k_x^{\pm} \pm ((\beta_0^2 + k_0^2)k_x^{\pm} + 2k_0k_y)} \delta(E - E_{\vec{k}}) dE_{\vec{k}} dk_y, \quad (3.3)$$

where  $\epsilon = -\frac{\hbar^2(\beta_0+k_0)^2}{2m_{RD}}$ ,

$$C^{\pm}(E) = \sqrt{(\beta_0^2 + k_0^2)(k_x^{\pm 2} + k_y^2) + 4\beta_0k_0k_x^{\pm}k_y}, \quad (3.4)$$

,  $\pm$  correspond to the  $E^+$  and  $E^-$  branches, respectively. From the calculation, the DOS of each branches are The total DOS can be obtained from

$$D_{total}(E) = D^+(E) + D^-(E) \quad (3.5)$$

$D_{total}(E)$ ,  $D^+(E)$ ,  $D^-(E)$  are plotted in Figure 3.2, where  $E_D = \frac{\hbar^2\beta_0^2}{2m_{RD}}$ . With  $m_{RD} = 0.05m_e$ ,  $\beta_0 = 0.025q_F$ , and  $k_0 = 0.05q_F$ , and  $E_{RD} = 9E_D$ . dotted line represents the DOS of electrons in the  $E^-$  branch, dashed line is  $E^+$  branch and the solid line is the total DOS. The DOS of the electrons in  $E^-$  branch becomes a singularities at  $-9E_D$  and  $-E_D$ , which are satisfied to the bottom and the saddle point of the band spectrum, respectively. Similarly, the DOS of the electrons in  $E^+$  branch starts at  $-E_D$ . For  $E > 0$ , the DOS is the usual 2DEG DOS.

## 3.2 Model and Formalism

### 3.2.1 Basic model

Similar to the previous junction in Chapter II, we modeled the M/RDS junction, as a two-dimensional infinite system, in which a normal metal is in  $x < 0$  and a 2DEG with RDSOC is in  $x > 0$  as shown in Figure 3.3. It is also assumed



that the interface is smooth and the barrier at the interface is represented by a Dirac delta-function potential,  $H\delta(x)$  where  $H$  is the scattering potential strength at the interface. Thus, the Hamiltonian of M/RDS junction is

$$H = \frac{\hat{p}^2}{2m(x)} + \frac{\hbar^2\beta_0}{m_{RD}}(\sigma_x(k_x \cos 2\theta + k_y \sin 2\theta) - \sigma_y(k_y \cos 2\theta - k_x \sin 2\theta)) + \frac{\hbar^2k_0}{m_{RD}}(\sigma_x k_y - \sigma_y k_x) - E_{FRD}(\Theta(x)) - E_F(\Theta(-x)) + H\delta(x), \quad (3.6)$$

where  $\hat{p} = -i\hbar(\hat{x}\frac{\partial}{\partial x} + \hat{y}\frac{\partial}{\partial y})$  is the momentum operator, the effective mass  $m(x) = m_e\Theta(-x) + m_{RD}\Theta(x)$ ,  $m_e$  and  $m_{RD}$  are the effective mass of an electron in the metal and in Rashba-Dresselhaus system, respectively,  $\Theta(x)$  is the Heaviside step function,  $\theta$  is the angle between the (100) crystal axis and the surface normal,  $E_F$  is the metal Fermi energy, and  $E_{FRD}$  is the Fermi energy of the Rashba-Dresselhaus system.

The energy dispersion relation of the electron in the metal is

$$E(q) = \frac{\hbar^2q^2}{2m_e}, \quad (3.7)$$

where  $\vec{q}$  is the wave vector of the electron in the metal,  $q = \sqrt{q_x^2 + q_y^2}$ . The eigenstates of electron with spin-up and spin-down are

$$|\uparrow\rangle = \frac{1}{\sqrt{2}} \begin{bmatrix} -i \\ 1 \end{bmatrix}, \quad (3.8)$$

and

$$|\downarrow\rangle = \frac{1}{\sqrt{2}} \begin{bmatrix} i \\ 1 \end{bmatrix}, \quad (3.9)$$

here the magnitude of the wave vector  $q_x$  as a function of energy is written as

$$q_x(E, q_y) = \sqrt{\frac{2m_e E}{\hbar^2} - q_y^2}, \quad (3.10)$$

For the electron in the Rashba-Dresselhaus system, the energy dispersion relation is equal to (see Figure 3.4)

$$E^\pm(k_x, k_y, \theta) = \frac{\hbar^2 k^2}{2m_{RD}} \pm \frac{\hbar^2}{m_{RD}} \sqrt{(\beta_0(k_x \cos 2\theta + k_y \sin 2\theta) + k_0 k_y)^2 + (\beta_0(k_y \cos 2\theta - k_x \sin 2\theta) + k_0 k_x)^2}, \quad (3.11)$$

where  $\vec{k} = (k_x, k_y)$  is the wave vector of the electron in the Rashba-Dresselhaus system. The eigenstates of the electrons with  $E^+$  and  $E^-$  states are

$$|+\rangle = \frac{1}{\sqrt{2}} \begin{bmatrix} \varphi(k_x^+, k_y, \theta) \\ 1 \end{bmatrix}, \quad (3.12)$$

and

$$|-\rangle = \frac{1}{\sqrt{2}} \begin{bmatrix} -\varphi(k_x^-, k_y, \theta) \\ 1 \end{bmatrix}, \quad (3.13)$$

where

$$\varphi(k_x^\pm, k_y, \theta) = \frac{(\beta_0(k_x^\pm \cos 2\theta + k_y \sin 2\theta) + k_0 k_y) + i(\beta_0 \kappa + k_0 k_x^\pm)}{\sqrt{(\beta_0(k_x^\pm \cos 2\theta + k_y \sin 2\theta) + k_0 k_y)^2 + (\beta_0 \kappa + k_0 k_x^\pm)^2}},$$

and  $\kappa = (k_y \cos 2\theta - k_x^\pm \sin 2\theta)$ .

The magnitude of the wave vector  $k_x$  as a function of  $E$ ,  $\theta$ , and  $k_y$  can be obtain from equation 3.11.

### 3.2.2 The Wave Functions and Matching Conditions

We consider ballistic transport across the interface; Thus, the wave function of the electron in the metal side takes the form

$$\begin{aligned} \Psi_M(q_x, q_y, x) = & \frac{1}{\sqrt{2}} \left( \begin{bmatrix} \pm i \\ 1 \end{bmatrix} e^{iq_x x} + r_{\uparrow} \begin{bmatrix} -i \\ 1 \end{bmatrix} e^{-iq_x x} \right. \\ & \left. + r_{\downarrow} \begin{bmatrix} i \\ 1 \end{bmatrix} e^{-iq_x x} \right) e^{iq_y y} \end{aligned} \quad (3.14)$$

where  $+$  and  $-$  are for the cases of the electron with spin-up (the spin state point to  $+y$  direction) and spin-down (the spin state point to  $-y$  direction), respectively. The wave function of the electron in the metal side is this a linear combination of an incoming and two reflecting eigenstates of the electron.  $r_{\uparrow}$  and  $r_{\downarrow}$  are the reflection probability amplitude of the spin-up and spin-down states, respectively.

The wave function of the electron in the Rashba-Dresselhaus system is a linear combination of two transmitted eigenstates:

$$\begin{aligned} \Psi_{RD}(k_x^+, k_y, \theta) = & \frac{1}{\sqrt{2}} \left( t_+ \begin{bmatrix} \varphi(k_x^+, k_y, \theta) \\ 1 \end{bmatrix} e^{ik_x^+} \right. \\ & \left. + t_- \begin{bmatrix} -\varphi(k_x^-, k_y, \theta) \\ 1 \end{bmatrix} e^{ik_x^-} \right) e^{ik_y y} \end{aligned} \quad (3.15)$$

$t_+$  and  $t_-$  are the transmission probability amplitudes of the electron in the  $E_+$  and  $E_-$  energy states, respectively.

The appropriated matching conditions at the interface for the two wave functions are the continuity and the discontinuity of slope of wave function. This

can be written as

$$\Psi_{RD}|_{x=0^+} = \Psi_M|_{x=0^-}, \quad (3.16)$$

and

$$\begin{aligned} & \frac{m_e}{m_{RD}} \frac{\partial \Psi_{RD}}{\partial x} \Big|_{x=0^+} - \frac{\partial \Psi_M}{\partial x} \Big|_{x=0^-} = \\ & \left( 2q_F - i \frac{m_e}{m_{RD}} (\sigma_x \beta_0 \cos 2\theta - \sigma_y (k_0 - \beta_0 \sin 2\theta)) \right) \Psi_{RD}|_{x=0^+}, \end{aligned} \quad (3.17)$$

where  $Z = \frac{m_e H}{\hbar^2 q_F}$  is a dimensionless parameter of the strength of the barrier at the interface.

### 3.2.3 Conductance and Normalized Spin Polarization of Conductance

By applying the appropriated matching, we will obtain the reflection and transmission amplitude and the corresponding probability can be obtained from

$$R_\sigma = |r_\sigma|^2, \quad (3.18)$$

$$T_+ = |t_+|^2 v_{qx}^+, \quad (3.19)$$

$$T_- = |t_-|^2 v_{qx}^-, \quad (3.20)$$

where

$$\begin{aligned} v_{qx}^\pm = & \frac{m_e}{m_{RD} q_x} \left( k_x^\pm \right. \\ & + \frac{\beta_0 \cos 2\theta (\beta_0 (k_x^\pm \cos 2\theta + k_y \sin 2\theta) + k_0 k_y)}{\sqrt{(\beta_0 (k_x^\pm \cos 2\theta + k_y \sin 2\theta) + k_0 k_y)^2 + (\beta_0 (k_y \cos 2\theta - k_x^\pm \sin 2\theta) + k_0 k_x^\pm)^2}} \\ & \left. + \frac{(k_0 - \beta_0 \sin 2\theta) (\beta_0 (k_y \cos 2\theta - k_x^\pm \sin 2\theta) + k_0 k_x^\pm)}{\sqrt{(\beta_0 (k_x^\pm \cos 2\theta + k_y \sin 2\theta) + k_0 k_y)^2 + (\beta_0 (k_y \cos 2\theta - k_x^\pm \sin 2\theta) + k_0 k_x^\pm)^2}} \right), \end{aligned} \quad (3.21)$$

$R_\sigma$  are the reflection probabilities of spin  $\sigma$  state, and  $T_+$ ,  $T_-$  are the corresponding transmission amplitudes for the plus and minus branches. We can also obtain the transmission probabilities for spin-up and spin-down states from

$$T_\uparrow = |\langle \uparrow | t_+ \rangle|^2 v_{qx}^+ + |\langle \uparrow | t_- \rangle|^2 v_{qx}^-, \quad (3.22)$$

$$T_\downarrow = |\langle \downarrow | t_+ \rangle|^2 v_{qx}^+ + |\langle \downarrow | t_- \rangle|^2 v_{qx}^-, \quad (3.23)$$

In the two-dimensional system, the electric current density flows across the junction when applied voltage is given as

$$J_x^e(eV) = \sum_{k_x > 0, k_y} e v_{qx} \sum_{i=1}^2 ((1 - R_{i\uparrow}(E_k) + R_{i\downarrow}(E_k))(f(E - eV) - f(E_k))), \quad (3.24)$$

which the electric current density flowing parallel to the junction under applied voltage can be written as

$$J_y^e(eV) = \sum_{k_x > 0, k_y} e v_{qy} \sum_{i=1}^2 (1 - R_{i\uparrow}(E_k) + R_{i\downarrow}(E_k))(f(E - eV) - f(E_k)), \quad (3.25)$$

where  $v_{qy} = v_{qx} \frac{\partial k_x}{k_y}$  is the group velocities in  $y$  direction. The tunneling conductance for the current density flowing parallel to and perpendicular to the junction normal are defined as

$$G_{xx}(V) = \frac{dJ_x^e(eV)}{dV}, \quad (3.26)$$

and

$$G_{xy}(V) = \frac{dJ_y^e(eV)}{dV}, \quad (3.27)$$

respectively. The total conductance spectrum of the electron can be obtained from

$$G(V) = \frac{e^2 A q_F}{h 2\pi} \int_{k_{y,min}}^{k_{y,max}} dk_y (1 - R_{i\uparrow}(eV) + R_{i\downarrow}(eV)) \quad (3.28)$$

The conductance spectrum of the electron with spin-up state can be obtained from

$$G_{\uparrow}(V) = \frac{e^2}{h} \frac{Aq_F}{2\pi} \int_{k_{y,min}}^{k_{y,max}} (1 - R_{i\uparrow}(eV) + R_{i\downarrow}(eV) - T_{i\downarrow}(eV)) dk_y, \quad (3.29)$$

and the conductance spectrum of the electron with spin-down state takes the form

$$G_{\downarrow}(V) = \frac{e^2}{h} \frac{Aq_F}{2\pi} \int_{k_{y,min}}^{k_{y,max}} (1 - R_{i\uparrow}(eV) + R_{i\downarrow}(eV) - T_{i\uparrow}(eV)) dk_y \quad (3.30)$$

We also defined the total conductance;  $G_{Total}$  is the summation of the conductance of electron with spin-up and electron with spin-down

$$G_{Total} = G_{\uparrow} + G_{\downarrow}. \quad (3.31)$$

For the different conductance,  $\Delta G$  is the differentiation between the conductance of electron with spin-up and electron with spin-down is defined from

$$\Delta G = G_{\uparrow} - G_{\downarrow}, \quad (3.32)$$

and the normalized spin polarization of conductance ;  $G_P$  is given by

$$G_P = \frac{\Delta G}{G_{Total}} \quad (3.33)$$

### 3.3 Results and Discussions

We studied the transport properties of the electron in metal/Rashba-Dresselhaus system junction. We set the effective mass of electron in Rashba-Dresselhaus system;  $m_{RD} = 0.05m_e$  through this section, and setting parameters as  $\beta_0 = 0.025q_F$ , and  $k_0 = 0.05q_F$  which makes  $E_{RD} = 9E_D$ . The conductance is in units of  $\frac{e^2}{h} \frac{Aq_F}{2\pi}$ . Firstly, we show the results  $\theta = \pm\pi/4$  rad, because these two cases possess the energy contours such that  $E(-k_x, k_y) = E(k_x, k_y)$  and  $E(k_x, -k_y) = E(k_x, k_y)$ .

Figure 3.5 shows the conductance spectrum for the junction when  $\theta = -\pi/4$  at various values of  $Z$ . As can be seen in the spectrum, there are three prominent features. The first one is at the bottom of the Rashba-Dresselhaus system band where the conductance value starts to be non zero. The second one is at the voltage value higher than the bottom of the Rashba-Dresselhaus system band by  $E_{RD} - E_{\Delta}$ , and the third one is at the voltage value being equal to zero. These can be used to determine the Rashba-Dresselhaus energy ( $E_{RD}$ ). It can also determine the  $E_{\Delta} = \frac{\hbar^2(k_0 - \beta_0)^2}{2m_{RD}}$  which is measured from the energy scale between the second and the third points of the prominent features.  $E_{\Delta}$  satisfied the different between the two spin-orbit strengths. These three features are robust against the change in  $Z$ .

The normalized spin polarization of conductance on the other hand, generally increases when  $Z$  increases. More specially, for  $eV < 0$ , the normalized spin polarization conductance is hardly change with  $Z$  as shown in Figure 3.6. Figure 3.7 shows both the total conductance and the normalized spin polarization of conductance as a function of  $Z$ . The optimum point which give high values of both total conductance and normalized spin polarization of conductance is between  $Z = 0.6$  and  $Z = 0.7$ .

We now plot the total conductance spectrum ( $G_{Total}$ ) as a function of applied voltage at various  $\theta$  when  $Z = 0$ . We show the conductance spectrum when  $\theta = 0, \pm\pi/4$ , the total conductance spectrum is dependence with  $\theta$ , which is different from the previous junction. When we rotate the crystallographic of the 2DEG, the energy contour of the system is changed so the total conductance spectrum is dependence with  $\theta$ . Moreover, these prominent features in the spectrum are robust against the change in  $\theta$  as shown in Figure 3.8. In addition, when we rotate the crystallographic of the 2DEG, the spin state of the electron of the system is also

changed, the normalized spin polarization of conductance depends on  $\theta$  as well as shown in Figure 3.9.

When consider the effect of the strength of Rashba spin-orbit coupling, we fix the strength of Dresselhaus spin orbit coupling equal to  $0.025q_F$ , and  $Z = 0$ . As we can see in the Figure 3.10, when  $k_0 = 0$  that is mean in this junction has only Dresselhaus spin-orbit coupling. They show similarly results being satisfied to the junction of metal and Dresselhaus system. The total conductance spectrum gives the same values for various  $\theta$  (at  $k_0 = 0$ ). Furthermore, the total conductance increases with increasing of the strength of the Rashba spin-orbit coupling, until the strength reaches to a critical value, after which the conductance spectrum decreases. In addition, the normalized spin polarization of conductance increases when the strength of the Rashba spin-orbit coupling increases as shown in Figure 3.11. Both of the total conductance and the normalized spin polarization of conductance also show the strange feature when  $\beta_0 = k_0$ .

The calculation of the conductance spectrum as a function of  $\theta$  at various values of applied voltage are shown in Figure 3.12. We set some parameters as  $Z = 0.5$ ,  $\beta_0 = 0.025q_F$ , and  $k_0 = 0.05q_F$ . In calculation processing, we vary in some angle which are  $\theta = 0, \pm\frac{\pi}{6}, \pm\frac{\pi}{4}, \pm\frac{\pi}{3},$  and  $\pm\frac{\pi}{2}$ . As we can see, in  $eV > 0$  region the conductance spectrum show an oscillation feature with period  $\pi$  rad which satisfies to the expression that is a function of  $2\theta$ . The conductance spectrum has a maximum value, when rotate the (100) crystal axis makes  $\theta = (2n + 1)\pi/4$  and minimum value at  $\theta = -(2n + 1)\pi/4$ , where  $n = 0, 1, 2, 3, \dots$ . In  $eV > 0$  region, the total conductance spectrum is slightly changed with the crystallographic orientation.

Figure 3.13 is the plot of the normalized spin polarization of conductance as a function of  $\theta$  at various values of applied voltage. Both of  $eV < 0$  and



$eV > 0$  regions, show an oscillation feature with period  $\pi$  rad. In contrast, the total conductance spectrum, in  $eV > 0$  region, the normalized spin polarization of conductance spectrum has a maximum value, when rotate the (100) crystal axis makes  $\theta = -(2n + 1)\pi/4$  and minimum value at  $\theta = (2n + 1)\pi/4$ . However in  $eV < 0$  region, it has a maximum value, when rotate the (100) crystal axis makes  $\theta = (2n + 1)\pi/4$  and minimum value at  $\theta = -(2n + 1)\pi/4$ .

Finally, we also calculate the conductance of the electrons which move parallel to the junction ( $G_{Total,XY}$ ). We found that there are not only the tunneling conductance in  $x$  axis but in some angle of the crystal rotation also generate the tunneling conductance in  $y$  direction. As shown in Figure 3.14 when  $\theta = 0$  and the applied voltage less than zero, the conductance spectra shows the negative values that is mean the conductance of the electrons which move along  $-y$  direction is more than the electrons move along  $+y$  direction. The conductance spectra gives the maximum value when  $eV = 0$ , and decreases when the applied voltage increases. But when  $\theta = \pi/4$ , there is no total conductance because of the energy contour of this case is symmetry around  $k_x$ . This means that there are the same value of group velocity of the electron but it is different in  $+y$  and  $-y$  direction, so the total conductance is becomes to zero.

### 3.4 Conclusions

In this chapter is the studied of a normal metal/Rashba-Dresselhaus system junction. We use a so-called scattering method to calculate the conductance spectra and the normalized spin polarization of conductance in the junction.

We found the total conductance spectra shows two distinctive features. From the positions of these existing features, the Rashba and Dresselhaus couples energy can be determined the Rashba-Dresselhaus energy and  $E_{\Delta}$ . The Rashba-

Dresselhaus energy can be determined from the beginning of the spectra to the second discontinuity point, which relate to the sum of two spin-orbit coupling strength.  $E_{\Delta}$  can be determined by the different scale between two discontinuity points, which relate to the different value between two spin-orbit coupling strength. And the total conductance spectrum is increased with the strength of the Rashba spin-orbit coupling, until the strength reaches to a critical value, after which the conductance spectrum is decreased with the strength.

Both of the conductance spectrum and the normalized spin polarization of conductance, show an oscillation features with period  $\pi$  rad. The conductance spectrum has a maximum value, when rotate the (100) crystal axis makes  $\theta = (2n + 1)\pi/4$  and minimum value at  $\theta = -(2n + 1)\pi/4$ , where  $n = 0, 1, 2, 3, \dots$ . In the other hand, the normalized spin polarization of conductance has a maximum value, when rotate the (100) crystal axis makes  $\theta = -(2n + 1)\pi/4$  with the junction normal and minimum value at  $\theta = (2n + 1)\pi/4$ .

Moreover, when we inject the electron across the junction along the  $x$  axis, normally it generates the tunneling conductance along  $x$  axis. However in junction which consists of both Rashba and Dresselhaus spin-orbit coupling, there is not only the tunneling conductance in  $x$  axis but in some  $\theta$  also generate the tunneling conductance in the direction parallel to the junction plane.

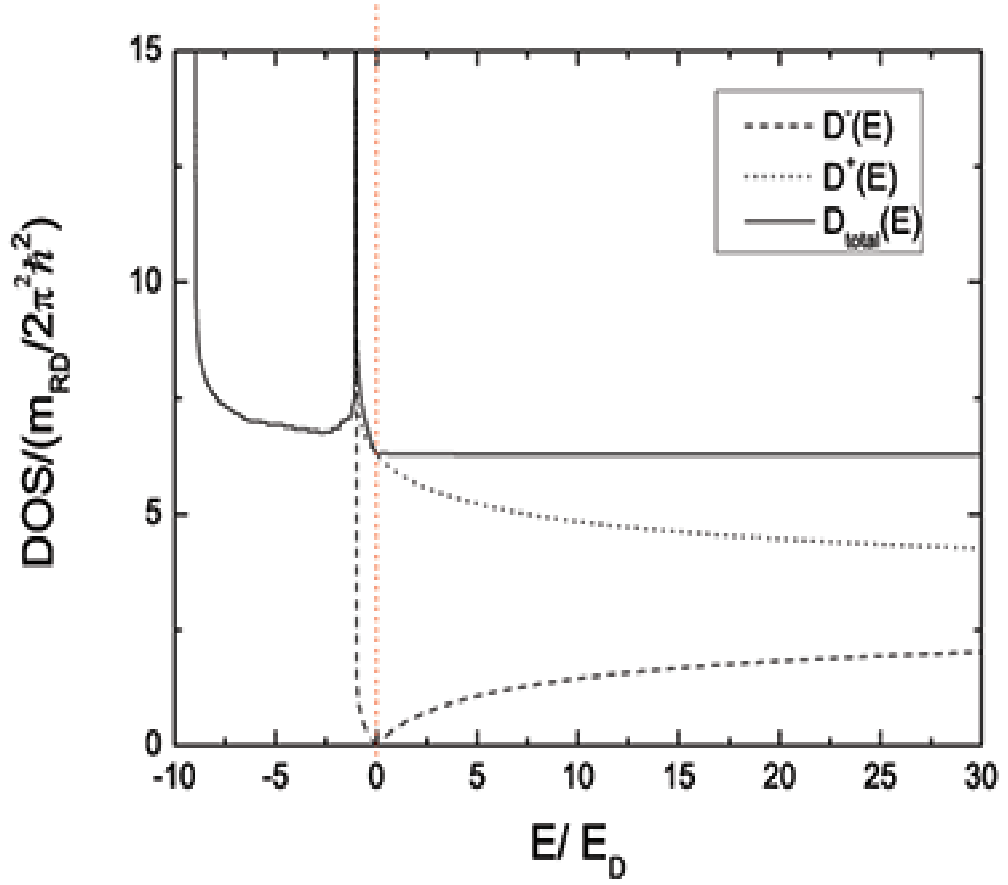


**Figure 3.2** The DOS of a 2DEG with Rashba and Dresselhaus spin-orbit coupling. The dotted line represents the DOS of the electron in the  $E^-$  branch, the dashed line represents the electron in the  $E^+$  branch and the solid line represents the total DOS, where  $E_D = \frac{\hbar^2 \beta_0^2}{2m_{RD}}$ ,  $m_{RD} = 0.05m_e$ ,  $\beta_0 = 0.025q_F$ , and  $k_0 = 0.05q_F$ .

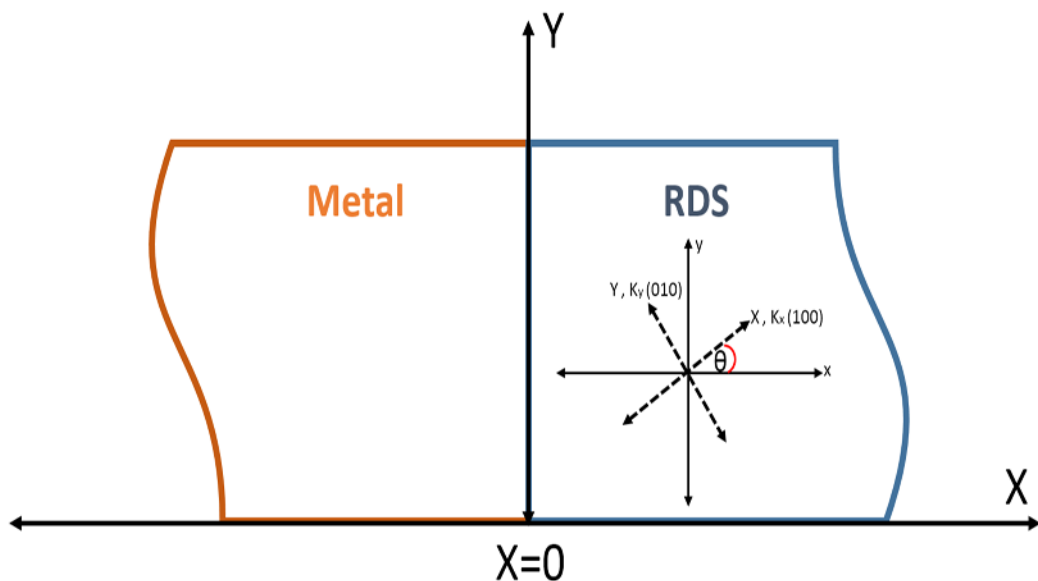


**Figure 3.3** A Metal/Rashba-Dresselhaus system junction.

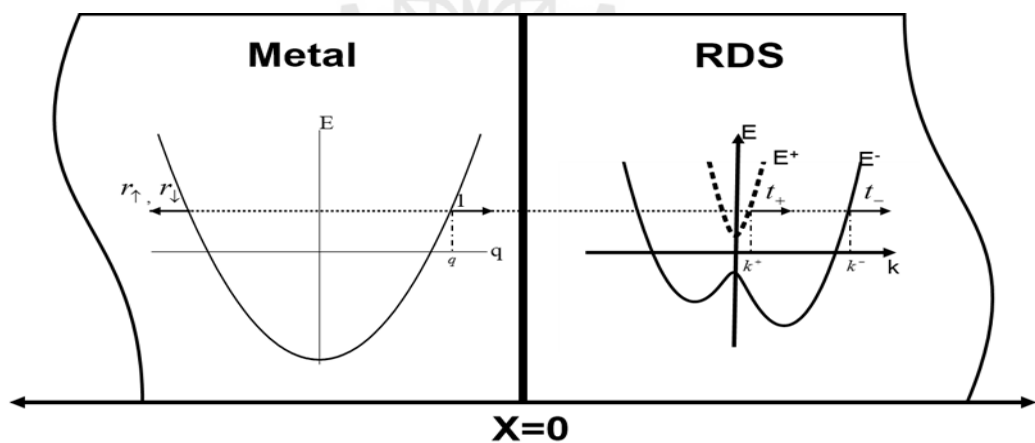


**Figure 3.4** The energy spectra of the electrons in a metal (left) and the Rashba-Dresselhaus system (right). The arrows pointing left or right, represent the electron states that are considered in the scattering process. We assumed the incoming state equal 1,  $r_{\uparrow}$  and  $r_{\downarrow}$  are reflected states with spin-up and spin-down, and  $t_{+}$  and  $t_{-}$  are outgoing states of the electron with  $E^{+}$  and  $E^{-}$ , respectively.

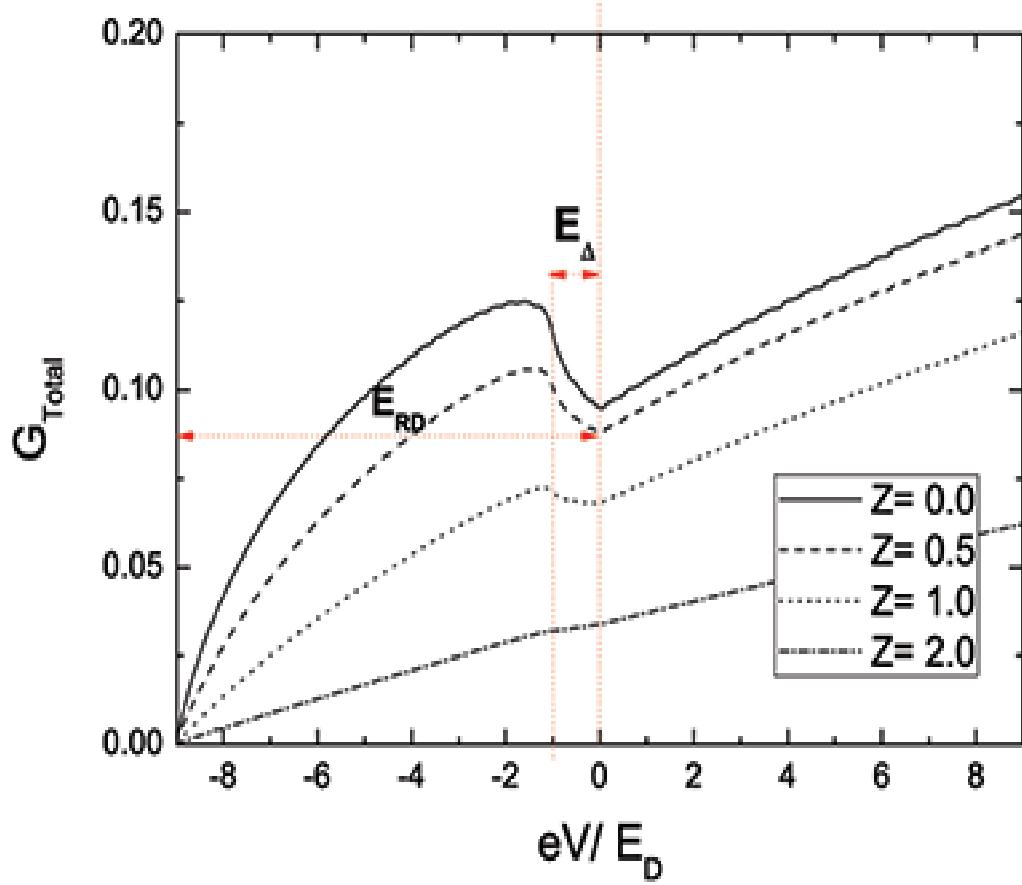


**Figure 3.5** The total conductance spectrum as a function of applied voltage at various values of  $Z$ , where  $k_0 = 0.05q_F$ ,  $\beta_0 = 0.025q_F$ ,  $m_{RD} = 0.05 m_e$ , and  $\theta = -\pi/4$  rad.

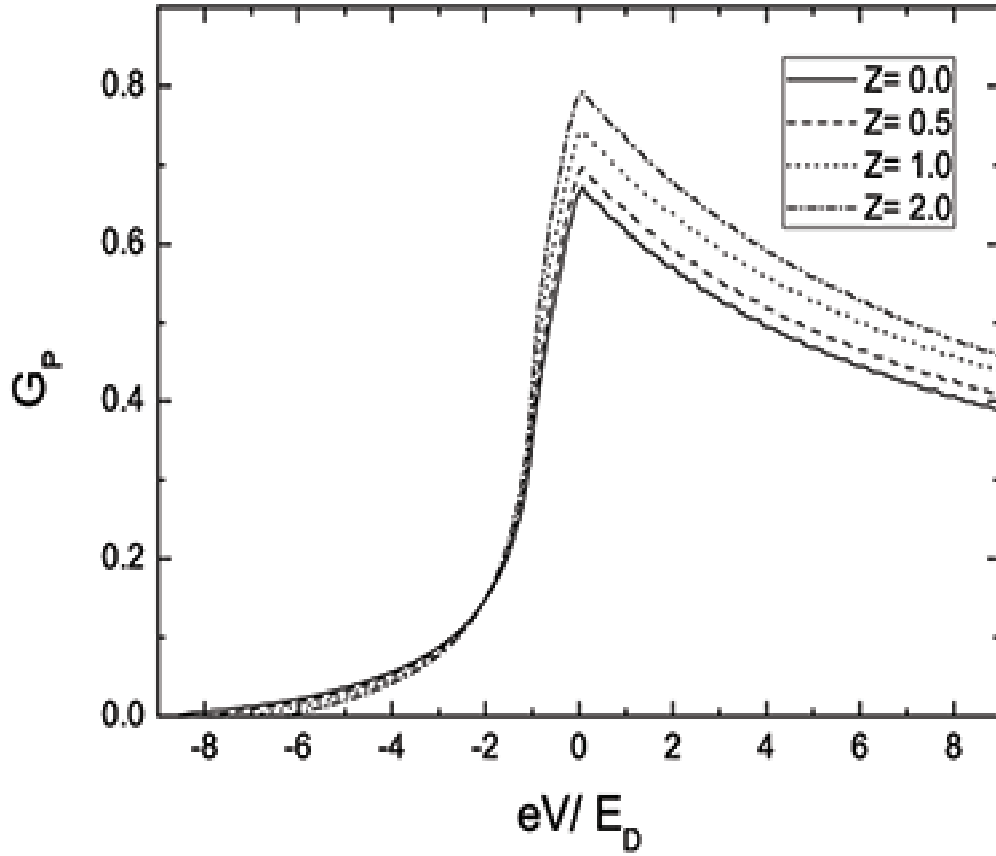


**Figure 3.6** Plots of the normalized spin polarization of conductance as a function of applied voltage at various values of  $Z$ , where  $m_{RD} = 0.05 m_e$ ,  $k_0 = 0.05q_F$ ,  $\beta_0 = 0.025q_F$ , and  $\theta = -\pi/4$  rad.

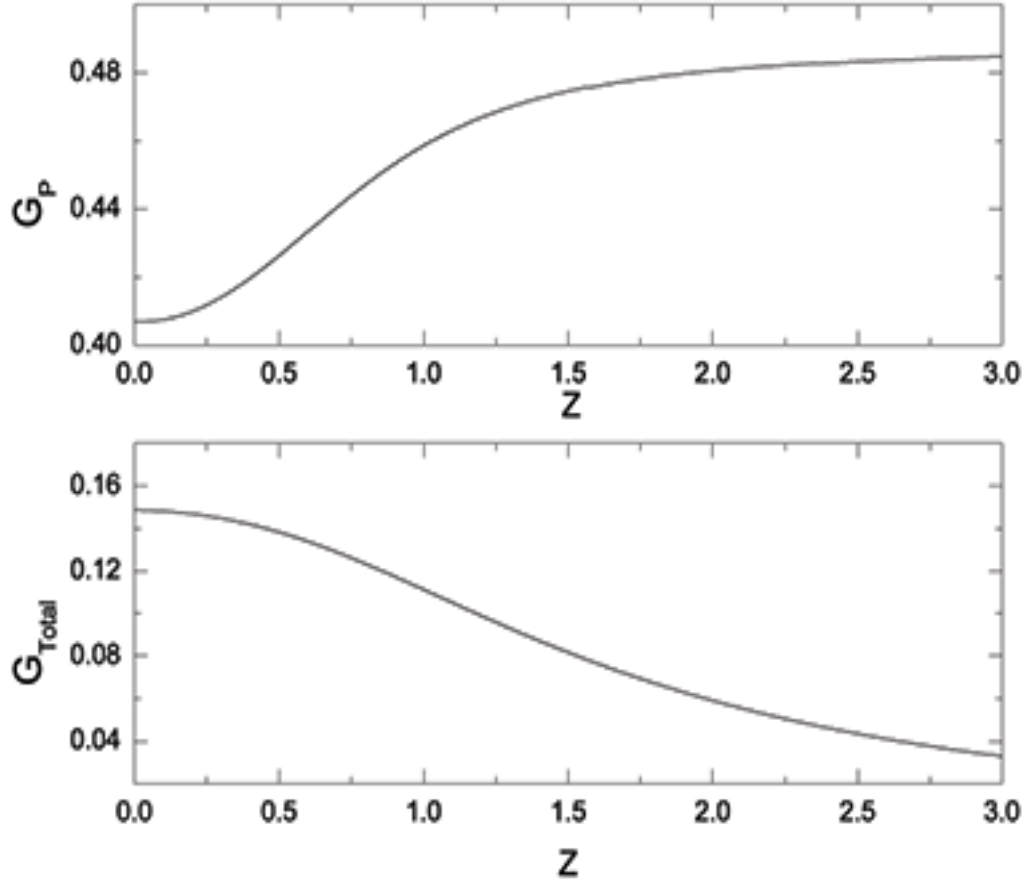


**Figure 3.7** Plots of the total conductance and the normalized spin polarization of conductance as a function of  $Z$ , where  $m_{RD} = 0.05 m_e$ ,  $k_0 = 0.05q_F$ ,  $\beta_0 = 0.025q_F$ , and  $\theta = 0$ .

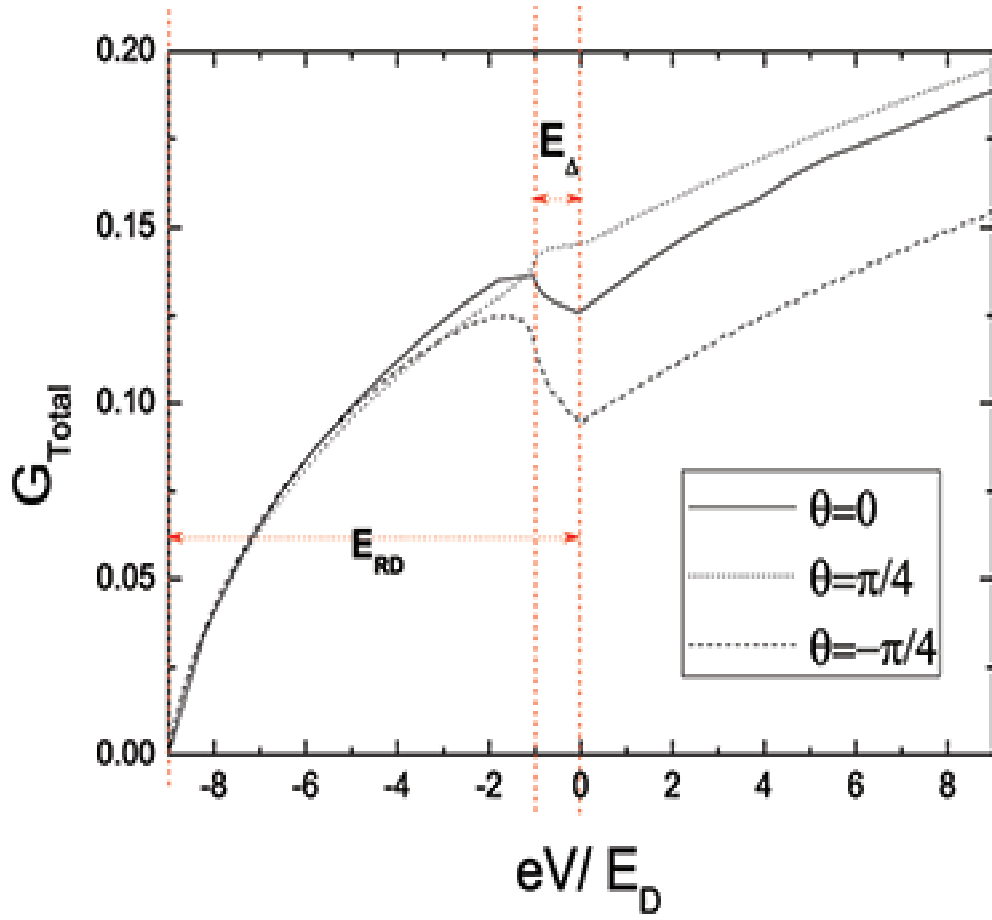


**Figure 3.8** The total conductance spectrum as a function of applied voltage at various  $\theta$ , where  $m_{RD} = 0.05 m_e$ ,  $k_0 = 0.05q_F$ ,  $\beta_0 = 0.025q_F$ ,  $Z = 0.0$ .



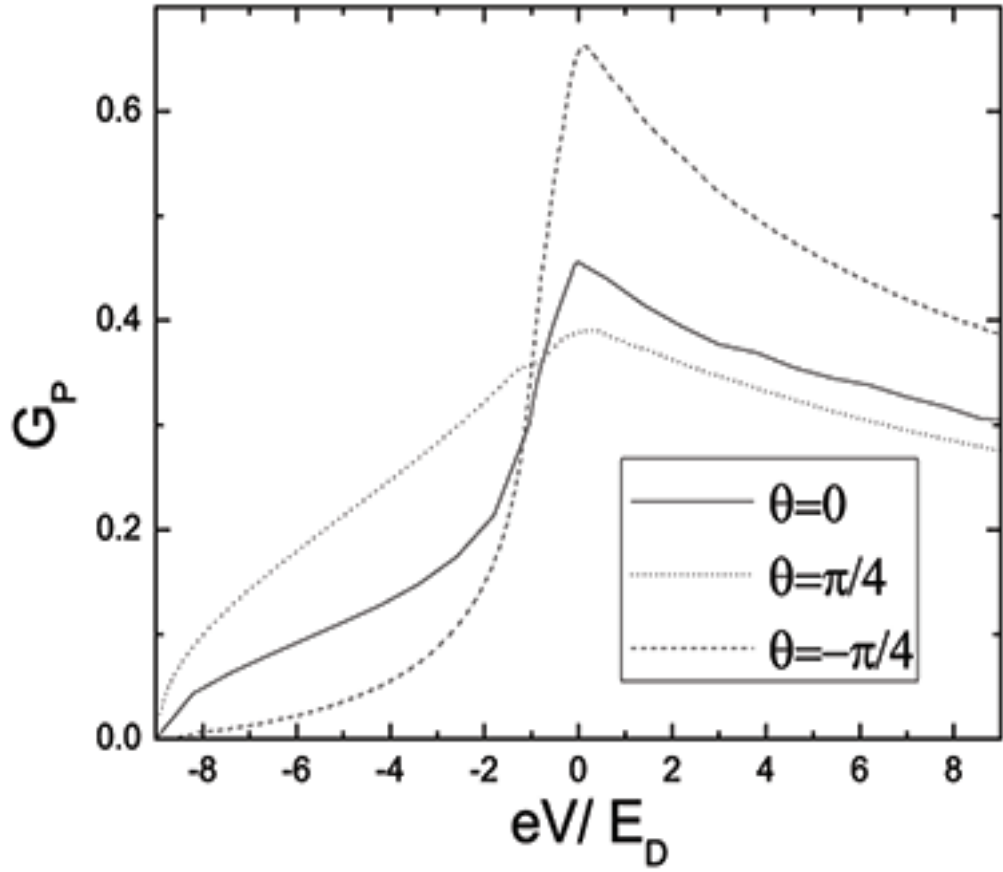


**Figure 3.9** Plots of the normalized spin polarization of conductance as a function of applied voltage at various  $\theta$ , where  $m_{RD} = 0.05 m_e$ ,  $k_0 = 0.05q_F$ ,  $\beta_0 = 0.025q_F$ , and  $Z = 0.0$ .

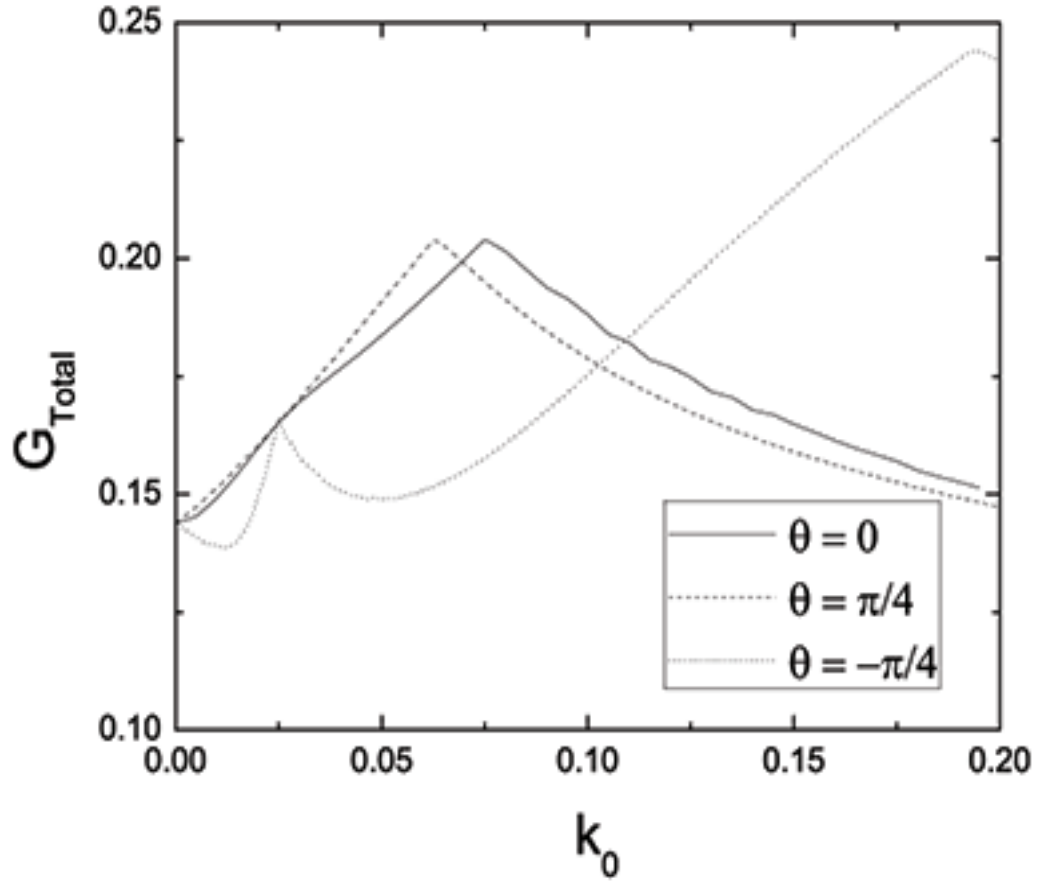


**Figure 3.10** The total conductance spectrum as a function of Rashba spin-orbit coupling strength at various values of  $\theta$ , where  $m_{RD} = 0.05 m_e$ ,  $\beta_0 = 0.025q_F$ ,  $Z = 0.0$ , and  $\theta = -\frac{\pi}{4}$  rad.

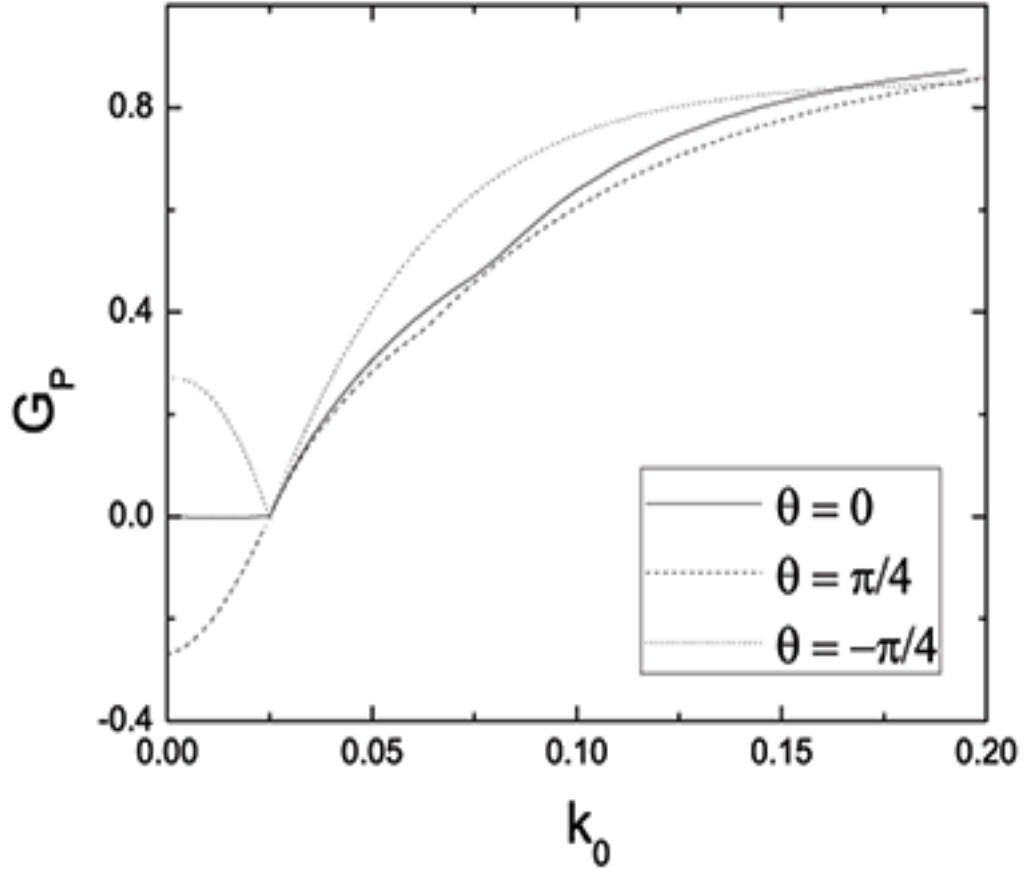


**Figure 3.11** Plot of the normalized spin polarization of conductance as a function of Rashba spin-orbit coupling strength at various values of  $\theta$ , where  $m_{RD} = 0.05 m_e$ ,  $\beta_0 = 0.025q_F$ , and  $\theta = -\frac{\pi}{4}$  rad.

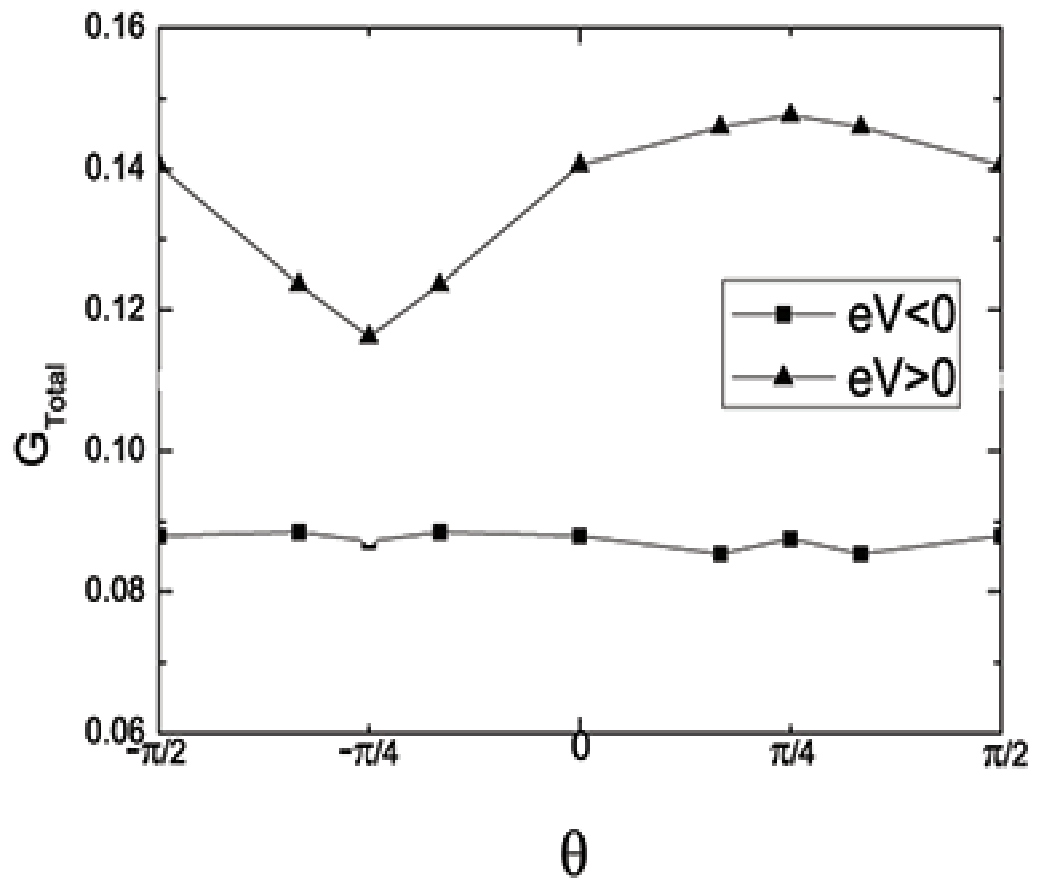


**Figure 3.12** Plot of the total conductance as a function of  $\theta$  at various values of applied voltage, where  $m_{RD} = 0.05 m_e$ ,  $k_0 = 0.05q_F$ ,  $\beta_0 = 0.025q_F$ , and  $Z = 0.0$ .

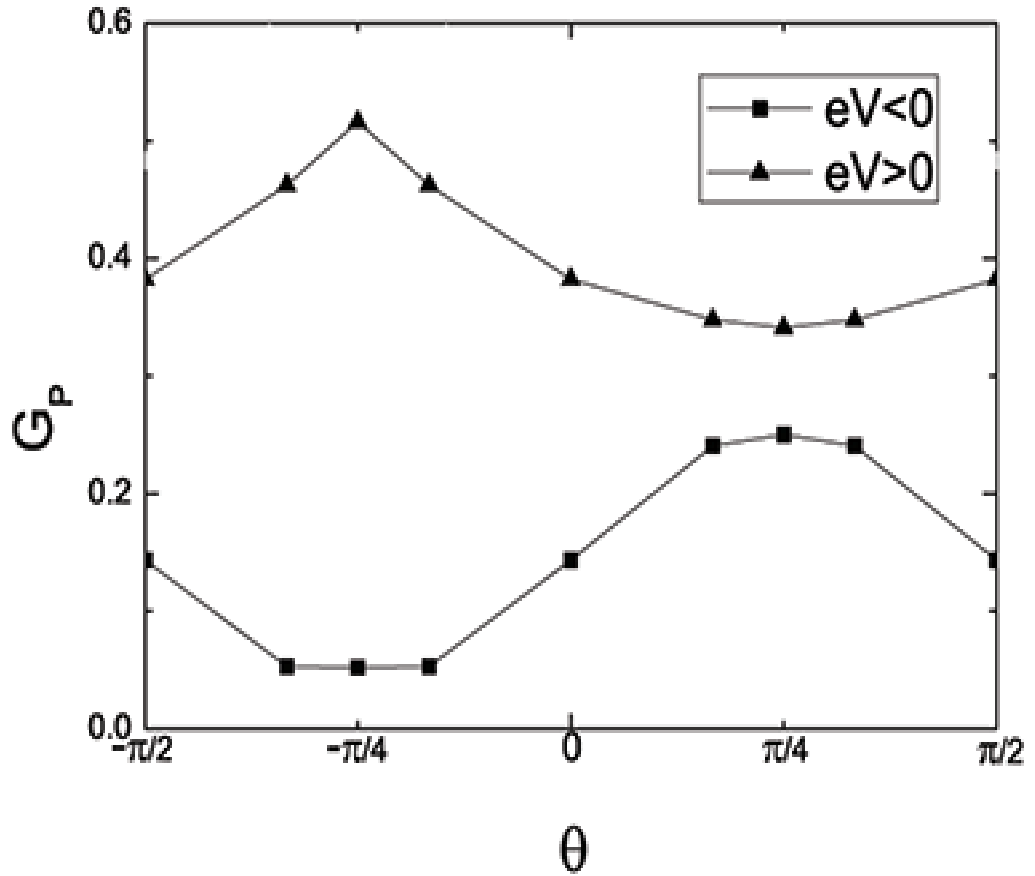


**Figure 3.13** Plot of the normalized spin polarization of conductance as a function of  $\theta$  at various values of applied voltage, where  $m_{RD} = 0.05 m_e$ ,  $k_0 = 0.05q_F$ ,  $\beta_0 = 0.025q_F$ , and  $Z = 0.0$ .

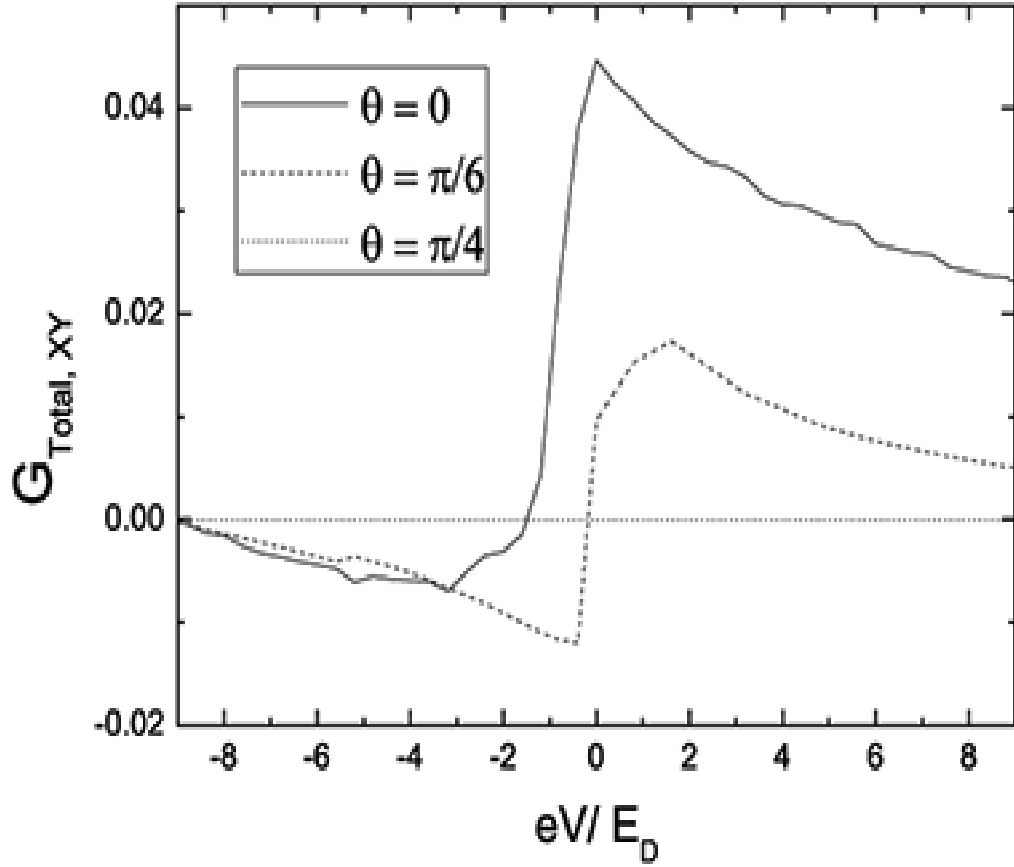


**Figure 3.14** The plot of the conductance perpendicular to the junction ( $G_{Total, XY}$ ) as a function of applied voltage at various values of  $\theta$ , where  $k_0 = 0.05q_F$ ,  $\beta_0 = 0.025q_F$ ,  $Z = 0.0$ , and  $\theta = 0$  rad.

# CHAPTER IV

## CONCLUSIONS

This thesis is a theoretical study of the particle and spin transport in systems with Rashba and Dresselhaus spin-orbit coupling by using a scattering method. According to both the energy contours and the spin states of the system with both types of spin-orbit coupling are not invariant with respect to the rotation about the  $z$  axis which lead to many interesting effects. This dependence is more explored on the crystallographic orientation of the particle and spin transport across the interface between a metal and 2DEG with both types of the spin-orbit coupling. Two types of junction are considered: the first one is the junction between a normal metal and a two-dimensional electron gas system with only Dresselhaus spin-orbit coupling and the second one is the junction between a normal metal and a two-dimensional electron gas system with both Rashba and Dresselhaus spin-orbit coupling.

In this formalism, the junction is represented by an infinite system. Each region in the system is modeled with a continuous Hamiltonian appropriate for each material. The reflection and transmission amplitudes can be obtained by applying the matching conditions for these wave functions at the interface. The conductance spectrum and the normalized spin polarization of conductance can be obtained as well. The effect of the crystallographic orientation of the 2DEG, the spin-orbit coupling strength, and the potential barrier strength are studied.

In chapter II is the study of the particle and spin transport in the junction between a normal metal and a two-dimensional electron with only Dresselhaus

spin-orbit coupling. The effect of the crystallographic orientation of 2DEG is studied, and found the total conductance spectra invariant with the crystallographic orientation. On the contrary, the normalized spin polarization of conductance is not invariant with the crystallographic orientation, they show an oscillation with period  $\pi$  rad. The magnitudes of the normalized spin polarization of conductance has a maximum value, when rotate the (100) crystal axis makes  $\theta = \pm(2n + 1)\pi/4$  and minimum value at  $\pm n\pi/2$  where  $n = 0, 1, 2, 3, \dots$ . In addition, both of the total conductance spectra and the normalized spin polarization of conductance can be enhanced by increasing the Dresselhaus strength, and be suppressed by increasing the potential barrier strength. The Dresselhaus couples energy can be determined from the beginning of the conductance spectra to the discontinuity point in the conductance spectra.

In Chapter III is the study of the particle and spin transport in the junction between a normal metal and a two-dimensional electron gas system with both Rashba and Dresselhaus spin-orbit coupling. The conductance spectrum shows two distinctive features. From the positions of these exist features, the Rashba and Dresselhaus couples energy can be determined the Rashba-Dresselhaus energy,  $E_{RD} = \frac{\hbar^2(k_0 + \beta_0)^2}{2m_{RD}}$ , and  $E_{\Delta} = \frac{\hbar^2(k_0 - \beta_0)^2}{2m_{RD}}$ . The Rashba-Dresselhaus energy can be determined from the beginning of the spectra to the second discontinuity point, which relate to the sum of two spin-orbit coupling strength.  $E_{\Delta}$  can be determined from the different scale between two discontinuity points, which relate to the different value between two spin-orbit coupling strength. Both the conductance spectrum and the normalized spin polarization of conductance are not invariant with the crystallographic orientation. The conductance spectrum has a maximum value, when the (100) crystal axis makes  $\theta = (2n + 1)\pi/4$  and minimum value at  $\theta = -(2n + 1)\pi/4$ , where  $n$  is non-negative integer. This is different from the



normalized spin polarization of conductance, it has a maximum value, when the (100) crystal axis makes  $\theta = -(2n+1)\pi/4$  and minimum value at  $\theta = (2n+1)\pi/4$ .

In case of fixed the Dresselhaus strength and varied the Rashba strength, the total conductance spectra is increased with the strength of the Rashba spin-orbit coupling, until the strength reaches to a critical value, after which the total conductance spectrum is decreased with the strength. On the other hand, the spin-polarization of conductance is increased with the Rashba spin-orbit coupling strength. Moreover, the total conductance spectra can be suppressed by increasing the potential barrier strength and the normalized spin polarization of conductance can be enhanced by increasing the potential barrier strength. One more interesting result is that there exists the current along the direction parallel to the junction place.

The results found in this thesis indicated that the normalized spin polarization of conductance can be controlled by varying the potential barrier strength, the applied voltage, and the spin-orbit coupling strength. Furthermore, by rotating the crystallographic of the 2DEG, we can control the normalized spin polarization of conductance. In the future, we expect to study more complex heterostructures that contain Rashba-Dresselhaus system, for example M/RDS/M, Ferromagnetic/RDS, Superconductor/RDS, DS/RDS, and RS/RDS junction.



## REFERENCES

## REFERENCES

- Ast, C. R., Henk, J., Ernst, A., Moreschini, L., Falub, M. C., Pacile, D., Bruno, P., Kern, K., and Grioni, M. (2007a). Giant spin splitting through surface alloying. **Physical Review Letters** 98: 186807.
- Ast, C. R., Wittich, G., Wahl, P., Vogelgesang, R., Pacile, D., Falub, M. C., Moreschini, L., Papagno, M., Grioni, M., and Kern, K. (2007b). Local detection of spin-orbit splitting by scanning tunneling spectroscopy. **Physical Review B** 75: 201401.
- Barnas, J., Fuss, A., Camley, R. E., GrUnberg, P., and Zinn, W. (1990). Novel magnetoresistance effect in layered magnetic structures: Theory and experiment. **Physical Review B** 42: 8110.
- Bychkov, Y. A. and Rashba, E. I. (1984). Oscillatory effects and the magnetic susceptibility of carriers in inversion layers. **Journal of Physics C** 17: 6039.
- Cercellier, H., Fagot-Revurat, Y., Kierren, B., Reinert, F., Popovic, D., and Malterre, D. (2004). Spin-orbit splitting of the Shockley state in the *Ag/Au(111)* interface. **Physical Review B** 70: 193412.
- Das, B., Miller, D. C., and Datta, S. (1989). Evidence for spin splitting in *In<sub>x</sub>Ga<sub>1-x</sub>As/In<sub>0.52</sub>Al<sub>0.48</sub>As* heterostructures as  $B \rightarrow 0$ . **Physical Review B** 39: 1411.
- Datta, S. and Das, B. (1989). Electronic analog of the electro-optic modulator. **Applied Physics Letters** 56: 7.

- Desrat, W., Maude, D. K., Wasilewski, Z. R., Airey, R., and Hill, G. (2006). Dresselhaus spin-orbit coupling in a symmetric (100) GaAs quantum well. **Physical Review B** 74: 193317.
- Dresselhaus, G. (1955). Spin-Orbit Coupling Effects in Zinc Blende Structures. **Physical Review** 100: 580.
- Dresselhaus, P. D., Papavassiliou, C. M. A., and Wheeler, R. G. (1992). Observation of spin precession in GaAs inversion layers using antilocalization. **Physical Review Letters** 68: 106.
- Engels, G., Lange, J., Schpers, T., and Lth, H. (1997). Experimental and theoretical approach to spin splitting in modulation-doped  $In_xGa_{1-x}As/InP$  quantum wells for  $B \rightarrow 0$ . **Physical Review B** 55: R1958.
- Frolov, S. M., Luscher, S., Yu, W., Ren, Y., Folk, J. A., and Wegscheider, W. (2009). Ballistic spin resonance. **Nature** 458: 868.
- Ganichev, S. D., Belkov, V. V., Ivchenko, L. E., Schneider, P., Giglberger, S., Eroms, J., Boeck, J. D., Borghs, G., Wegscheider, W., Weiss, D., and Prettl, W. (2004). Experimental separation of Rashba and Dresselhaus spin splittings in semiconductor quantum wells. **Physical Review Letters** 92: 256601.
- Giglberger, S., Golub, L. E., Belkov, V. V., Danilov, S. N., Schuh, D., Gerl, C., Rohlfing, F., Stahl, J., Wegscheider, W., Weiss, D., Prettl, W., and Ganichev, S. D. (2007). Rashba and Dresselhaus spin splittings in semiconductor quantum wells measured by spin photocurrents. **Physical Review B** 75: 035327.

- Grundler, D. (2000). Large Rashba Splitting in InAs Quantum Wells due to Electron Wave Function Penetration into the Barrier Layers. **Physical Review Letters** 84: 6074.
- Henk, J., Hoesch, M., Osterwalder, J., Ernst, A., and Bruno, P. (2004). Spin-Orbit coupling in the L-gap surface states of Au(111): spin-resolved photoemission experiments and first-principles calculations. **Journal of Physics: Condensed Matter** 16: 7581–7597.
- Hu, C. M. and Matsuyama, T. (2001). Spin injection across a heterojunction: A ballistic picture. **Physical Review Letters** 87: 066803.
- Hu, C. M., Nitta, J., Akazaki, T., Takayanagi, H., Osaka, J., Pfeffer, P., and Zawadzki, W. (1999). Zero-field spin splitting in an inverted  $In_{0.53}Ga_{0.47}As/In_{0.52}Al_{0.48}As$  heterostructure: Band nonparabolicity influence and the subband dependence. **Physical Review B** 60: 7736.
- Jantayod, A. (2013). Spin-dependent tunneling through a symmetric semiconductor barrier. **Superlattices Microstruct** 54: 54.
- Jiang, Y. and Jalil, M. B. A. (2003). Enhanced spin injection and magnetoconductance by controllable Rashba coupling in a *ferromagnet/two – dimensional* electron gas structure. **Journal of Physics: Condensed Matter** 15: 31.
- Jusserand, B., Richards, D., Peric, H., and Etienne, B. (1992). Zero-magnetic-field spin splitting in the GaAs conduction band from Raman scattering on the modulation-doped quantum wells. **Physical Review Letters** 69: 848.

- Knap, W., Skierbiszewski, C., Zduniak, A., Litwin-Staszewska, E., Bertho, D., Kobbi, F., Robert, J. L., Pikus, G. E., Pikus, F. G., Iordanskii, S. V., Mosser, V., Zekentes, K., and Lyanda-Geller, Y. B. (1996). Weak antilocalization and spin precession in quantum wells. **Physical Review B** 53: 3912.
- Koga, T., Nitta, J., Akazaki, T., and Takayanagi, H. (2002). Rashba Spin-Orbit Coupling Probed by the Weak Antilocalization Analysis in *InAlAs/InGaAs/InAlAs* Quantum Wells as a Function of Quantum Well Asymmetry. **Physical Review Letters** 89: 046801.
- Krich, J. J. and Halperin, B. I. (2007). Cubic Dresselhaus Spin-Orbit Coupling in 2D Electron Quantum Dots. **Physical Review Letters** 98: 226802.
- LaShell, S., McDougall, B. A., and Jensen, E. (1996). Spin Splitting of an Au(111) Surface State Band Observed with Angle Resolved Photoelectron Spectroscopy. **Physical Review Letters** 77: 3419.
- Lee, M. and Choi, M. (2005). Ballistic spin currents in mesoscopic *metal/In(GA)As/metal* junctions. **Physical Review B** 71: 153306.
- Liang, F., Yang, Y. H., and Wang, J. (2009). Electrical generation of pure spin current with oscillating spin-orbit interaction. **European Physical Journal B** 69: 337–341.
- Linder, J., Yokoyama, T., and Sudbø, A. (1997). Pure spin current generated by reflection at a normal *metal/two* dimensional electron gas interface. **Physical Review B** 56: 075312.
- Lu, J. D. and Li, J. W. (2010). The effects of Dresselhaus and Rashba spin-orbit

interactions on the electron tunneling in a non-magnetic heterostructure. **Applied Surface Science** 256: 4027–4030.

Maiti, s. K. (2011). Determination of Rashba and Dresselhaus spin-orbit fields. **Journal of Applied Physics** 110: 064306.

Meier, L., Salis, G., Shorubalko, I., Gini, E., Schon, S., and Ensslin, K. (2007). Measurement of Rashba and Dresselhaus spin-orbit magnetic fields. **Nature Physics** 3: 650–654.

Miller, J. B., Zumbuhl, D. M., Marcus, C. M., Lyanda-Geller, Y. B., Goldhaber-Gordon, D., Campman, K., and Goddard, A. C. (2003). Gate-Controlled Spin-Orbit Quantum Interference Effects in Lateral Transport. **Physical Review Letters** 90: 076807.

Nitta, J., Akazaki, T., Henk, J., and Takayanagi, H. (1997). Gate control of spin-orbit interaction in an inverted  $In_{0.53}Ga_{0.47}As/In_{0.52}Al_{0.48}As$  heterostructure. **Physical Review B** 78: 1335.

Pacile, D., Ast, C. R., Papagno, M., silva, C. D., Moreschini, L., Falub, M. C., Seitsonen, A. P., and Grioni, M. (2006). Electronic structure of an ordered  $Pb/Ag(111)$  surface alloy: Theory and experiment. **Physical Review B** 73: 245429.

Park, Y. H., Kim, H., Chang, J., Han, S. H., Eom, J., Choi, H., and Koo, H. C. (2013). Separation of Rashba and Dresselhaus spin-orbit interactions using crystal direction dependent transport measurements. **Applied Physics Letters** 103: 252407.

Perel, V. I., Tarasenko, S. A., Yassievich, I. N., Ganichev, S. D., Bel'kov, V. V.,

- and Prettl, W. (2003). Spin-dependent tunneling through a symmetric semiconductor barrier. **Physical Review B** 67: 201304.
- Pfeffer, P. and Zawadzki, W. (1999). Spin splitting of conduction subbands in III-V heterostructures due to inversion asymmetry. **Physical Review B** 59: R5312.
- Popovic, D., Reinert, F., Hufner, S., Grigoryan, V. G., Springborg, M., Cercellier, H., Fagot-Revurat, Y., Kierren, B., and Malterre, D. (2005). High-resolution photoemission on *Ag/Au(111)*: Spin-orbit splitting and electronic localization of the surface state. **Physical Review B** 72: 045419.
- Premper, J., Trautmann, M., Henk, J., and Bruno, P. (2007). Spin-orbit splitting in an anisotropic two-dimensional electron gas. **Physical Review B** 76: 073310.
- Rashba, E. I. (1960). Properties of semiconductors with an extremum loop I. Cyclotron and combinational resonance in a magnetic field perpendicular to the plane of the loop. **Solid State Ionics** 2: 1109.
- Sawa, Y., Yokoyama, T., and Tanaka, Y. (2007). Charge transport in *2DEG/s - wave* superconductor junction with Dresselhaus-type spin-orbit coupling. **Journal of Magnetism and Magnetic Materials** 310: 2277.
- Silva, E. A. (1992). Conduction-subband anisotropic spin splitting in III-V semiconductor heterojunctions. **Physical Review B** 46: 1921.
- Srisongmuang, B. and Kaoey, A. (2012). Tunneling conductance of a two-dimensional electron gas with Dresselhaus spin-orbit coupling. **Journal of Magnetism and Magnetic Materials** 324: 475.



- Studer, M., Salis, S., Ensslin, K., Driscoll, D. C., and Gossard, A. C. (2009a). Gate-Controlled Spin-Orbit Interaction in a Parabolic *GaAs/AlGaAs* Quantum Well. **Physical Review Letters** 103: 027201.
- Studer, M., Schon, G., Ensslin, K., and Salis, G. (2009b). Spin-orbit interaction and spin relaxation in a two-dimensional electron gas. **Physical Review B** 79: 045302.
- Studer, M., Walszer, M. P., Baer, S., Rusterhol, H., Schon, G., Schuh, D., Wegscheider, W., Ensslin, K., and Salis, G. (2010). Role of linear and cubic terms for drift-induced Dresselhaus spin-orbit splitting in a two-dimensional electron gas. **Physical Review B** 82: 235320.
- Tolozá Sandoval, M. A., de Andrada e Silva, E. A., Ferreira da Silva, A., and La Rocca, G. C. (2010). Variational Rashba Effect in *GaAlAs/GaAs* Heterojunctions. **Journal of Superconductivity and Novel Magnetism** 23: 171–173.
- Tolozá Sandoval, M. A., Silva, A. F., Ferreira da Silva, E. A., and La Rocca, G. C. (2012). Rashba and Dresselhaus spin-orbit interaction strength in *GaAs/GaAlAs* heterojunctions. **Physics Procedia** 28: 95–98.
- Usaj, G. and Balseiro, C. A. (2004). Transverse electron focusing in systems with spin-orbit coupling. **Physical Review B** 70: 041031.
- Vajna, S., Simon, E., Szilva, A., Palotas, K., Ujfalussy, B., and Szunyogh, L. (2012). Higher-order contributions to the Rashba-Bychkov effect with application to the *Bi/Ag(111)* surface alloy. **Physical Review B** 85: 075404.

- Wepfer, G. G., Collins, T. C., and Euwema, R. N. (1971). Calculated spin-orbit splittings of some group IV, III-V, and II-VI semiconductors. **Physical Review B** 4: 1296.
- Wolf, S. A., Awschalom, D. D., Buhrman, R. A., Daughton, J. M., von Malnar, S., Roukes, M. L., Chtchelkanova, A. Y., and Treger, D. M. (2001). Spintronics: A Spin-Based Electronics Vision for the Future. **Science** 294: 1488.
- Xiao, Y. C. and Deng, W. J. (2010). Rashba-Dresselhaus double refraction in a two-dimensional electron gas. **Superlattices Microstruct** 48: 181–189.
- Xu, W. and Guo, Y. (2005). Rashba and Dresselhaus spin-orbit coupling effects on tunneling through two-dimensional magnetic quantum systems. **Physics Letters A** 340: 281–289.
- Yokoyama, T., Tanaka, Y., and Inoue, J. (2006). Charge transport in two-dimensional electron *gas/insulator/superconductor* junctions with Rashba spin-orbit coupling. **Physical Review B** 74: 035318.
- Zutic, I., Fabian, J., and Sarma, S. D. (2004). Spintronics: Fundamentals and applications. **Reviews of Modern Physics** 76: 323.



## APPENDICES

# APPENDIX A

## TUNNELING BETWEEN A NORMAL METAL AND A 2DEG WITH ONLY RASHBA SPIN-ORBIT COUPLING DOUBLE JUNCTIONS

We modeled our junction (M/RS/M junction) as a two-dimensional infinite system, in which a normal metal is in  $x < 0$  and  $x < L$ , and a 2DEG with RSOC is in  $0 < x < L$  as shown in Figure A.1. It is assumed that the interface is smooth and the barrier at the interface is represented by a Dirac delta-function potential,  $H_1\delta(x = 0)$  and  $H_2\delta(x = L)$  where  $H_{1(2)}$  is the scattering potential strength at the interface. The Hamiltonian of the electron in M/RS/M junction is written as

$$\begin{aligned}
 H(x) = & \frac{\hat{p}^2}{2m(x)} + H_1\delta(x) + H_2\delta(x - L) + \frac{\hbar^2 k_0 \Theta(x)}{m_R} (\sigma_x k_z - \sigma_z k_x) \\
 & - E_F \Theta(-x) + \Theta(x - L) - E_{FR} \Theta(x) - \Theta(x - L), \tag{A.1}
 \end{aligned}$$

where  $\hat{p} = -i\hbar(\hat{x}\frac{\partial}{\partial x} + \hat{z}\frac{\partial}{\partial z})$  is the momentum operator, the effective mass  $m(x) = m_e(\Theta(-x) + \Theta(x - L)) + m_R(\Theta(x) - \Theta(x - L))$  which is position dependent,  $m_e$  and  $m_R$  are the effective electron mass in the metal and in Rashba system, respectively,  $\Theta(x)$  is the Heaviside step function,  $E_F$  is the Fermi energy of the metal, and  $E_{FR}$  is the Fermi energy of the Rashba system.

In the metal, the energy dispersion relation for both spin-up and spin-down

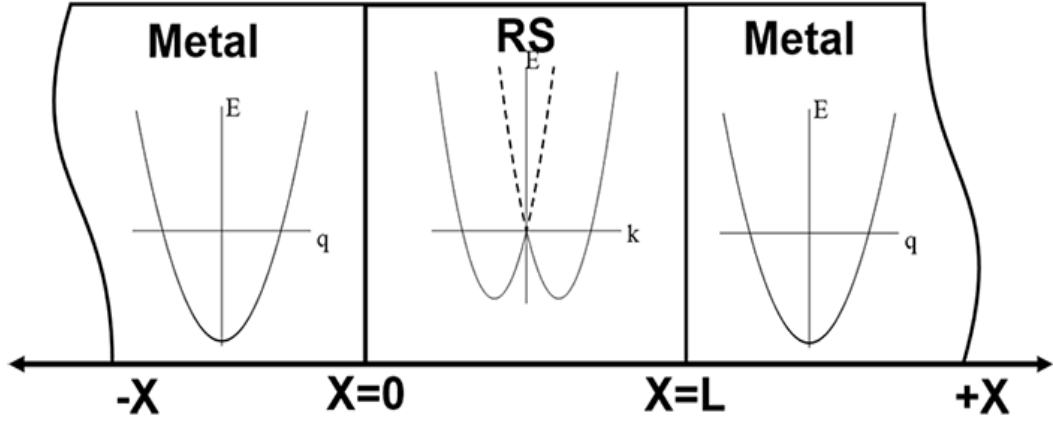


**Figure A.1** A Metal/Rashba system/Metal double junction.

are equal. The energy dispersion relation of the electron in the metal is

$$E(q) = \frac{\hbar^2 q^2}{2m_e}, \quad (\text{A.2})$$

where  $\vec{q}$  is the wave vector of the electron in the metal,  $q = \sqrt{q_x^2 + q_z^2}$ . The wave function of the electron in metal side takes form

$$\begin{aligned} \Psi_{M1}(q_x, q_z, x) = \frac{1}{\sqrt{2}} & \left( \begin{bmatrix} \pm i \\ 1 \end{bmatrix} e^{iq_x x} + r_{\uparrow} \begin{bmatrix} -i \\ 1 \end{bmatrix} e^{-iq_x x} \right. \\ & \left. + r_{\downarrow} \begin{bmatrix} i \\ 1 \end{bmatrix} e^{-iq_x x} \right) e^{iq_z z} \end{aligned} \quad (\text{A.3})$$

where the  $\pm$  in the first term refer to the electron with spin-up (the spin state point to  $+z$  direction) and spin-down (the spin state point to  $-z$  direction) respectively. The first term represents the incoming state, the second and third terms are the reflecting state, where  $R_{\uparrow}$  and  $R_{\downarrow}$  are the reflection probability amplitude of electron with spin-up and spin-down respectively, and  $\vec{q} = (q_x, q_z)$  is the wave vectors of electron in the normal metal.

here the magnitude of the wave vector  $q_x$  as a function of energy is written as

$$q_x(E, q_z) = \sqrt{\frac{2m_e E}{\hbar^2} - q_z^2}, \quad (\text{A.4})$$

In the  $0 < x < L$  region, the wave function is obtained as a linear combination of two transmitted and two reflected eigenstates of the same energy and  $k_z$ ,

$$\begin{aligned} \psi_{RS}^{(j)}(x, z) = & \left( \begin{bmatrix} \cos \frac{\alpha}{2} \\ \mp \sin \frac{\alpha}{2} \end{bmatrix} t_{j+} e^{\pm i k_x^+ x} + \begin{bmatrix} \sin \frac{\alpha}{2} \\ \mp \cos \frac{\alpha}{2} \end{bmatrix} r_{j+} e^{\mp i k_x^+ x} \right) e^{i k_z^+ z} \\ & + \left( \begin{bmatrix} \sin \frac{\beta}{2} \\ \cos \frac{\beta}{2} \end{bmatrix} t_{j-} e^{i k_x^- x} + \begin{bmatrix} \cos \frac{\beta}{2} \\ \sin \frac{\beta}{2} \end{bmatrix} r_{j-} e^{-i k_x^- x} \right) e^{i k_z^- z}, \quad (\text{A.5}) \end{aligned}$$

where the upper and lower signs refer to the energy above and below  $U_0$  respectively,  $\alpha$  and  $\beta$  are the angles between of  $k^+, k^-$  and the  $x$  axis, respectively.  $t_{+/-}, r_{+/-}$  are the transmission and reflection amplitudes for electrons in the plus/minus branch of the RSOC system. Because the wave vector along the  $z$  axis is conserved, we have the following relations  $q_z = k_z^+ = k_z^-$ , or  $k^+ \sin \alpha = k^- \sin \beta = q \sin \gamma$ , where

$$k^- = k_0 + \sqrt{k_0^2 + \frac{2m^*}{\hbar^2}(E - U_0)}, \quad (\text{A.6})$$

and

$$k^+ = \pm \left( k_0 - \sqrt{k_0^2 + \frac{2m^*}{\hbar^2}(E - U_0)} \right). \quad (\text{A.7})$$

The + and - signs in equation (A.7) are for  $E > 0$  and  $E < 0$ , respectively.

In the  $x > L$  region, the electron wave function can be expressed as a

transmitted eigenstate;

$$\psi_{M_R}^{(j)}(x, z) = \left( \begin{bmatrix} t_{j\uparrow} \\ t_{j\downarrow} \end{bmatrix} e^{iq_x x} \right) e^{iq_z z}, \quad (\text{A.8})$$

where  $t_{j\sigma}$  is the transmission coefficient of the particle with spin  $\sigma$ .

All the coefficients in Eqs.(A.3)-(A.5), and (A.8) can be obtained from the four boundary conditions at  $x = 0$  and  $x = L$ .

$$\psi_{M_L}^{(j)}(x = 0^+, z) = \psi_{R_S}^{(j)}(x = 0^-, z) = \psi^{(j)}(0), \quad (\text{A.9})$$

$$\psi_R^{(j)}(x = L^+, z) = \psi_{M_R}^{(j)}(x = L^-, z) = \psi^{(j)}(L), \quad (\text{A.10})$$

$$\left( \frac{m}{m^*} \frac{\partial \psi_R^{(j)}}{\partial x} - \frac{\partial \psi_{M_L}^{(j)}}{\partial x} \right) \Big|_0 = \left( 2k_F Z_1 - ik_0 \frac{m}{m^*} \sigma_z \right) \psi^{(j)}(0), \quad (\text{A.11})$$

$$\left( \frac{\partial \psi_{M_R}^{(j)}}{\partial x} - \frac{m}{m^*} \frac{\partial \psi_R^{(j)}}{\partial x} \right) \Big|_L = \left( 2k_F Z_2 + ik_0 \frac{m}{m^*} \sigma_z \right) \psi^{(j)}(L), \quad (\text{A.12})$$

where  $Z_i = \frac{mH_i}{\hbar^2 q_F}$  is the dimensionless parameter, referring to the interfacial scattering at  $x = 0$  for  $i = 1$  and at  $x = L$  for  $i = 2$ .  $Z \rightarrow 0$  is in the high transparency limit, whereas  $Z \rightarrow \infty$  is in the low transparency, or tunneling, limit. The conductance spectrum of the electron can be obtained from

$$G(eV) = \frac{e^2}{h} \frac{Aq_F}{2\pi} \int_{-\gamma_m}^{\gamma_m} d\gamma \cos\gamma \sqrt{1 + \frac{eV}{E_F} \sum_{j=1}^2 (T_{j\uparrow}(eV, \gamma) + T_{j\downarrow}(eV, \gamma))}. \quad (\text{A.13})$$

where  $A$  is the total area of the metallic electrode and  $\gamma_m = \sin^{-1}[k^-(E)/q(E)]$  is the maximum incident angle for the electron with energy  $E$ .  $T_{j\sigma}(eV, \gamma)$  are the transmission probabilities in case  $j$  with spin  $\sigma$ .

We define the spin polarization of conductance  $G_P$ , which is the difference between the up-spin and down-spin conductance normalized by the total conductance.

$$G_P(eV) = \frac{G_{\downarrow}(eV) - G_{\uparrow}(eV)}{G_{\downarrow}(eV) + G_{\uparrow}(eV)}. \quad (\text{A.14})$$

We set the effective mass of the electron in Rashba system;  $m_R = 0.05m_e$  through this section, and the Rashba spin-orbit coupling strength;  $k_0 = 0.05q_F$ . We calculate all of the conductance in the unit of  $\frac{e^2}{h} \frac{Aq_F}{2\pi}$ .

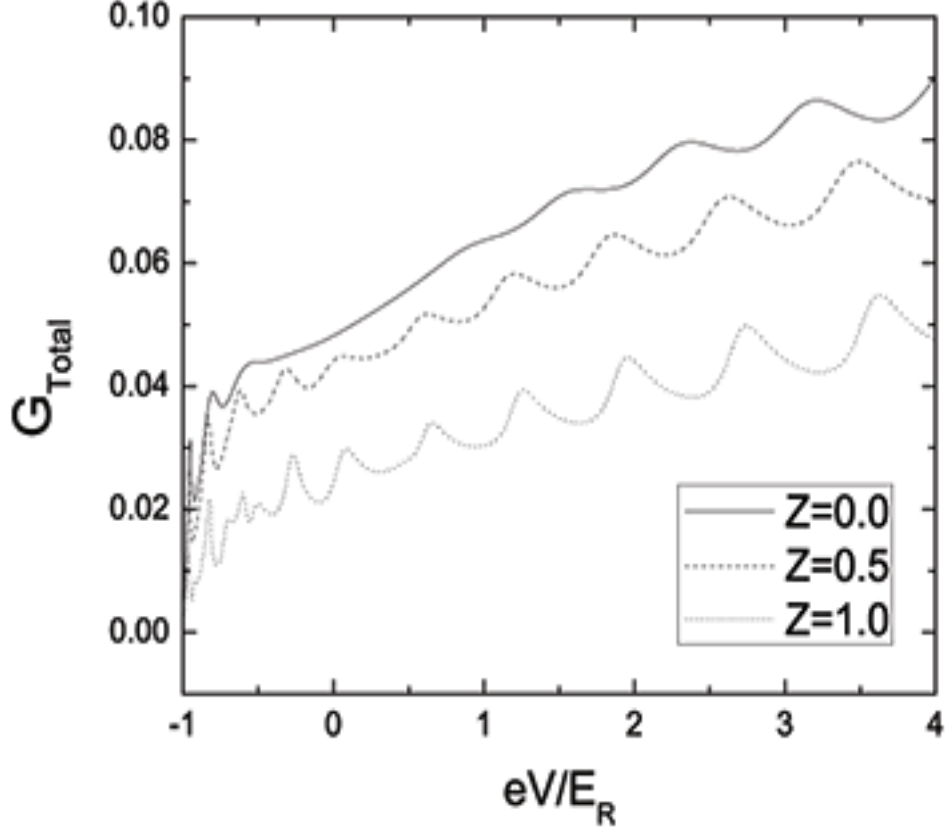


**Figure A.2** The total conductance of the M/RS/M double junctions as a function of applied voltage ( $eV$ ) when we set  $Z_1 = Z_2 = Z$ , where  $k_0 = 0.05 q_F$ ,  $m_R = 0.05 m_e$ , and  $L = 280//q_F$ .

The plots of total conductance and normalized spin polarization of conductance of the double junctions between a normal metal and a two-dimensional electron with only Rashba spin-orbit coupling as a function of applied voltage ( $eV$ ) at various values of  $Z$  shown in Figure A.2 and Figure A.3. Both of the conductance spectra and the normalized spin polarization of conductance show



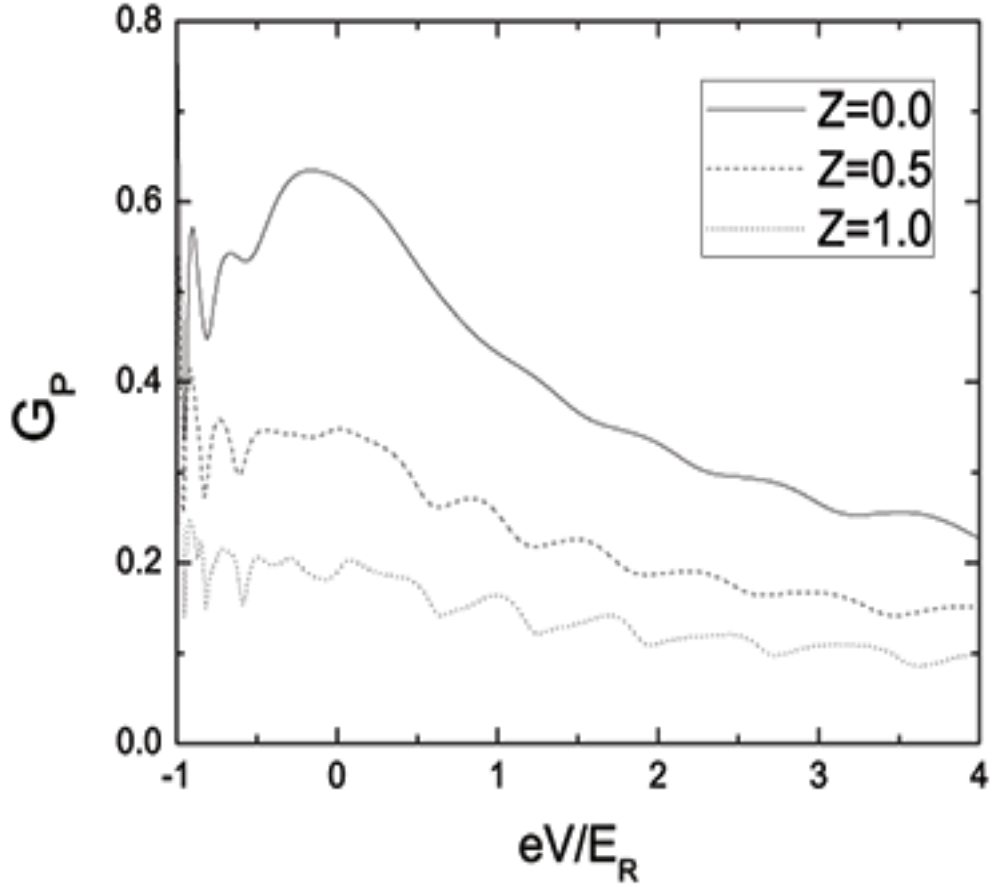
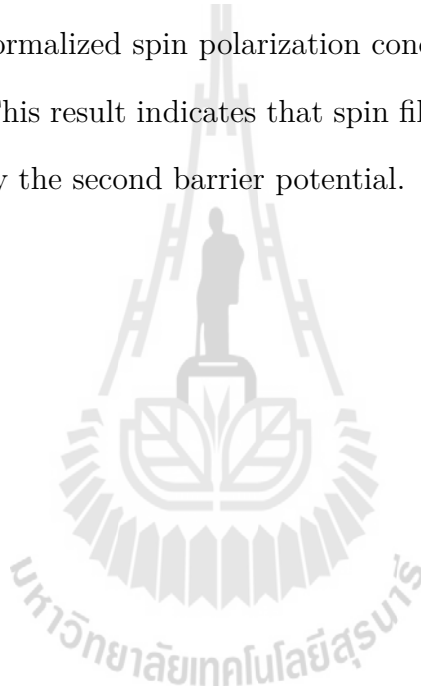


**Figure A.3** The normalized of spin polarization of conductance of the M/RS/M double junctions as a function of applied voltage ( $eV$ ) when we set  $Z_1 = Z_2 = Z$ , where  $k_0 = 0.05 q_F$ ,  $m_R = 0.05 m_e$ , and  $L = 280/q_F$ .

the oscillatory behaviors, reflecting the resonance due to the finite thickness of the Rashba layer. The period of this oscillation is not affected by the interfacial scattering potential. However, their magnitudes were suppressed by the interfacial scattering potential which is similarly to the result of M/DS junction.

Figure A.4 shows the total conductance and the normalized spin polarization of conductance as a function of  $Z_1$ . In both regions of the energy scales, the total conductance decrease when  $Z_1$  increases, but the normalized spin polarization conductance is slightly increase when  $Z_1$  is increased. Moreover, when  $Z_2$  is

varied, the normalized spin polarization conductance is decreased as  $Z_2$  is larger. The plot of the total conductance and the normalized spin polarization of conductance as a function of  $Z_2$  are shown in Figure A.5. The total conductance decrease when  $Z_2$  increases for both energy scales. The normalized spin polarization of conductance in  $eV = -0.5 E_R$  region is slightly increase when  $Z_2$  is increased, but in  $eV = E_R$  region is decrease when  $Z_2$  is increased. In addition, when  $Z_1$  is varied, the normalized spin polarization conductance is hardly changes with  $Z_1$ . We found that the normalized spin polarization conductance is much more sensitive to  $Z_2$  than  $Z_1$ . This result indicates that spin filtering in a double junction is determined mainly by the second barrier potential.



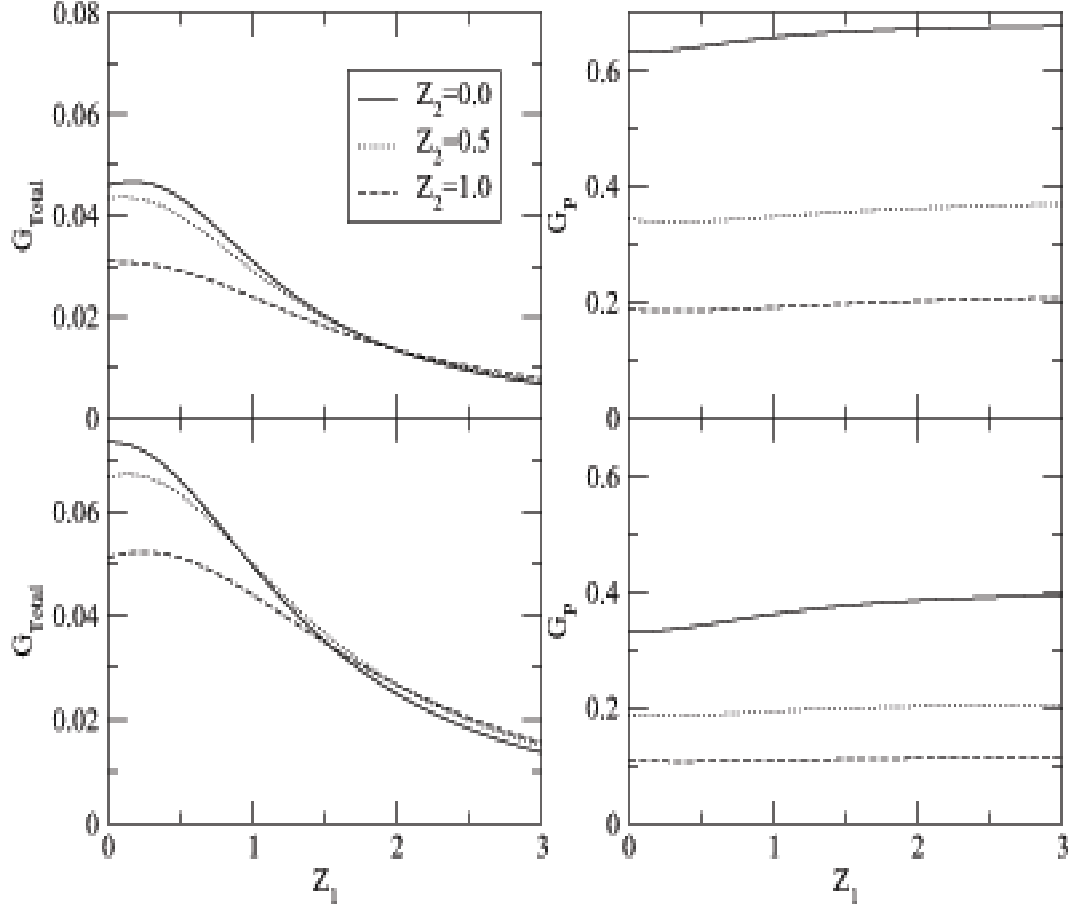


**Figure A.4** The total conductance and the normalized spin polarization of conductance of the M/RS/M double junctions as a function of the interfacial scattering potential between a normal metal and a 2DEG with RSOC ( $Z_1$ ) when fixed  $Z_2 = 0$ , where  $k_0 = 0.05 q_F$ ,  $m_R = 0.05 m_e$ , and  $L = 280/q_F$ . The left column shows the total conductance and the right column shows the normalized spin polarization of conductance, when the top figure for  $eV = -0.5 E_R$  and the bottom figure for  $eV = E_R$ .

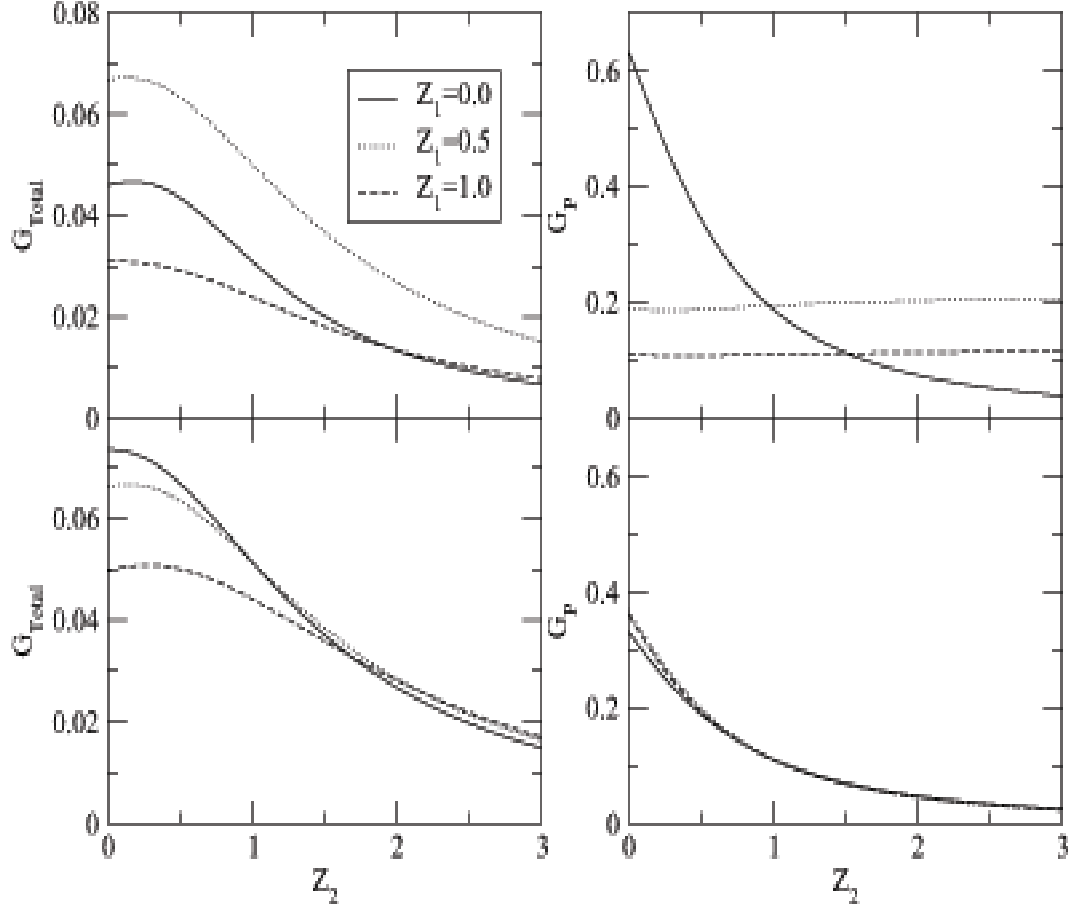


**Figure A.5** The total conductance and the normalized spin polarization of conductance of the M/RS/M double junctions as a function of the interfacial scattering potential between a 2DEG with RSOC and a normal metal ( $Z_2$ ) when fixed  $Z_1 = 0$ , where  $k_0 = 0.05 q_F$ ,  $m_R = 0.05 m_e$ , and  $L = 280/q_F$ . The left column shows the total conductance and the right column shows the normalized spin polarization of conductance, when the top figure for  $eV = -0.5 E_R$  and the bottom figure for  $eV = E_R$ .

# APPENDIX B

## PUBLICATION I

Journal of Magnetism and Magnetic Materials 324 (2012) 475–478



Contents lists available at SciVerse ScienceDirect

Journal of Magnetism and Magnetic Materials

journal homepage: [www.elsevier.com/locate/jmmm](http://www.elsevier.com/locate/jmmm)



### Tunneling conductance of a two-dimensional electron gas with Dresselhaus spin-orbit coupling

B. Srisongmuang<sup>a,\*</sup>, A. Ka-oeay<sup>b</sup>

<sup>a</sup> Ratchaburi Campus, Faculty of Industrial Education and Technology, King Mongkut's University of Technology Thonburi, Bangkok 10140, Thailand

<sup>b</sup> School of Physics, Suranaree University of Technology, Nakhon Ratchasima 30000, Thailand

#### ARTICLE INFO

Article history:  
Received 26 April 2011  
Received in revised form  
10 August 2011  
Available online 22 August 2011

Keywords:  
Dresselhaus spin-orbit coupling  
Tunneling spectroscopy  
Tunneling conductance

#### ABSTRACT

We theoretically studied the spin-dependent charge transport in a two-dimensional electron gas with Dresselhaus spin-orbit coupling (DSOC) and metal junctions. It is shown that the DSOC energy can be directly measured from the tunneling conductance spectrum. We found that spin polarization of the conductance in the propagation direction can be obtained by injecting from the DSOC system. We also considered the effect of the interfacial scattering barrier (both spin-flip and non-spin-flip scattering) on the overall conductance and the spin polarization of the conductance. It is found that the increase of spin-flip scattering can enhance the conductance under certain conditions. Moreover, both types of scattering can increase the spin polarization below the branches crossing of the energy band.

© 2011 Elsevier B.V. All rights reserved.

#### 1. Introduction

The generation of spin-polarized carriers is one of the main focuses in the new field "spintronics", which aims to utilize the spin degree of freedom of electrons in electronic devices. The generation of spin polarization can be achieved in several ways, for example, through optical pumping [1] and electrical spin injection [2]. However, for device applications, electrical spin injection into semiconductor is more desirable [3].

Spin injection from ferromagnetic metal into the semiconductor was first proposed by Aronov and Pikus [2]. Preliminary experiments have resulted in very similar ways and the spin injection effect measured was only about 1% [4–6]. In 2000, Schmidt et al. revealed that the conductivity mismatch between the ferromagnetic metal and the semiconductor was the fundamental problem for injecting spins from metal to semiconductors [7]. In the same year, to solve the problem of the mismatch in the conductivities of a ferromagnetic metal and a semiconductor, the injection through tunnel contacts was proposed by Rashba [8]. Then, the higher efficiency electrical spin injection from metal to semiconductor was realized in different systems [9–13]. Besides the use of tunnel barriers, the spin injection from the ferromagnetic semiconductor into the semiconductor has been demonstrated. High degree of spin polarization has been achieved in this way [14–16], where there is no conductivity mismatch problem between two semiconductors. However, researchers in many

different areas are still trying to find alternative spin-polarized sources.

Recently, there has been growing interest in the electron transport properties through a non-magnetic semiconductor after it was found that large spin polarization can be obtained in such a structure due to the spin-orbit coupling interaction [17–25]. The spin-orbit coupling in semiconductors is induced by symmetry-breaking, which is mainly classified into two types. One is the Rashba spin-orbit coupling (RSOC) [26–28], which is due to the structure-inversion asymmetry. The other is the spin splitting induced by the bulk-inversion asymmetry known as the DSOC [29]. However, the measurement of spin splitting still remains a challenge. It has been studied using many different techniques, which are briefly discussed in our previous work and references therein [22].

In this paper, we deal with the junction composed of a metal and a two-dimensional electron gas (2DEG) with Dresselhaus-type spin-orbit coupling. We show that the in-plane tunneling spectroscopy can also be used to measure the strength of DSOC as well as that of the RSOC [22]. We also find that large spin polarization in the propagation direction is obtained in this system. We also study how the interfacial scattering barrier affects both the conductance spectrum and the spin polarization of conductance.

#### 2. Formulation

The 2DEG/M junction is modeled as an infinite 2D system. Our system lies on  $xz$  plane, where the Dresselhaus and the metal

\* Corresponding author.

E-mail address: [benjamats@hotmail.com](mailto:benjamats@hotmail.com) (B. Srisongmuang).

system occupy the  $x < 0$  and  $x > 0$ , respectively. The two regions are separated by the flat interface at  $x=0$ . The interfacial scattering is modeled by a Dirac delta-function potential [30]. We describe our system by the following Hamiltonian:

$$H = \hat{p} \frac{1}{2m(x)} \hat{p} + U(x,z) + H_D \quad (1)$$

Each term is a  $2 \times 2$  matrix acting on spinor states and  $\hat{p}$  is the momentum operator. The effective mass  $m(x)$  is position dependent; i.e.  $[m(x)]^{-1} = m^{-1}\Theta(x) + (m^*)^{-1}\Theta(-x)$ , where  $m$  and  $m^*$  are effective electron masses in the metal and the Dresselhaus system, respectively, and  $\Theta(x)$  is the Heaviside step function.  $U(x,z)$  is also a position-dependent function and is modeled by the expression

$$U(x,z) = H\delta(x) + E_0\Theta(-x) - E_F\Theta(x) \quad (2)$$

where  $H$  represents the scattering potential at the interface; the diagonal elements of  $H$  corresponding to the non-spin-flip scattering potential, while off-diagonal elements govern the spin-flip scattering [31].  $E_0$  is the energy difference between the Fermi level and the crossing point of two branches in Dresselhaus system, and  $E_F$  is the Fermi energy of the metal. The Dresselhaus Hamiltonian is written as

$$H_D = \frac{\beta}{\hbar} (\sigma_z p_z + \sigma_x p_x) \quad (3)$$

where  $\beta$  represents the DSOC strength.

From the Hamiltonian, one can obtain the eigenenergy for electrons in each region. The wave function of electrons with energy  $E$  in the Dresselhaus system is written as a linear combination of incident momentum state and reflected states of the same energy and  $k_x$ . The energy dispersion of the system is depicted in Fig. 1. There are two equal possibilities for an incident electron. Thus, the two wave functions in the Dresselhaus side become

$$\Psi^{(1)}_{DS}(x,z) = \left( \begin{bmatrix} \cos(\frac{\phi_2}{2} + \frac{\pi}{4}) \\ \sin(\frac{\phi_2}{2} + \frac{\pi}{4}) \end{bmatrix} e^{k_z z} + b_1 + \begin{bmatrix} \cos(\frac{\phi_2}{2} - \frac{\pi}{4}) \\ -\sin(\frac{\phi_2}{2} - \frac{\pi}{4}) \end{bmatrix} e^{-k_z z} \right) \quad (4)$$

$$\Psi^{(2)}_{DS}(x,z) = \left( \begin{bmatrix} \pm \cos(\frac{\phi_2}{2} + \frac{\pi}{4}) \\ \sin(\frac{\phi_2}{2} + \frac{\pi}{4}) \end{bmatrix} e^{\pm k_z x} + b_1 - \begin{bmatrix} \pm \cos(\frac{\phi_2}{2} \mp \frac{\pi}{4}) \\ \mp \sin(\frac{\phi_2}{2} - \frac{\pi}{4}) \end{bmatrix} \right) \times e^{\mp k_z z} + b_2 - \begin{bmatrix} -\cos(\frac{\phi_2}{2} + \frac{\pi}{4}) \\ \sin(\frac{\phi_2}{2} + \frac{\pi}{4}) \end{bmatrix} e^{-k_z x} \right) e^{k_z x} \quad (4)$$

where  $\phi_{2\pm}$  are the angles between  $k$  and the  $x$  axis as shown in Fig. 1. For  $E > E_0$ ,  $b_1$  and  $b_2$  are the amplitudes of reflection of electrons to the plus and minus branches, respectively. When  $E < E_0$ ,  $b_1$  and  $b_2$  refer to the amplitudes of reflection of electrons with smaller and larger  $k$  of the minus branch, respectively. The upper and lower signs in Eq. (4) are for  $E \leq E_0$  and  $E > E_0$ , respectively.

Similarly, in the metal system, the wave function is obtained as a linear combination of two outgoing states of the same energy and  $k_x$ . In order to observe the electron spin in the  $x$  direction, we choose the spins of transmitted electrons to be along the  $x$  direction. The corresponding electron wave function in the metal is written as

$$\Psi_M(x,z) = \frac{c_1}{\sqrt{2}} \begin{bmatrix} 1 \\ 1 \end{bmatrix} e^{i k_x x} + \frac{c_2}{\sqrt{2}} \begin{bmatrix} 1 \\ -1 \end{bmatrix} e^{i k_x x} \quad (5)$$

where  $c_1$  and  $c_2$  are the transmission amplitudes of electrons with spin orientation in  $+x$  and  $-x$  respectively.

We obtain all the reflection and transmission amplitudes from the following matching conditions that ensure the probability conservation [32]:

$$\Psi_{DS}(x=0, z) = \Psi_M(x=0, z) \quad (6)$$

$$\left( \frac{m}{m^*} \frac{d\Psi_{DS}}{dx} - \frac{d\Psi_M}{dx} \right) \Big|_{x=0} = \left( i \frac{m}{m^*} k_D \sigma_x - 2q_z Z \right) \Psi(0) \quad (7)$$

where  $Z = mH/\hbar^2 q_z$ ; the diagonal elements of  $Z$  refer to non-spin-flip scattering strength ( $Z$ ) and off-diagonal elements refer to that of spin-flip scattering ( $Z_f$ ).

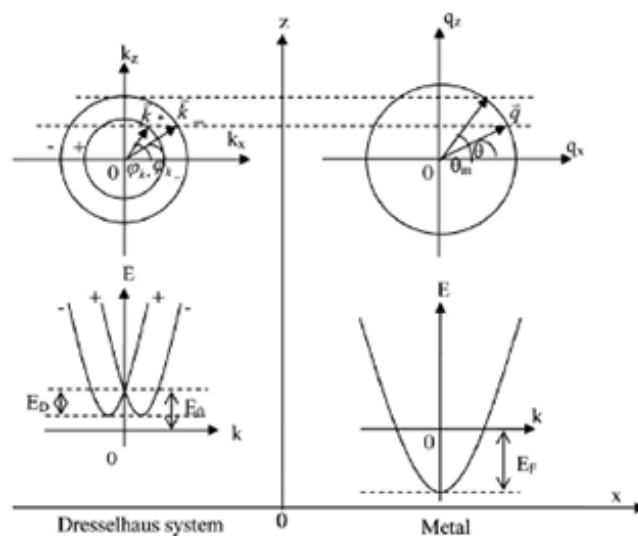


Fig. 1. Top sketches are the energy contours of the electron in a metal (right) and the Dresselhaus system (left). The angles  $\phi$  and  $\theta$  are defined as those between the  $x$  axis and the momenta of electrons in the Dresselhaus system and the metal, respectively. The dashed line that crosses both sides shows the momentum states with the same  $k_x$ . The lower sketches are the corresponding energy spectra.  $E_0$  and  $E_F$  are the off-set energy of the Dresselhaus system and the metal Fermi energy, respectively.

From the transmission amplitudes, the differential conductance at zero temperature can be calculated from the following:

$$G(eV) = \frac{L^2 e^2}{4\pi^2 \hbar} \int_{-\theta_m}^{\theta_m} d\theta \cos\theta (C_1(eV, \theta) + C_2(eV, \theta)) \quad (8)$$

where  $L^2$  is the area of the metal,  $C_1(eV, \theta)$  and  $C_2(eV, \theta)$  are the transmission probabilities to states with spin  $+x$  and  $-x$ , respectively, and  $\theta_m$  is the maximum angle of the transmission electron in the metal (see Fig. 1).

We can obtain the expression for the spin polarization of conductance as

$$P = \frac{\int_{-\theta_m}^{\theta_m} d\theta \cos\theta (C_1(eV, \theta) - C_2(eV, \theta))}{\int_{-\theta_m}^{\theta_m} d\theta \cos\theta (C_1(eV, \theta) + C_2(eV, \theta))} \quad (9)$$

### 3. Results and discussion

In this section, we discuss the effect of the interfacial scattering on the differential conductance spectra and the spin polarization of conductance. In our numerical calculation, for the purpose of illustration, we set  $m/m^* = 10$  and  $k_D = 0.05k_F$ . The main results are not affected by the choice of these parameters. In all conductance plots, the conductance is in units of  $L^2 e^2 / (4\pi^2 \hbar)$ .

The plot of the differential conductance as a function of electron energy ( $eV/E_F$ ) is shown in Fig. 2. There are two distinguished features at the voltage corresponding to the bottom and the branch crossing of the energy band. The energy spacing between them is equal to the Dresselhaus energy ( $E_D$ ), which is the quantity of interest. This predicted behavior should be displayed in the hybrid structure composed of metal and semiconductor-based heterostructures such as InSb [29], GaSb [33], InAsSb [34], and InSb-based alloys [35] since they exhibit Dresselhaus spin-orbit coupling.

The effect of the interfacial scattering on the overall conductance can be seen in Fig. 3. As expected, the spin-flip scattering suppresses the conductance in transparency junction (see Fig. 3(a)). However, in the tunneling limit ( $Z=1$ ), the results are surprising. As can be seen in Fig. 3 (b), an increase in  $Z_F$  (form zero to 1) can enhance conductance. The conductance spectrum, which is usually decreased in the presence of the interfacial scattering, can be enhanced by the combined effect of both types of scattering. This effect was also found in the previous study of the tunneling conductance spectrum of a semiconductor

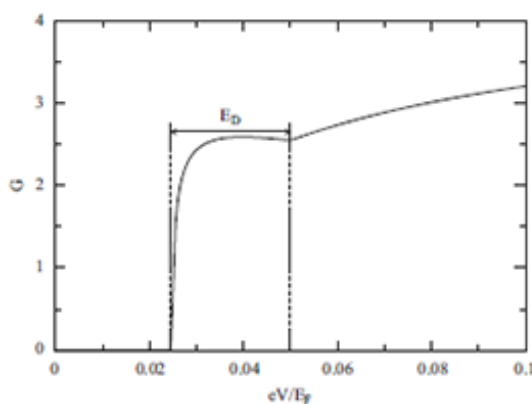


Fig. 2. Differential conductance spectra  $G$  for  $Z=Z_F=0$ .

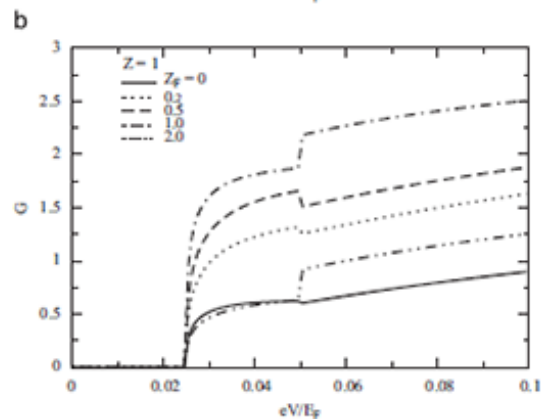
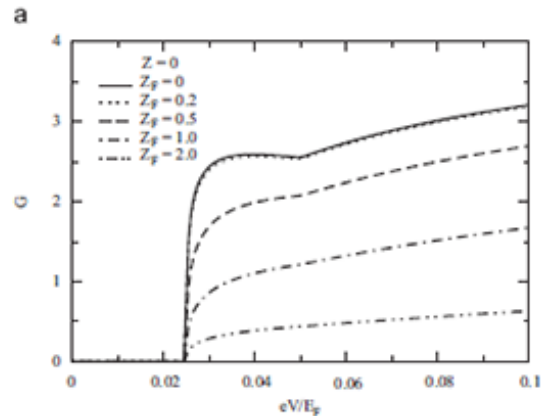


Fig. 3. Differential conductance spectra for different  $Z_F$  where (a)  $Z=0$  and (b)  $Z=1$ .

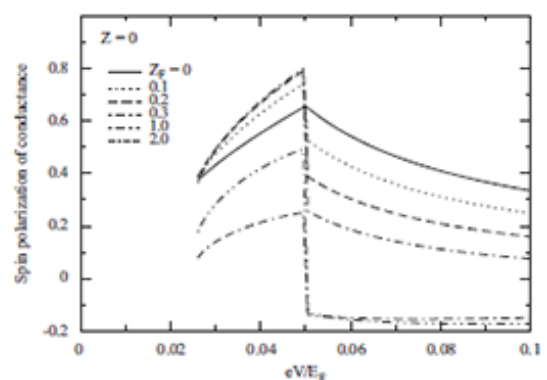


Fig. 4. Plots of the spin polarization of the conductance as a function of energy for different  $Z_F$ , where  $Z=0$ .

and superconductor hybrid structures by Zutic and Das Sarma [31] as well as by Das Sarma et al. [36]. In addition, not just in ballistic junction, interfacial spin-flip scattering was shown to be also important for spin injection in diffusive regime [37].



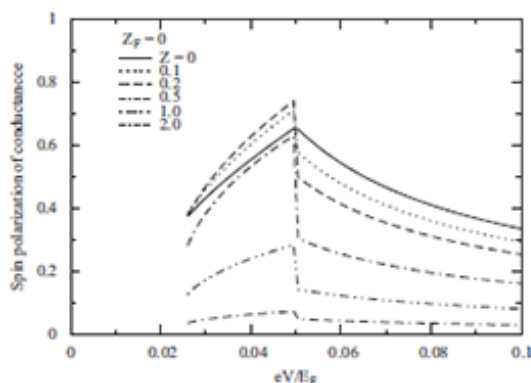


Fig. 5. Plots of the spin polarization of the conductance as a function of energy for different  $Z$ , where  $Z_F=0$ .

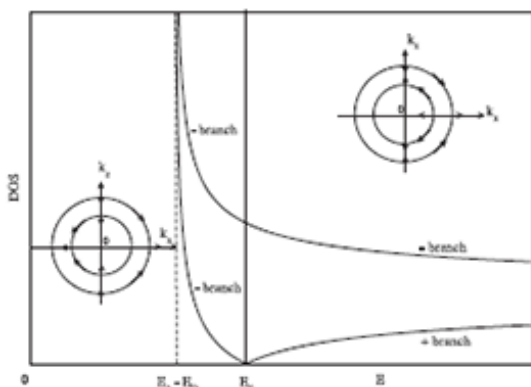


Fig. 6. Density of states of each branch of 2DEG with the Dresselhaus spin-orbit coupling. The contour plots on the left and on the right are those in the case where  $E < E_0$  and  $E > E_0$ , respectively. When  $E > E_0$ , the outer contour is that of the minus branch and the inner one is that of the plus branch. When  $E < E_0$ , both energy contours belong to the  $-$ branch. The arrows represent the spin direction of the states with positive  $s_x$ .

At last, plots of the spin polarization of the conductance as a function of  $eV/E_F$  are shown in Figs. 4 and 5. In the absence of both types of scattering, large spin polarization is always positive. This is because the density of states of the minus branch is larger than that of the plus branch, and the spins of the incident states of the minus branch are mostly oriented along the  $+x$  direction, see Fig. 6. Moreover, at energy below the branches crossing, the increase in  $Z$  or  $Z_F$  from zero to a small value (from 0 to  $\sim 0.3$ ) can enhance the spin polarization (see Figs. 4 and 5). It is also found in the absence of  $Z$ , when  $Z_F$  is high, e.g.,  $Z_F=1.0$  and  $2.0$ , that the spin polarization of the energy above  $E_0$  is negative (see Fig. 4).

#### 4. Conclusions

In conclusion, the spin-dependent transport properties of 2DEG/M junction with Dresselhaus spin-orbit coupling have been investigated. We showed that the in-plane tunneling conductance

spectrum can also be used to measure the Dresselhaus energy as well as obtained it in the system with Rashba spin-orbit coupling. We find that the spin-flip scattering can enhance both conductance and the spin polarization of the conductance in certain conditions, and also can change the sign of the spin polarization of the conductance when  $Z_F$  is high. It is found that non-spin-flip scattering can increase the spin polarization of conductance in certain conditions as well. Large spin polarization found in this system indicates the potential of tunable spin-dependent electric devices such as spin switches and spin filters.

#### Acknowledgments

We thank P. Pairor for useful discussion. This work was supported by Ratchaburi Campus, King Mongkut's University of Technology Thonburi. A. Ka-oy was supported by the Thailand Research Fund through the Royal Golden Jubilee Ph. D. program (Grant No. PHD/0218/2548).

#### References

- [1] F. Meir, B.P. Zakharchenya, *Optical Orientation*, vol. 8, North-Holland, Amsterdam, 1984.
- [2] A.G. Aronov, G.E. Plus, *Soviet Physics—Semiconductors* 10 (1976) 698.
- [3] I. Zutic, J. Fabian, S. Das Sarma, *Reviews of Modern Physics* 76 (2004) 323.
- [4] P. Hammer, B.R. Bennet, M.J. Yang, M. Johnson, *Physical Review Letters* 83 (1999) 203.
- [5] S. Gardesiu, C.G. Smith, G.H.W. Barnes, E.H. Linfield, D.A. Ritchie, *Physical Review B* 60 (1999) 7764.
- [6] A.T. Filip, B.H. Hoving, F.J. Jedema, B.J. van Wees, B. Dutta, S. Borghs, *Physical Review B* 62 (2000) 9996.
- [7] G. Schmidt, D. Ferrand, L.W. Molenkamp, A.T. Filip, B.J. van Wees, *Physical Review B* 62 (2000) R4790.
- [8] E.I. Rashba, *Physical Review B* 62 (2000) R16267.
- [9] H. Zhu, et al., *Physical Review Letters* 87 (2001) 016601.
- [10] A.T. Hanbidi, B.T. Jonker, G. Itskos, G. Kioseoglou, A. Petrou, *Applied Physics Letters* 80 (2002) 1240.
- [11] C. Adedmann, X. Lou, J. Strand, C.J. Palmstrom, P.A. Crowell, *Physical Review B* 71 (2005) 121301.
- [12] X. Jiang, R. Wang, R.M. Shelby, R.M. Macfarlane, S.R. Bank, J.S. Harris, S.S.P. Parkin, *Physical Review Letters* 94 (2005) 056601.
- [13] W. Han, K.M. McCreary, Y. Li, J.L. Jared, A.G. Wong, Swartz, R.K. Kawakami, *Physical Review Letters* 105 (2010) 167202.
- [14] R. Fiederling, M. Heim, G. Reuscher, W. Ossau, G. Schmidt, A. Waag, L.W. Molenkamp, *Nature (London)* 402 (1999) 787.
- [15] Y. Ohno, D.K. Young, B. Beschoten, F. Matsukura, H. Ohno, D.D. Awschalom, *Nature (London)* 402 (1999) 790.
- [16] B.T. Jonker, Y.D. Park, B.R. Bennett, *Physical Review B* 62 (2000) 8180.
- [17] J.-F. Liu, W.-J. Deng, K. Xia, C. Zhang, Z. Ma, *Physical Review B* 73 (2006) 155308.
- [18] M. Lee, M.-S. Choi, *Physical Review B* 71 (2005) 153306.
- [19] V. Marigliano Ramaglia, V. Cataudella, G. De Filippis, C.A. Perroni, *Physical Review B* 73 (2006) 155328.
- [20] T. Yokoyama, Y. Tanaka, J. Inoue, *Physical Review B* 74 (2006) 035318.
- [21] Y. Sawo, T. Yokoyama, Y. Tanaka, *Journal of Magnetism and Magnetic Materials* 310 (2007) 2277.
- [22] B. Srirongmuang, P. Pairor, M. Berciu, *Physical Review B* 78 (2008) 155317.
- [23] C.-Z. Ye, R. Xue, Y.-H. Nie, J.-Q. Lian, *Physical Letters A* 373 (2009) 1290.
- [24] I. Villegas-Lelovsky, C. Trallero-Giner, M. Rebello Sousa Dias, V. Lopez-Richard, G.E. Marques, *Physical Review B* 79 (2009) 155306.
- [25] J.-D. Ia, J.-W. Li, *Applied Surface Science* 256 (2010) 4027.
- [26] E.I. Rashba, *Soviet Physics-Solid State* 2 (1960) 1109.
- [27] Y.A. Bychkov, E.I. Rashba, *Journal of Physical Chemistry* 17 (1984) 6039.
- [28] Y.A. Bychkov, E.I. Rashba, *JETP Letters* 39 (1984) 78.
- [29] G. Dresselhaus, *Physical Review* 100 (1955) 580.
- [30] G.E. Blonder, M. Tinkham, T.M. Klapwijk, *Physical Review B* 25 (1982) 4515.
- [31] I. Zutic, S. Das Sarma, *Physical Review B* 60 (1999) R16322.
- [32] U. Zulicke, C. Schroll, *Physical Review Letters* 88 (2001) 029701.
- [33] D.G. Semler, W.M. Becker, Laura M. Roth, *Physical Review B* 1 (1970) 764.
- [34] N. Nishizako, T. Manago, S. Ishida, H. Geka, I. Shibasaki, *Physica E* 42 (2010) 975.
- [35] M. Akabori, V.A. Guzenko, T. Sato, Th. Schapers, T. Suzuki, S. Yamada, *Physical Review B* 77 (2008) 205320.
- [36] S. Das Sarma, J. Fabian, X. Hu, I. Zutic, *Superlattices and Microstructures* 27 (2000) 289.
- [37] S. Garzon, I. Zutic, R.A. Webb, *Physical Review Letters* 94 (2005) 176601.



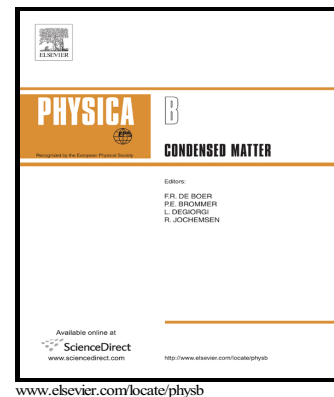
# APPENDIX C

## PUBLICATION II

### Author's Accepted Manuscript

Impact of interfacial scattering on the spin polarization of a metal/semiconductor/metal with Rashba spin-orbit coupling junction

A. Ka-oey, A. Jantayod, P. Pairor



PII: S0921-4526(14)00854-0  
DOI: <http://dx.doi.org/10.1016/j.physb.2014.11.020>  
Reference: PHYSB308737

To appear in: *Physica B: Physics of Condensed Matter*

Received date: 26 June 2014  
Revised date: 9 September 2014  
Accepted date: 13 November 2014

Cite this article as: A. Ka-oey, A. Jantayod and P. Pairor, Impact of interfacial scattering on the spin polarization of a metal/semiconductor/metal with Rashba spin-orbit coupling junction, *Physica B: Physics of Condensed Matter*, <http://dx.doi.org/10.1016/j.physb.2014.11.020>

This is a PDF file of an unedited manuscript that has been accepted for publication. As a service to our customers we are providing this early version of the manuscript. The manuscript will undergo copyediting, typesetting, and review of the resulting galley proof before it is published in its final citable form. Please note that during the production process errors may be discovered which could affect the content, and all legal disclaimers that apply to the journal pertain.

# Impact of interfacial scattering on the spin polarization of a metal/semiconductor/metal with Rashba spin-orbit coupling junction

A. Ka-oeey <sup>a</sup>, A. Jantayod <sup>b,c,\*</sup>, and P. Pairor <sup>a</sup>

<sup>a</sup>*School of Physics, Institute of Science, Suranaree University of Technology, Nakhon Ratchasima 30000, Thailand*

<sup>b</sup>*Department of Physics, Faculty of Science, Naresuan University, Phitsanulok 65000, Thailand*

<sup>c</sup>*Research Center for Academic Excellence in Applied Physics, Faculty of Science, Naresuan University, Phitsanulok 65000, Thailand*

---

## Abstract

The conductance spectrum and the normalized spin polarization due to the spin-dependent conductance of a metal/semiconductor/metal with Rashba spin-orbit coupling junction are theoretically studied within a free electron approximation and a scattering method. The effect of the first and the second interfacial scattering potentials on the two quantities are considered, especially when both of the potential strengths are not equal. While the conductance is determined by the higher interfacial scattering potential, the spin polarization is determined by the second interfacial barrier potential of the junction.

*Keywords:* A metal/semiconductor/metal with Rashba spin-orbit coupling, Tunneling conductance, interfacial scattering, spin polarization

---

## 1. Introduction

Understanding the mechanism of spin injection offers a huge potential for many fundamental and practical applications in spintronics [1, 2, 3, 4, 5, 6, 7, 8, 9]. Conventionally, the spin injection can be achieved by sourcing the currents from ferromagnetic metal electrodes. Thus, much effort has been put

---

*Email address:* aekj@nu.ac.th (A. Jantayod <sup>b,c,\*</sup>)

towards the study of the spin transport across a ferromagnet/semiconductor interface [10, 11, 12, 13]. It was found that there is a fundamental obstacle for effective spin injection in this case, due to the conductivity mismatch between the two materials [14, 11, 13]; however, a simple solution to this problem is to insert an insulating barrier at the interface [15, 16].

Another way to overcome this problem is to avoid ferromagnets altogether and instead use the spin filtering device based on the intrinsic properties of mesoscopic systems, such as strong spin-orbit interaction [17, 18, 19]. One of the heterojunctions that can be used as spin filtering devices is a metal/Rashba spin-orbit coupling system/metal (M/RSOC/M) double junction. It was shown that the Rashba spin-orbit coupling in a semiconductor heterostructure can help produce and control a spin-polarized current. Assuming identical interfacial scattering potential strengths, one finds that the transmission and spin polarization in such structures depend strongly on the electron incident angle [20].

It is known that the interfacial scattering potentials have an important impact on the particle and spin transmission across a heterostructure. It is not easy to fabricate the double junction with the same interface scattering strength. We, therefore, are interested in the impact of the inequality of these two interfacial scattering strengths in the double junction on the spin filtering. In this article, we theoretically examine the conductance and the spin polarization of conductance of M/RSOC/M double junction, in which the two interfacial scattering potential strengths may not be equal. In the next section we present the assumptions and formalism used in this study. Section 3 contains the results and discussion, and finally, the conclusion is presented in Section 4.

## 2. Method and Assumptions

We model our junction as a two-dimensional system, which lies in the  $xz$  plane. A semiconductor layer of thickness  $L$  with the Rashba spin-orbit coupling is sandwiched between two identical metallic electrodes. We set the first interface at  $x = 0$  and the second one at  $x = L$ . We represent each interfacial scattering barrier by a Dirac-delta function potential [21]. In order to consider in the ballistic regime, the thickness of the Rashba system is also set to be much shorter than the typical mean free path of an electron in the system. The energy dispersion relation of the electron in each region of the double junction is shown in Fig. 1.

We describe our system by the following Hamiltonian:

$$\vec{H} = \left\{ \hat{p} \frac{1}{2m(x)} \hat{p} + V(x) \right\} \hat{I} + \vec{H}_{RS}(x), \quad (1)$$

where  $\hat{p} = -i\hbar(\hat{x}\frac{\partial}{\partial x} + \hat{z}\frac{\partial}{\partial z})$  is the momentum operator. The effective mass  $m(x)$  is position-dependent; i.e.,  $[m(x)]^{-1} = m^{-1}\Theta(-x) + (m^*)^{-1}\Theta(x)$ , where  $m$  and  $m^*$  are the effective electron masses in the metallic and the Rashba region, respectively.  $\Theta(x)$  is the Heaviside step function.  $V(x)$  is also the position-dependent and is defined by the following expression.

$$V(x) = H_1\delta(x) + H_2\delta(x-L) - E_F [\Theta(-x) + \Theta(x-L)] + U_0 [\Theta(x) - \Theta(x-L)], \quad (2)$$

where  $H_1, H_2$  represent the scattering potential strengths at  $x = 0$  and  $x = L$  respectively.  $U_0$  is the offset gate voltage, which is much smaller than the Fermi energy,  $E_F = \frac{\hbar^2 q_F^2}{2m}$  of electrons in the metallic electrodes.  $\vec{H}_{RS}$  is the Rashba spin-orbit coupling term, which is expressed as [17, 18, 19]

$$\vec{H}_{RS}(x) = -\lambda(x) [\vec{\sigma} \times \vec{k}] \cdot \hat{j}, \quad (3)$$

where  $\lambda(x) = \lambda\Theta(x)$  and  $\lambda$  is the Rashba spin-orbit coupling strength parameter, which can be tuned by applying the external electric field perpendicular to the 2D plane [22, 23, 24, 25, 26, 27],  $\hat{j}$  is a unit vector pointing in the direction perpendicular to the plane of the junction,  $\vec{\sigma} = (\sigma_x, \sigma_y, \sigma_z)$  are the Pauli spin matrices, and  $\vec{k}$  is the wave vector of the electron.

The electron energy dispersion relation in the Rashba system can be obtained as

$$E_{\pm}(k) = \frac{\hbar^2}{2m^*} [k^2 \pm 2k_0k] + U_0, \quad (4)$$

where  $k = \sqrt{k_x^2 + k_z^2}$  is the magnitude of the wave vector and  $k_0 = m^*\lambda/\hbar$  is the wave vector associated with the Rashba spin-orbit coupling.

We first consider the electrons in the  $x < 0$  region. The wave function is written as a linear combination of an incident state and a reflected state of the same energy and  $k_z$ . Because there are equal number of electrons with opposite spin directions in a metal, there are two possibilities of the wave function. That is,

$$\psi_M^{(1)}(x, z) = \left( \begin{bmatrix} 1 \\ 0 \end{bmatrix} e^{iq_x x} + \begin{bmatrix} r_{1\uparrow} \\ r_{1\downarrow} \end{bmatrix} e^{-iq_x x} \right) e^{iq_z z}, \quad (5)$$

$$\psi_M^{(2)}(x, z) = \left( \begin{bmatrix} 0 \\ 1 \end{bmatrix} e^{iq_x x} + \begin{bmatrix} r_{2\uparrow} \\ r_{2\downarrow} \end{bmatrix} e^{-iq_x x} \right) e^{iq_z z}, \quad (6)$$

where  $q_x = q \cos \gamma$ ,  $q_z = q \sin \gamma$ , with  $\gamma$  being the angle between the wave vector and the  $x$  axis, and  $q = \sqrt{2m(E_F - E)/\hbar^2}$ .  $r_{j\sigma}$  is the reflection coefficient for spin  $\sigma$ , where  $j = 1, 2$  referring to the wave function of an incident electron with up spin and down spin respectively.

In the  $0 < x < L$  region, the wave function is obtained as a linear combination of two transmitted and two reflected eigenstates of the same energy and  $k_z$ ,

$$\begin{aligned} \psi_{RS}^{(j)}(x, z) = & \left( \begin{bmatrix} \cos \frac{\alpha}{2} \\ \mp \sin \frac{\alpha}{2} \end{bmatrix} t_{j+} e^{\pm i k_x^+ x} + \begin{bmatrix} \sin \frac{\alpha}{2} \\ \mp \cos \frac{\alpha}{2} \end{bmatrix} r_{j+} e^{\mp i k_x^+ x} \right) e^{i k_z^+ z} \\ & + \left( \begin{bmatrix} \sin \frac{\beta}{2} \\ \cos \frac{\beta}{2} \end{bmatrix} t_{j-} e^{i k_x^- x} + \begin{bmatrix} \cos \frac{\beta}{2} \\ \sin \frac{\beta}{2} \end{bmatrix} r_{j-} e^{-i k_x^- x} \right) e^{i k_z^- z}, \end{aligned} \quad (7)$$

where the upper and lower signs refer to the energy above and below  $U_0$  respectively,  $\alpha$  and  $\beta$  are the angles between of  $k^+, k^-$  and the  $x$  axis, respectively.  $t_{+/-}, r_{+/-}$  are the transmission and reflection amplitudes for electrons in the plus/minus branch of the RSOC system. Because the wave vector along the  $z$  axis is conserved, we have the following relations  $q_z = k_z^+ = k_z^-$ , or  $k^+ \sin \alpha = k^- \sin \beta = q \sin \gamma$ , where

$$k^- = k_0 + \sqrt{k_0^2 + \frac{2m^*}{\hbar^2}(E - U_0)}, \quad (8)$$

and

$$k^+ = \pm \left( k_0 - \sqrt{k_0^2 + \frac{2m^*}{\hbar^2}(E - U_0)} \right). \quad (9)$$

The + and - signs in equation (9) are for  $E > U_0$  and  $E < U_0$ , respectively.

In the  $x > L$  region, the electron wave function can be expressed as a transmitted eigenstate;

$$\psi_{MR}^{(j)}(x, z) = \left( \begin{bmatrix} t_{j\uparrow} \\ t_{j\downarrow} \end{bmatrix} e^{i q_x x} \right) e^{i q_z z}, \quad (10)$$

where  $t_{j\sigma}$  is the transmission coefficient of the particle with spin  $\sigma$ .

All the coefficients in Eqs.(5)-(7), and (10) can be obtained from the four boundary conditions at  $x = 0$  and  $x = L$ .

$$\psi_{ML}^{(j)}(x = 0^+, z) = \psi_{RS}^{(j)}(x = 0^-, z) = \psi^{(j)}(0), \quad (11)$$

$$\psi_R^{(j)}(x = L^+, z) = \psi_{M_R}^{(j)}(x = L^-, z) = \psi^{(j)}(L), \quad (12)$$

$$\left( \frac{m}{m^*} \frac{\partial \psi_R^{(j)}}{\partial x} - \frac{\partial \psi_{M_L}^{(j)}}{\partial x} \right) \Big|_0 = \left( 2k_F Z_1 - ik_0 \frac{m}{m^*} \sigma_z \right) \psi^{(j)}(0), \quad (13)$$

$$\left( \frac{\partial \psi_{M_R}^{(j)}}{\partial x} - \frac{m}{m^*} \frac{\partial \psi_R^{(j)}}{\partial x} \right) \Big|_L = \left( 2k_F Z_2 + ik_0 \frac{m}{m^*} \sigma_z \right) \psi^{(j)}(L), \quad (14)$$

where  $Z_i = \frac{mH_i}{\hbar^2 q_F}$  is the dimensionless parameter, referring to the interfacial scattering at  $x = 0$  for  $i = 1$  and at  $x = L$  for  $i = 2$ .  $Z \rightarrow 0$  is in the high transparency limit, whereas  $Z \rightarrow \infty$  is in the low transparency, or tunneling, limit.

The differential conductance at a zero temperature is therefore

$$G(eV) = \frac{e^2}{h} \frac{Aq_F}{2\pi} \int_{-\gamma_m}^{\gamma_m} d\gamma \cos \gamma \sqrt{1 + \frac{eV}{E_F}} \sum_{j=1}^2 (T_{j\uparrow}(eV, \gamma) + T_{j\downarrow}(eV, \gamma)). \quad (15)$$

where  $A$  is the total area of the metallic electrode and  $\gamma_m = \sin^{-1}[k^-(E)/q(E)]$  is the maximum incident angle for the electron with energy  $E$ .  $T_{j\sigma}(eV, \gamma)$  are the transmission probabilities in case  $j$  with spin  $\sigma$ .

We define the spin polarization of conductance  $P$ , which is the difference between the up-spin and down-spin conductance normalized by the total conductance

$$P(eV) = \frac{G_{\downarrow}(eV) - G_{\uparrow}(eV)}{G_{\downarrow}(eV) + G_{\uparrow}(eV)}. \quad (16)$$

### 3. Results and Discussion

The numerical calculation results of the conductance spectrum in a unit of  $e^2 A k_F / \pi h$  and the spin polarization of conductance across the M/RSOC/M junction are presented in this section. We focus on the effect of the interfacial scattering potential on these two quantities. That is, the dimensionless parameter  $Z_1 = mH_1/q_F \hbar^2$  and  $Z_2 = mH_2/q_F \hbar^2$  will be varied, whereas the electron effective mass in the Rashba layer is set to  $m^* = 0.05m_e$ , where  $m_e$  is the free electron mass. Also the thickness of the RSOC layer is set to  $L = 280/q_F$ ,  $k_0 = 0.05q_F$ , and the offset gate voltage is set to  $U_0 = 2E_\lambda$ .

The scattering potential at the interfaces generally limit the particle ability to transmit across the structures as can be seen in the following plots.

The conductance spectrum ( $G$ ) as a function of bias voltage ( $eV$ ) for various values of  $Z_1, Z_2$  are shown in Fig. 2. In all plots, the oscillatory behaviors are present, reflecting the resonance due to the finite thickness of the Rashba layer. The period of this oscillation is not affected by the interfacial scattering potential strengths. As seen in Fig. 2(a), when we consider the case where both barriers have the same potential strength:  $Z_1 = Z_2 = Z$ , the oscillation peaks are more prominent in the tunneling limit. When  $Z_1, Z_2$  are not equal, the conductance spectrum shows similar structures and the value of the conductance depends on the interfacial scattering potential that is higher.

The spin polarization of conductance  $P$  as a function of applied voltage for various values of  $Z_1, Z_2$  is plotted in Fig. 3. The plots contain similar oscillations as seen in the conductance spectrum. When  $Z_1 = Z_2 = Z$ ,  $P$  is decreased as  $Z$  is larger. When  $Z_1$  is fixed and  $Z_2$  is varied,  $P$  is decreased with the increase in  $Z_2$ . However, when  $Z_2$  is fixed and  $Z_1$  is varied,  $P$  is hardly changes. These results can be seen more clearly in the plots of  $P$  vs  $Z_1$  and  $Z_2$  in Fig. 4. The values of  $P$  at the voltages either higher or lower than  $U_0$  is much more sensitive to  $Z_2$  than  $Z_1$ . This result indicates that spin filtering in a double junction is determined mainly by the second barrier potential.

#### 4. Conclusions

The free electron model and the scattering method are used to calculate the conductance and the normalized spin polarization of conductance across a double junction, M/RSOC/M. The conductance is decreased as the interfacial scattering potential is increased and it is determined by the stronger interfacial scattering potential. As for the case of the spin polarization, its valued is surprisingly determined by the second barrier strength of the double junction.

#### Acknowledgments

A. Jantayod would like to acknowledge financial supported from Naresuan University. A. Ka-oey and P. Pairor thank Thailand Research Fund through the Royal Golden Jubilee Ph.D. Program (Grant No. PHD/0218/2548) and the office of the Higher Education Commission under NRU Project of Thailand (RU 4/2555) for financial support.

- [1] G. Prinz, Phys. Today 48 (1995) 58.
- [2] H. Ohno, Science. 281 (1998) 5379.
- [3] M. Oestreich, Nature (London) 402 (1999) 735.
- [4] S. A. Wolf, D. D. Awschalom, R. A. Buhrman, J. M. Daughton, S. V. Molnar, M. L. Roukes, A. Y. Chtchelkanova, and D. M. Treger, Science 294 (2001) 1488.
- [5] Z. W. Xie and B. Z. Li, J. Appl. Phys. 93 (2003) 9111.
- [6] A. Saffarzadeh, J. Magn. Magn. Mater. 269 (2004) 327.
- [7] I. Zutic, J. Fabian, and S. D. Sarma, Rev. Mod. Phys. 76 (2004) 323.
- [8] U. Lders, M. Bibes, S. Fusil, K. Bouzehouane, E. Jacquet, C. B. Sommers, J. -P. Contour, J. -F. Bobob, A. Barthlmy, A. Fert, and P. M. Levy, Phys. Rev. B 76 (2007) 134412.
- [9] A. Fert, Rev. Mod. Phys. 80 (2008) 1517.
- [10] W. Y. Lee, S. Gardelis, B. -C. Choi, Y. B. Xu, C. G. Smith, C. H. W. Barnes, D. A. Ritchie, E. H. Linfield, and J. A. C. Bland, J. Appl. Phys. 85 (1999) 6682.
- [11] G. Schmidt, D. Ferrand, L. W. Molenkamp, A. T. Filip, and B. J. van Wees, Phys. Rev. B 62 (2000) 4790R.
- [12] C. -M. Hu and T. Matsuyama, Phys. Rev. Lett. 87 (2001) 066803.
- [13] Y. Jiang and M. B. A. Jalil, J. Phys.:Condens. Matter 15 (2003) 31.
- [14] P. R. Hammar, B. R. Bennett, M. J. Yang, and M. Johnson, Phys. Rev. Lett. 83 (1999) 203.
- [15] E. I. Rashba, Phys. Rev. B 62 (2000) 16267R.
- [16] H. B. Heersche, Th. Schpers, J. Nitta, and H. Takayanagi, Phys. Rev. B 64 (2001) 161307R.
- [17] E. I. Rashba, Sov. phys. Solid State 2 (1960) 1109.



- [18] Y. A. Bychkov and E. I. Rashba, *J. phys. C* 17 (1984) 6039.
- [19] Y. A. Bychkov and E. I. Rashba, *JETP Lett*, 39 (1984) 78.
- [20] V. M. Ramaglia, D. Bercioux, V. Cataudella, G. D. Filippis, and C. A. Perroni, *J. Phys.:Condens. Matter* 16 (2004) 9143.
- [21] G. E. Blonder, M. Tinkham, and T. M. Klapwijk, *Phys. Rev. B* 25 (1982) 4515.
- [22] G. Engels, J. Lange, Th. Schapers, and H. Luth, *Phys. Rev. B* 55 (1997) 1958.
- [23] J. Nitta, T. Akazaki, H. Takayanagi, and T. Enoki, *Phys. Rev. Lett.* 78 (1997) 1335.
- [24] J. P. Heida, B. J. van Wees, J. J. Kuipers, T. M. Klapwijk, and G. Borghs, *Phys. Rev. B* 57 (1998) 11911.
- [25] C.-M. Hu, J. Nitta, T. Akazaki, H. Takayanagi, J. Osaka, P. Pfeffer, and W. Zawadzki, *Phys. Rev. B* 60 (1999) 7736.
- [26] Y. Sato, T. Kita, S. Gozu, and S. Yamada, *J. Appl. Phys.* 89 (2001) 8017.
- [27] T. Koga, J. Nitta, T. Akazaki, and H. Takayanagi, *Phys. Rev. Lett.* 89 (2002) 046801.

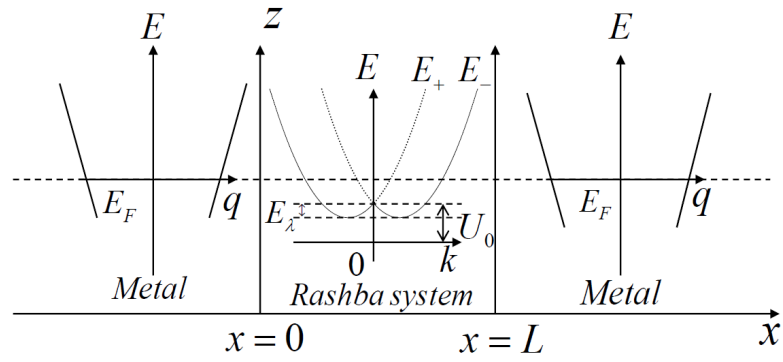


Figure 1: The sketch of the energy dispersion relation of the electron in each region of the double junction.  $E_F$ ,  $U_0$ , and  $E_\lambda = \hbar^2 k_0^2 / 2m^*$  are the Fermi energy of electron in the metallic leads, the offset gate voltage and the Rashba spin-orbit coupling energy, respectively.

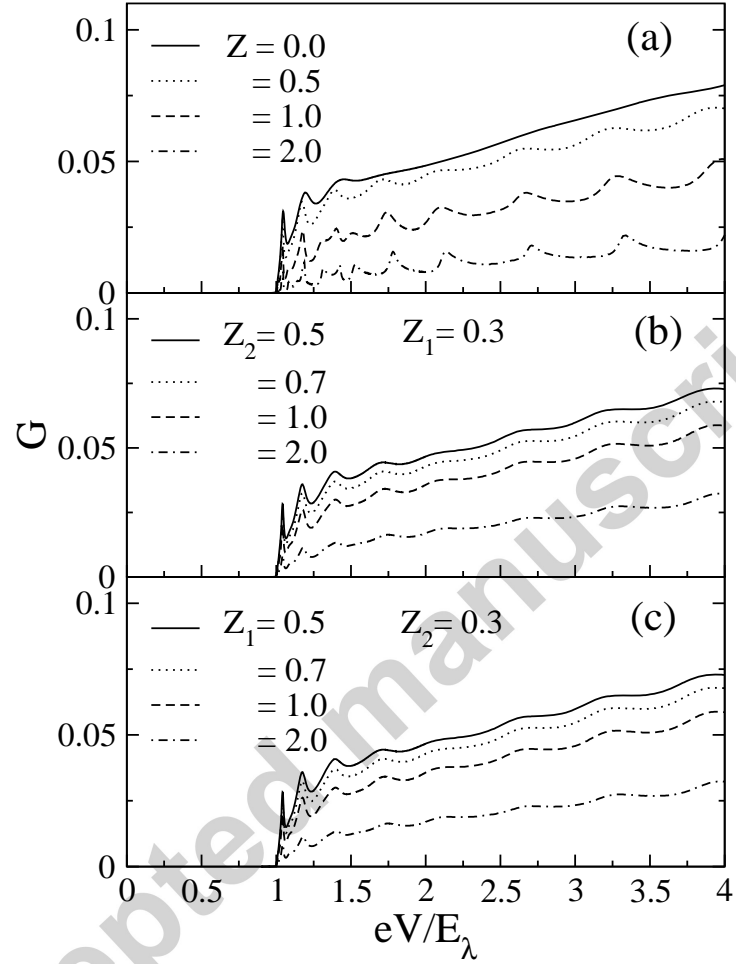


Figure 2: The plots of conductance spectra as a function of applied voltage, (a) for identical barrier strength ( $Z_1 = Z_2 = Z$ ), (b) for  $Z_1 = 0.3$  and  $Z_2$  is varied, and (c) for  $Z_2 = 0.3$  and  $Z_1$  is varied.

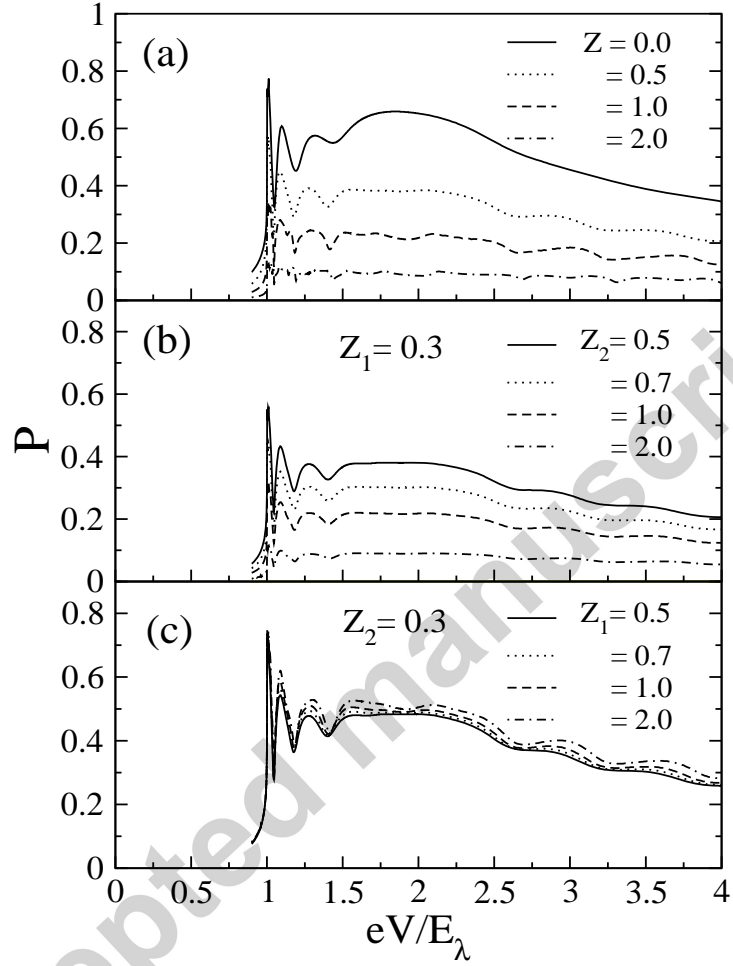


Figure 3: The plots of spin polarization of conductance as a function of applied voltage, (a) for identical barrier strength ( $Z_1 = Z_2 = Z$ ), (b) for  $Z_1 = 0.3$  and  $Z_2$  is varied, and (c) for  $Z_2 = 0.3$  and  $Z_1$  is varied.

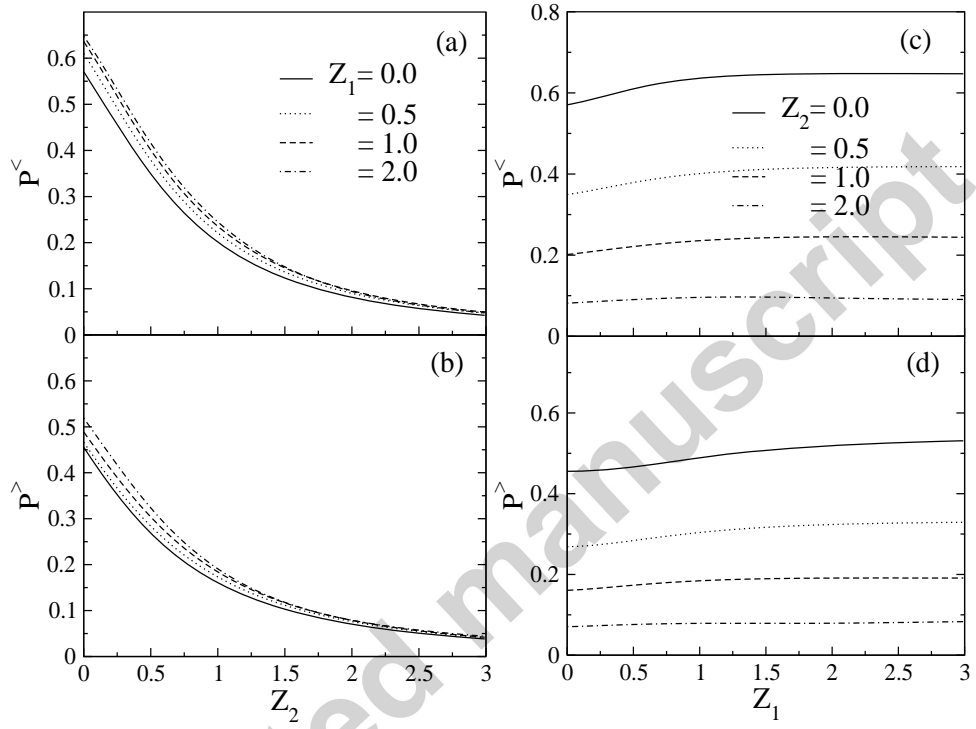


Figure 4: The plots of spin polarization of conductance as a function  $Z_2$  and  $Z_1$ . (a) and (c) contain the plots of  $P$  at the applied voltage is slightly below  $U_0$  and (b) and (d) contain the plots of  $P$  at the applied voltage is above  $U_0$ .

# CURRICULUM VITAE

**NAME** Miss Achara Ka-oey  
**DATE OF BIRTH** January 23, 1983  
**PLACE OF BIRTH** Chiangmai, Thailand  
**PERSONAL ADDRESS** 71 M.15, Thumbol Sansai Phrao District,  
Chiangmai 50190, Thailand  
Mobile. 66-84-0372496  
**E-MAIL** t\_taro23@hotmail.com

## EDUCATIONS

PhD candidate (2006 - present)

School of Physics, Suranaree University of Technology, Nakhon Ratchasima,  
Thailand

Title of Thesis: Particle and spin transport in systems with Rashba and  
Dresselhaus spin-orbit coupling

Supervisor: Assoc. Prof. Dr. Puangratana Pairor

Diploma of Education (2005 - 2006)

Faculty of Education, Chiangmai University, Chiangmai, Thailand

Bachelor of Science (2002 - 2005)

Department of Physics, Faculty of Science, Naresuan University, Phitsanu-  
lok, Thailand

Advisor: Dr. Chanun Sricheewin